

**The Yakima Air Wintertime Nitrate Study
(YAWNS)**

Final Report

Prepared by:
Laboratory for Atmospheric Research
Department of Civil & Environmental Engineering
Washington State University

Preface

The Laboratory for Atmospheric Research at Washington State University submits this Final Report as part of a contract project from the Washington Department of Ecology to conduct the Yakima Air Wintertime Nitrate Study (YAWNS).

Contacts:

Tim VanReken (Project PI and Lead Author)
Laboratory for Atmospheric Research
Department of Civil & Environmental Engineering
Washington State University
Phone: (509) 335-5055
Email: vanreken@wsu.edu

Tom Jobson
Laboratory for Atmospheric Research
Department of Civil & Environmental Engineering
Washington State University
Phone: (509) 335-2692
Email: tjobson@wsu.edu

Brian Lamb
Laboratory for Atmospheric Research
Department of Civil & Environmental Engineering
Washington State University
Phone: (509) 335-5702
Email: blamb@wsu.edu

Heping Liu
Laboratory for Atmospheric Research
Department of Civil & Environmental Engineering
Washington State University
Phone: (509) 335-1529
Email: heping.liu@wsu.edu

Susan Kaspari
Department of Geology
Central Washington University
Phone: (509) 963-2738
Email: kaspari@geology.cwu.edu

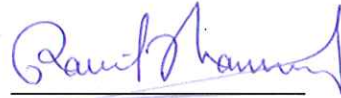
Approval Page

Washington Department
of Ecology
Air quality Program



Jeff Johnston 2/25/14
Date
Phone: 360-407-6115
Email: jeff.johnston@ecy.wa.gov

Washington Department
of Ecology
Air quality Program



Ranil Dhammapala 2/25/2014
Date
Phone: 360-407-6807
Email: ranil.dhammapala@ecy.wa.gov

Executive Summary

The Yakima region in Washington is in attainment for the 24-hour $PM_{2.5}$ Federal standard but monitored concentrations are frequently close to the standard, primarily during winter, and a nonattainment classification has been considered a possibility. At present, the primary strategy employed in Washington to reduce $PM_{2.5}$ during wintertime is to control the emissions from biomass burning, including burning wood for home heating and outdoor burning of yard debris and orchard tear-outs. The Washington Department of Ecology desired a more complete understanding of the conditions that led to elevated $PM_{2.5}$ levels in the Yakima region; Yakima is unusual within Washington in that a significant fraction of the wintertime $PM_{2.5}$ is comprised of particulate nitrate. To understand the atmospheric processes leading to elevated particulate nitrate, researchers at Washington State University and Central Washington University were contracted to complete the Yakima Air Wintertime Nitrate Study (YAWNS).

Observations for YAWNS were completed in the Yakima region during January 2013. The primary measurement site was located in central Yakima on the campus of Yakima Valley Community College. Measurements there included meteorological conditions including surface mixing layer height and stability, trace gas pollutants including CO, NO_x , and VOCs, and the particle size distribution and composition. A secondary site was located in Toppenish at the permanent monitoring site operated by the Yakama Nation. YAWNS measurements at that site included CO and NO_x .

Several periods of elevated PM occurred during YAWNS. The analysis for this report focused largely on two periods with a mesoscale stagnation episode lasting for approximately two weeks in mid-January. During the Clear Sky period, from 10-16 January, the diurnal cycle of the mixing layer followed a typical pattern. A shallow stable surface layer overnight led to the elevated pollution, followed by meteorologically driven dilution each afternoon. This Clear Sky period at night was characterized by elevated levels of both primary (directly-emitted) and secondary (produced chemically in the atmosphere) PM components, including nitrate.

The Clear Sky period was followed by a period of Persistent Cloud, which lasted through 23 January. Unexpectedly, persistent low levels of all primary pollutants, both trace gases and particulate material, characterized this period. Our results indicate that this result was driven by the meteorology; the low-level cloud enhanced surface mixing and increased dilution. However, concentrations of secondary particulate material remained elevated, most notably particulate nitrate.

The elevated particulate nitrate concentrations found in Yakima during winter are driven primarily by three factors: meteorology, and the availability of ammonia and nitrate precursors. The wintertime meteorology of the region drives gas-particle equilibrium of ammonium nitrate strongly toward the particle phase, and high relative humidity conditions enhance this effect. High ammonia emissions from agricultural sources in the area lead to elevated atmospheric concentrations, which drives virtually all available nitric acid into the particulate phase, and results in a condition where any additional nitric acid production would lead directly to greater particulate nitrate levels. The production of particulate nitrate precursors is

complicated and sensitive to the varying meteorological and chemical conditions in the valley. Given the presence of excess gaseous ammonia, there is almost always sufficient reactive nitrogen available to produce elevated levels of particulate nitrate if the right meteorological conditions take hold.

Little evidence was found that pollution in Yakima is significantly impacted from regional transport via the Lower Yakima Valley. While meteorological conditions and PM_{2.5} levels were typically similar at Yakima and Toppenish, the analysis shows clearly that Yakima air quality is dominated by local sources. Though of limited duration, it was found that the YAWNS study period was representative of the typical wintertime meteorology and air quality conditions at Yakima. Furthermore, the air quality in Yakima itself is consistent with other regional cities with a similar mix of emissions sources. In general, when elevated ammonia concentrations from agriculture mix with urban NO_x emissions on humid winter days, elevated particulate nitrate is common.

The YAWNS study has several implications for air quality management in Washington State:

1. Ammonia emissions reductions are unlikely to result in significant reductions in wintertime particulate nitrate unless order-of-magnitude reductions are viable. As it stands, the ammonia levels in winter are high enough that all available nitric acid is driven to particulate nitrate.
2. The pathway to reducing the available nitric acid / particulate nitrate pool is not obvious. Particulate nitrate is the major atmospheric endpoint for NO_x, so

NO_x reductions would reduce the potential particulate nitrate pool. However, NO also inhibits the formation of particulate nitrate by destroying the nitrate radical, which is an important intermediate species. Therefore, it is possible that local NO_x reductions would drive the local atmospheric chemistry toward increased particulate nitrate production. A numerical modeling effort is required to determine the specific system behavior.

3. During persistent cloud conditions, mixing occurs throughout the cloud layer and perhaps beyond, resulting in reduced levels of some pollutants, including primary PM. While a reduction in the relative contribution of wood smoke to organic PM is apparent during burn bans, calling or continuing burn bans during persistent cloud conditions might be less critical than during clear sky stagnation events. However, in addition to reducing exposure to the direct wood smoke emissions, burn bans may also reduce exposure to secondary organic aerosol.
4. The cloud-capped condition is linked to elevated secondary PM levels. Thus the onset of cloud shifts the type of PM present, but elevated concentrations would still be expected to be associated with the meteorological condition.
5. During YAWNS, burn bans appear to have been called at the correct times in Yakima, especially during clear sky and mixed meteorological conditions. It may be possible to adjust responses to anticipate the likely increased mixing associated with persistent low-level cloud. While meteorological models do not reliably predict such cloudy periods, once they set in they are clearly

identifiable. It may be possible to relax policy responses more confidently when persistent cloud is accompanied by slight reductions in observed $PM_{2.5}$ levels.

List of Abbreviations

AGL	Above Ground Level
AIRPACT-4	Air Indicator Report for Public Awareness and Community Tracking- version 4
AMS	Aerosol Mass Spectrometer
BBOA	Biomass Burning Organic Aerosol
CMAQ	Community Multi-Scale Air Quality (model)
CMU	Carnegie Mellon University
CO	Carbon monoxide
CO ₂	Carbon dioxide
CPC	Condensation Particle Counter
CWU	Central Washington University
DMA	Differential Particle Analyzer
D_p	Particle Diameter
EC	Elemental Carbon
EI	Emissions Inventory
elev.	Elevation
EPA	Environmental Protection Agency
EPCRA	The Emergency Planning and Community Right-to-Know Act
equiv.	Equivalent
est.	Estimated
FEM	Federal Equivalent Method
FRM	Federal Reference Method
H ₂ O	Water
H ₃ O ⁺	Hydronium ion
HCHO	Formaldehyde
HCO	Formyl radical
HEPA	High-efficiency particulate absorption (filter)
HNO ₃	Nitric acid
HO ₂	Hydroperoxyl radical
HOA	Hydrocarbon-like Organic Aerosol
HONO	Nitrous acid

HR	High Resolution
HR-AMS	High-Resolution Aerosol Mass Spectrometer
IMPROVE	Interagency Monitoring of Protected Visual Environments (monitoring network)
$K_p(T)$	Partitioning coefficient
Lat	Latitude
Lon	Longitude
lpm	Liters per minute
M	A generic molecule in a chemical reaction, typically nitrogen or oxygen in air
m/z	Mass-to-charge ratio
MACL	Mobile Atmospheric Chemistry Laboratory
meas.	Measured
MOVES	Motor Vehicle Emission Simulator
MS	Mass Spectral
N_2O_5	Dinitrogen pentoxide
NEMA	National Electrical Manufacturers Association
NH_3	Ammonia
NH_4^+	Ammonium ion
$(NH_4)_2SO_4$	Ammonium sulfate
NH_4NO_3	Ammonium nitrate
NIST	National Institute of Standards and Technology
NO	Nitric oxide
NO_2	Nitrogen dioxide
NO_3	Nitrate radical
NO_3^-	Nitrate ion
NOAA	National Oceanic and Atmospheric Administration
NO_x	Nitrogen oxides (the sum of NO and NO_2)
NO_y	NO_x plus the compounds that result from the oxidation of NO_x
NO_z	The compounds that result from NO_z oxidation (= $NO_y - NO_x$)
N_{tot}	Total particle number concentration
O_2	Oxygen
O_3	Ozone

OH	Hydroxyl radical
OMC	Organic Matter Carbon
OOA	Oxidized Organic Aerosol
PAN	Peroxy acetyl nitrate
PBL	Planetary Boundary Layer
PFA	Perfluoroalkoxy alkanes (polymer)
PM	Particulate Mass
PM _{2.5}	Fine Particulate Mass (particles smaller than 2.5 µm)
PMF	Positive Matrix Factorization
ppbv	Parts per billion by volume
ppmv	Parts per million by volume
pptv	Parts per trillion by volume
PSL	Polystyrene latex (polymer)
PST	Pacific Standard Time
PTOF	Particle Time-of-Flight
PTR-MS	Proton Transfer Reaction Mass Spectrometer
QA	Quality Assurance
QC	Quality Control
RCW	Regulatory Code of Washington
RH	Relative Humidity
SMPS	Scanning Mobility Particle Sizer
SO ₄ ²⁻	Sulfate ion
SP2	Single Particle Soot Photometer
Td	Townsend (unit of measure for the ratio of electric field strength to molecular concentration)
UMR	Unit Mass Resolution
USDA	United States Department of Agriculture
VOCs	Volatile Organic Compounds
WRF	Weather Research and Forecasting (model)
WSDA	Washington State Department of Agriculture
WSU	Washington State University
WXT	Weather transmitter

YAWNS

Yakima Air Wintertime Nitrate Study

YRCAA

Yakima Regional Clean Air Authority

YVCC

Yakima Valley Community College

Table of Contents

1. INTRODUCTION	15
1.1. CONTROL OF WOOD SMOKE EMISSIONS	18
1.2. PARTICULATE NITRATE	20
2. PROJECT OBJECTIVES AND TASKS	24
3. REPORT FORMAT	27
4. STUDY CONDITIONS	28
4.1. SITE DESCRIPTIONS	28
4.1.1. YAKIMA SITE	29
4.1.2. TOPPENISH SITE	31
4.2. ATMOSPHERIC CONDITIONS DURING YAWNS	32
5. INSTRUMENTATION	35
5.1. PARTICLE INSTRUMENTATION	36
5.1.1. AEROSOL INLET	36
5.1.2. CONDENSATION PARTICLE COUNTER (CPC)	36
5.1.3. SCANNING MOBILITY PARTICLE SIZER (SMPS)	37
5.1.4. HIGH-RESOLUTION AEROSOL MASS SPECTROMETER (HR-AMS)	38
5.1.5. SINGLE-PARTICLE SOOT PHOTOMETER (SP2)	39
5.2. TRACE GAS INSTRUMENTATION	40
5.2.1. GAS PHASE INSTRUMENTATION INLET	40
5.2.2. NO _x /NO _y ANALYZER	40
5.2.3. AEROLASER VACUUM UV CARBON MONOXIDE ANALYZER	41
5.2.4. PROTON TRANSFER REACTION MASS SPECTROMETER (PTR-MS)	42
5.2.5. AMMONIA (NH ₃) DENUDER SAMPLER	44
5.2.6. CO ₂ AND H ₂ O ANALYZER	45
5.2.7. OZONE MONITOR	46
5.3. METEOROLOGICAL INSTRUMENTS	46
5.3.1. CEILOMETER	46
5.3.2. WEATHER STATION	47
5.3.3. FLUX TOWER MEASUREMENTS	47
5.4. TOPPENISH MEASUREMENTS	48
5.5. EXISTING MEASUREMENTS IN THE AREA	49
6. DATA	50
6.1. DATA QUALITY	50
6.2. TIME SERIES	52
7. POSITIVE MATRIX FACTORIZATION OF PM ORGANIC COMPOSITION	58
8. METEOROLOGICAL AND CHEMICAL DRIVERS OF PM LEVELS	63
8.1. CLASSIFICATION OF STUDY PERIODS	63
8.2. COMPARISON OF CLEAR SKY AND PERSISTENT CLOUD PERIODS	65

8.3. NEUTRALIZATION STATE OF MAJOR PARTICULATE INORGANIC IONS	76
8.4. POTENTIAL CAUSES OF OBSERVED PARTICULATE NITRATE LEVELS AT YAKIMA	79
8.5. PARTICULATE NITRATE FORMATION MECHANISMS	84
8.6. MIXED METEOROLOGY PERIOD	93
8.7. SOURCES OF NO_x	96
8.8. SOURCES OF AMMONIA	98
8.9. INTERVALLEY POLLUTION TRANSPORT	102
8.10. REPRESENTATIVENESS OF RESULTS	107
<u>9. SUMMARY AND FUTURE PLANS</u>	<u>111</u>
9.1. AIR QUALITY MANAGEMENT IMPLICATIONS	113
9.2. RECOMMENDATIONS FOR ADDITIONAL STUDY	114
<u>10. REFERENCES</u>	<u>117</u>
<u>11. APPENDICES</u>	<u>121</u>
11.1. SMPS OPERATION AND CALIBRATION	121
11.2. HR-AMS OPERATION AND DATA ANALYSIS	124
11.3. NO_x/NO_y ANALYZER OPERATION AND CALIBRATION	133
11.4. AEROLASER VUV CO INSTRUMENT OPERATION AND CALIBRATION	141
11.5. PTR-MS OPERATION AND CALIBRATION	144
11.6. AMMONIA DENUDER PREPARATION	148
11.7. AMMONIA DENUDER ANALYSIS	150

1. Introduction

Fine atmospheric particles, those having diameters of $2.5\ \mu\text{m}$ ($\text{PM}_{2.5}$), have demonstrable adverse impacts on human health (Pope et al., 2002). These impacts are primarily cardio-respiratory in nature. A major study released in *The Lancet* in 2012 determined that fine particulates were among the leading risk factors contributing to global burden of human disease (Lim et al., 2012). Both household air pollution from solid fuels and ambient PM pollution were in the top ten risk factors, ranking at #2 and #8, respectively. To avoid these adverse health impacts, under the authority of the Clean Air Act, the U.S. Environmental Protection Agency has instituted a National Ambient Air Quality Standard for $\text{PM}_{2.5}$. Currently the primary standard for ambient $\text{PM}_{2.5}$ is a $35\ \mu\text{g m}^{-3}$ mean concentration over an 24-hour period (US EPA, 2013b). If the three-year average of the 98th percentile for daily $\text{PM}_{2.5}$ concentrations exceeds that limit, then a region is classified as being in non-attainment of the $\text{PM}_{2.5}$ standard. Such a classification carries substantial regulatory requirements.

In urban areas and especially in warmer climates, summertime air pollution associated with photochemical smog is the main concern with respect to particulate air pollution. However, in cooler climates and especially in populated areas with valley topography, the worst particulate air pollution is usually associated with wintertime stagnation conditions. Stagnant conditions result from a combination of meteorological and topographic factors. Typically the stagnation occurs under large-scale high pressure systems including subsidence (downward atmospheric motion),

clear skies, and low surface wind speeds. During the wintertime in the absence of strong solar heating of the surface, the planetary boundary layer (PBL) is shallow with minimal vertical mixing. At night under clear skies, a strong surface temperature inversion can occur and, with snow-covered surfaces, this can extend through the daylight hours. Dilution of pollutants is dampened and high pollutant concentrations are often observed. This phenomenon is exacerbated by valley topography where cold air pooling can occur. Thus stagnant conditions within valleys can lead to exceptionally high pollution levels. Such wintertime valley stagnation events have been studied previously in Idaho's Treasure Valley (Kuhns et al., 2003; Stockwell et al., 2003), in the Cache Valley in Utah (Silva et al., 2007), and in the Chamonix Valley in France (Chazette et al., 2005).

Currently, the Yakima region in Washington is in attainment for $PM_{2.5}$. However there had been an upward trend in $PM_{2.5}$ in recent years, primarily during winter, and for a time a nonattainment classification was considered a possibility. Values have since dropped, but nonetheless the Washington Department of Ecology desired a more complete understanding of the conditions that led to elevated $PM_{2.5}$ levels in the Yakima region. To achieve this goal, they contracted with researchers at Washington State University in Pullman (WSU) and at Central Washington University in Ellensburg (CWU) to complete the Yakima Air Wintertime Nitrate Study (YAWNS). The major focus of YAWNS was an intensive observation period in the Yakima region during January 2013. The resulting data were analyzed during the rest of 2013. This report describes the data and the resulting analysis.

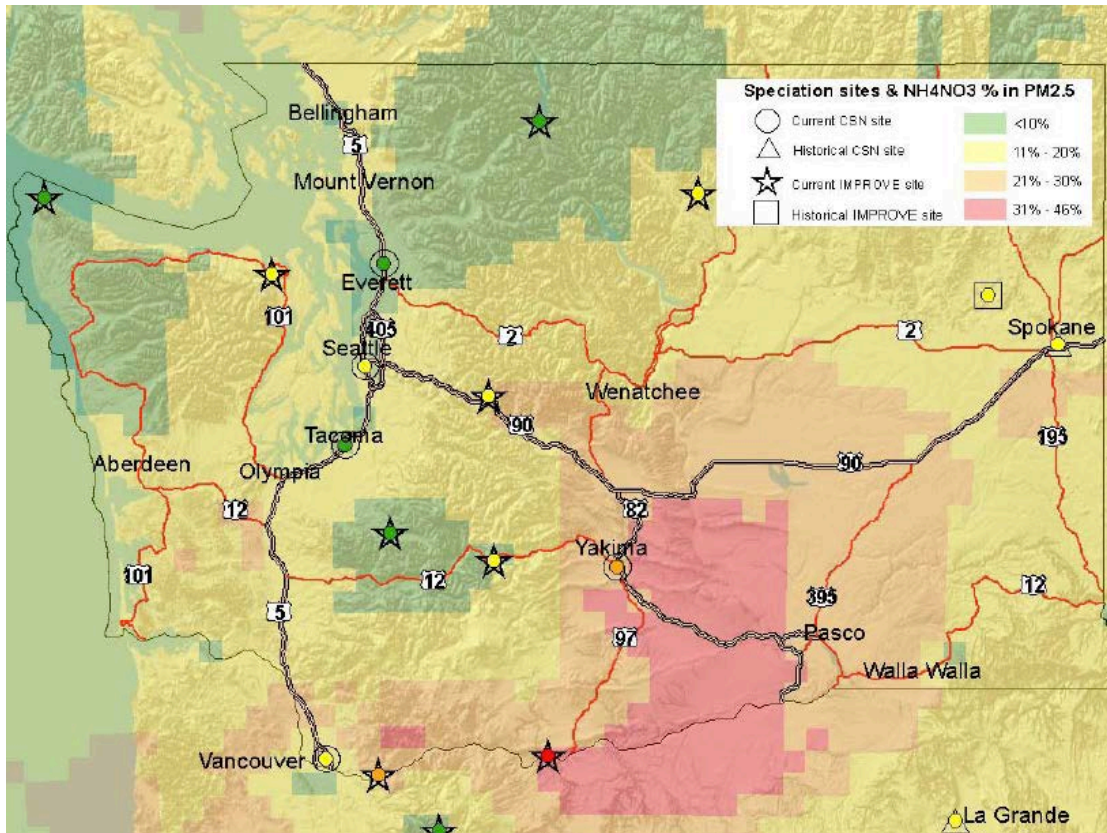


Figure 1.1. Contribution of ammonium nitrate (NH_4NO_3) to total $\text{PM}_{2.5}$ in Washington. Map is based on measured aerosol speciation data collected through 2009, spatially interpolated with CMAQ-modeled data at a 12km resolution. Map created and provided by Dr. Ranil Dhammapala, Washington Department of Ecology.

Yakima is unusual within Washington in that a significant fraction of the $\text{PM}_{2.5}$ during winter is comprised of particulate nitrate, usually in the chemical form of ammonium nitrate (NH_4NO_3). Particulate nitrate makes up a larger fraction of $\text{PM}_{2.5}$ in Yakima and south central Washington than it does anywhere else in the state (Figure 1.1). Nitrate levels are especially important during episodes of high $\text{PM}_{2.5}$. Figure 1.2 shows the fractional contribution of ammonium nitrate to total $\text{PM}_{2.5}$ on days representing the 75th percentile (in terms of $\text{PM}_{2.5}$ mass load) during the heating season, in Yakima. The contribution of ammonium nitrate varied year by

year, but was always 15-25% of the total PM_{2.5} on these days with elevated particulate pollution.

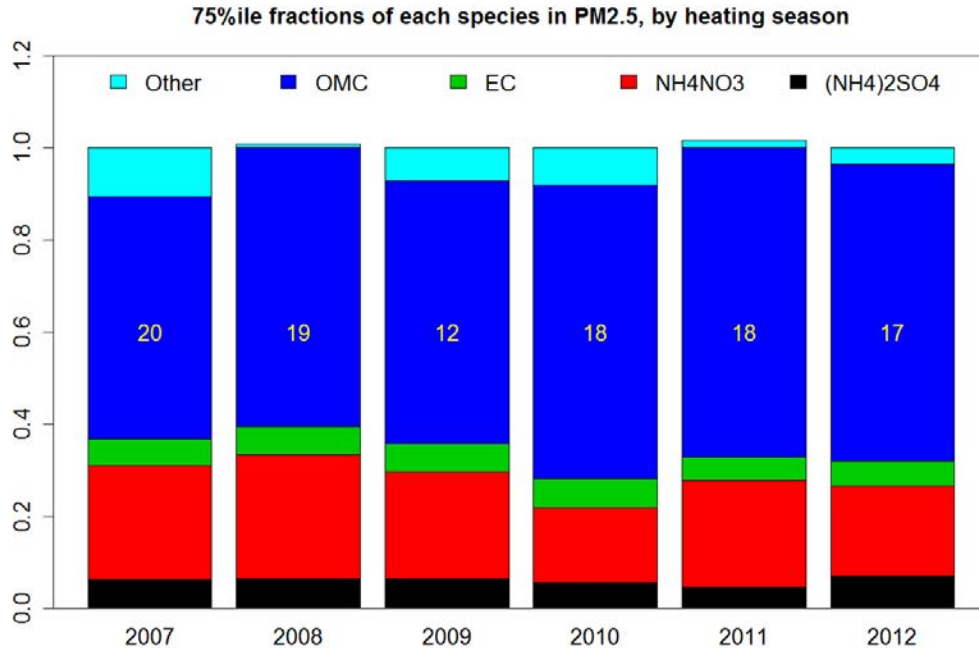


Figure 1.2. Fractional contribution of major chemical constituents to PM_{2.5} on elevated particulate pollution days during the heating season in Yakima. The data shown represent the 75th percentile in PM_{2.5} concentration for each year's heating season when speciation data are available. Numbers on each bar indicate the PM_{2.5} mass measured at the 75th percentile for each year. (NH₄)₂SO₄ is ammonium sulfate; NH₄NO₃ is ammonium nitrate, EC is elemental carbon (i.e., soot); and OMC is organic matter carbon. Figure created and provided by Dr. Ranil Dhammapala, Washington Department of Ecology.

1.1. Control of Wood Smoke Emissions

The dominant component of wintertime PM_{2.5} in Yakima is organic matter. At present, the primary strategy employed in Washington to reduce PM_{2.5} during wintertime is to control the emissions from biomass burning, including burning wood for home heating and outdoor burning of yard debris and orchard tearouts. This is the case in the Yakima region as well. The Yakima Regional Clean Air Agency (YRCAA) has a successful wood stove exchange that provides financial incentives to encourage residents to exchange older, dirtier, less efficient wood stoves for less

polluting certified models. In addition, during periods when PM_{2.5} levels are expected to reach unhealthy level, air quality managers can implement burn bans. These bans can be either a Stage 1 or Stage 2 level.

During a Stage 1 burn ban:

- 1) No burning is allowed in fireplaces and uncertified wood stoves, unless it is your only adequate source of heat. This includes the use of manufactured logs such as Duraflame or Javalogs.
- 2) Pellet stoves, EPA-certified wood stoves and natural gas or propane fireplaces may be used.
- 3) No visible smoke is allowed from any solid fuel burning devices, beyond a 20 minute start-up period.

During a Stage 2 burn ban:

- 1) No burning is allowed in any fireplace, pellet stove or wood stove (certified or not), unless it is your only adequate source of heat.
- 2) Natural gas or propane stoves and fireplaces may be used.
- 3) No visible smoke is allowed from any solid fuel-burning device at any time.

All outdoor burning is prohibited during a burn ban, even in areas where otherwise permitted by law (RCW 70.94.473).

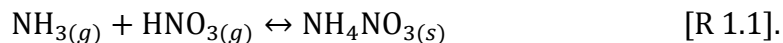
While burn bans have proven effective as a means of reducing particulate pollution levels and avoiding adverse health effects on occasion (Washington

Department of Ecology, 2011), there remain implementation challenges and questions as to their effectiveness.

1.2. Particulate Nitrate

The presence of elevated nitrate in PM_{2.5} during wintertime in the Yakima region provides an additional target for control strategies, potentially complementing the strategies in place to control PM_{2.5} from wood smoke. Evaluating this possibility requires first obtaining an improved understanding of the sources and chemical transformations that lead to the presence of elevated nitrate in the region's PM_{2.5}. Gaining that understanding is the primary motivation for the YAWNS project and for this report. An additional motivation is to provide a more general characterization of the atmospheric environment of the Yakima region during winter and describe how emissions, atmospheric chemistry, and meteorology interact to drive the PM_{2.5} observed.

Particulate nitrate exists primarily as ammonium nitrate (NH₄NO₃), either as a solid or dissolved as part of an aqueous solution. A good review of the atmospheric chemistry leading to ammonium nitrate formation can be found in Seinfeld and Pandis (2006). In the absence of water or other species, ammonium nitrate in the particle phase exists in equilibrium with gas-phase nitric acid (HNO₃) and ammonia (NH₃):



When only these species are present, then the equilibrium can be straightforwardly described using an equilibrium constant $K_p(T)$, which is equal to the product of the

gas-phase ammonia and nitric acid partial pressures. If the product of the gas-phase HNO_3 and NH_3 concentrations is less than the value of the equilibrium constant then no particulate nitrate will condense. Once the gas phase is saturated with ammonia and nitric acid, any excess must condense into the particle phase to form ammonium nitrate. At wintertime temperatures, the equilibrium is driven strongly toward the condensed phase, meaning that relatively more ammonium nitrate will form in winter than in summer for the same initial gas concentrations.

The introduction of water, sulfate, and organic species, all of which are present in the ambient atmosphere, adds more complexity to the ammonium nitrate formation mechanism. When sufficient water is present, a condensed aqueous phase will form, and ammonium, nitrate, and sulfate will each exist primarily in their ionic forms. Ammonia will condense preferentially with sulfate compounds (which condense irreversibly), so in practical terms all sulfate must be fully neutralized before any ammonia is available to react with nitric acid to form nitrate aerosol. The aqueous phase also affects the equilibration of ammonium nitrate independently—some fraction of the ammonia and nitric acid will condense even if the product of their gas-phase partial pressures is below the value indicated by $K_p(T)$. In these cases, the equilibration calculation is complex enough to usually require a numerical solution.

Ammonia in the atmosphere results mostly from primary agricultural emissions, with smaller contributions from natural sources, biomass burning, and human activities (Seinfeld and Pandis, 2006). In contrast, primary emissions of nitric acid are relatively small. Nitric acid forms in the atmosphere as a result of the

oxidation of NO and NO₂, the major nitrogen oxide species (NO_x). NO_x is released to the atmosphere mostly as a byproduct of fossil fuel and other fuel combustion. There are two major mechanisms for converting NO_x to HNO₃. During daytime, HNO₃ forms from the reaction of NO₂ with photolytically-generated hydroxyl radical:



Here, OH is the hydroxyl radical and M is any third molecule (typically nitrogen or oxygen) that absorbs energy during the reactive collision. At night, OH concentrations are low due to the absence of sunlight but can be formed in other reactions, such those between O₃ and alkenes. In winter months daytime OH concentrations would be low due to reduced ultra-violet photon flux compared to summer. Thus nitric acid production rates from R1.2 would be low and may not be significant in winter. At night, two other chemical reactions are possible to produce particulate nitrate. Both reaction pathways involve the nitrate radical (NO₃, distinct from particulate nitrate). During the day, NO₃ is rapidly photolyzed and thus does not exist at significant concentrations during the day, even in winter. NO₃ is rapidly removed through reaction with NO, so NO₃ chemistry only occurs when NO mixing ratios are suitably low. NO₃ radical is made at night when O₃ reacts with NO₂ and can lead to PM nitrate production through N₂O₅ uptake and subsequent hydrolysis on particles:





Another pathway is reaction of NO_3 radical with aldehydes, such as formaldehyde (HCHO) and acetaldehyde, associated with vehicle emissions:



Together the HNO_3 production mechanisms are the major pathways for removal of NO_x from the atmosphere and the source for particulate nitrate.

2. Project Objectives and Tasks

The motivation for the YAWNS study was the need to determine the causes of the particulate nitrate frequently observed at Yakima during winter. Meeting this goal required obtaining field observation data that could be analyzed to improve current understanding of the sources, meteorological conditions, and atmospheric chemistry that leads to elevated particulate nitrate levels in the region. An additional motivation was to provide a more general characterization of the atmospheric environment in Yakima during winter for comparison with and evaluation of the AIRPACT-4 regional air quality forecast model.

To achieve the project objectives, the YAWNS study was divided into the following major tasks:

- 1) Instrument Calibration and MACL Integration at WSU;
- 2) Field Observations;
- 3) Data Reduction and Validation;
- 4) Data Analysis to Address Project Objectives; and
- 5) Reporting of Results.

Task 1: The equipment listed in Table 5.1 were extensively tested at WSU and CWU and integrated into the MACL trailer for deployment to Yakima. Arrangements were made to allow continuous sampling at the two project sites for a three-week period in January 2013. Data logging capabilities and outputs of each

instrument were finalized at this time, including the required modifications to data acquisition systems. Task 1 was completed on December 31, 2012.

Task 2: Continuous on-site air monitoring operations were conducted in Yakima (5-27 January 2013) and Toppenish (11 December 2012 - 28 January 2013). On-site activities were carried out by WSU and CWU staff with assistance from the Washington Department of Ecology. On-site operations included: 1) inspection of instruments and data from the acquisition systems; 2) periodic performance tests; 3) documentation of instrument, station, and meteorological conditions; 4) preventive and corrective maintenance; and 6) transmission of data and documentation. On-site operations were supported by additional Pullman-based WSU staff; this support included: 1) periodic download and examination of field data; 2) replenishment of consumables and supplies; 3) operations review with field staff; 4) laboratory analysis of collected samples; and 5) site visits as needed for instrument calibration, repair, and maintenance. Uploaded data were assembled into a comprehensive database in preparation for post-study validation. Task 2 was completed on January 28, 2013.

Task 3: Time series and scatterplots for all primary data products were examined to identify outliers. Validation levels were assigned to aid users in assessing the reliability of the data sets for analysis. All validated data was compiled in an organized, secure online data repository available to both WSU and Ecology staff. This was completed by August 30, 2013.

Task 4: Advanced data analysis was conducted to address Ecology's and WSU's major project objectives. This included analyzing correlations among measured chemical and meteorological parameters, assessing the contributions of woodsmoke, describing the stagnation conditions during the study period, and conducting a positive matrix factorization analysis on the PM composition data. This work was completed in part by WSU researchers in Pullman, and in part by Graham VanderSchelden, a WSU graduate student working directly with Ecology staff during the summer of 2013. Data analysis activities within the project scope were completed on February 1, 2014.

Task 5: WSU has prepared this final report summarizing the project activities and data assessment. Summaries of major data analysis activities are provided, but full reports of all post-experiment research are beyond this scope of this report. We anticipate that WSU and Ecology staff will continue to collaborate to produce manuscripts for the peer-reviewed literature as an outcome of the YAWNS, but such efforts are beyond the specific requirements of this project. With the exception of these final manuscripts, final reporting will be complete by February 28, 2014.

3. Report Format

This report is organized into nine major chapters, with references and appendices also included. Chapter 1 of this report introduces the background knowledge to place the YAWNS study in context with other work. Chapter 2 presents the objectives and tasks of the YAWNS project as detailed in our initial work plan. This chapter describes the report format. Chapter 4 describes the study conditions, including discussions of the two YAWNS measurement sites as well as the overall meteorological conditions and the burn ban properties during the study period. Chapter 5 discusses the instrumentation deployed from WSU and CWU, with additional detail provided in the report appendices. Chapter 6 discusses our quality assurance and quality control approach, and also provides basic time series results for most parameters studied during YAWNS. Chapter 7 describes the positive matrix factorization analysis used to derive source factors for the organic PM. Chapter 8 describes our detailed analysis of our collected data, designed to address our primary and secondary motivating questions for the study. Chapter 9 summarizes the reports major findings and outlines expected future research directions for the research team.

4. Study Conditions

The YAWNS field study took place during a three-week period from 5-27 January 2013, based in Yakima, Washington. Yakima is a small city (population 93,101, estimated 2012) located within the Upper Yakima Valley. The valley is bounded by the Cascade Mountains to the immediate west, and by lines of hills to the north and south that eventually merge several miles to the east. The topography forms an enclosed basin at the surface that restricts horizontal air flow within the valley. The Upper Yakima Valley connects to the Lower Yakima Valley via Union Gap, located a few miles south of central Yakima. The Upper Valley also connects to the Wenas Valley to the north of Yakima.

Yakima has a semi-arid climate due largely to its location in the rain shadow of the Cascade Mountains. January is its second wettest month (after December), with 28.7 mm of precipitation falling on average (1981-2010 mean). Mean daily high and low temperatures during January are 38.8 and 23.8 °F, respectively, making it the second coldest month of the year on average (trailing December) (NOAA NOWData, 2013).

4.1. Site Descriptions

To address the study objectives, a primary site was established in central Yakima. The goal at this site was to measure a comprehensive suite of pollutant concentrations and local meteorology at a location that would be representative of the city's air quality. Additional instrumentation was located at an existing air

quality monitoring station at Toppenish. The goal for this secondary site was to evaluate the degree to which Yakima air quality is affected by pollution transported from south central Washington via the lower Yakima Valley. A regional satellite map showing the locations of both sites is provided in Figure 4.1.

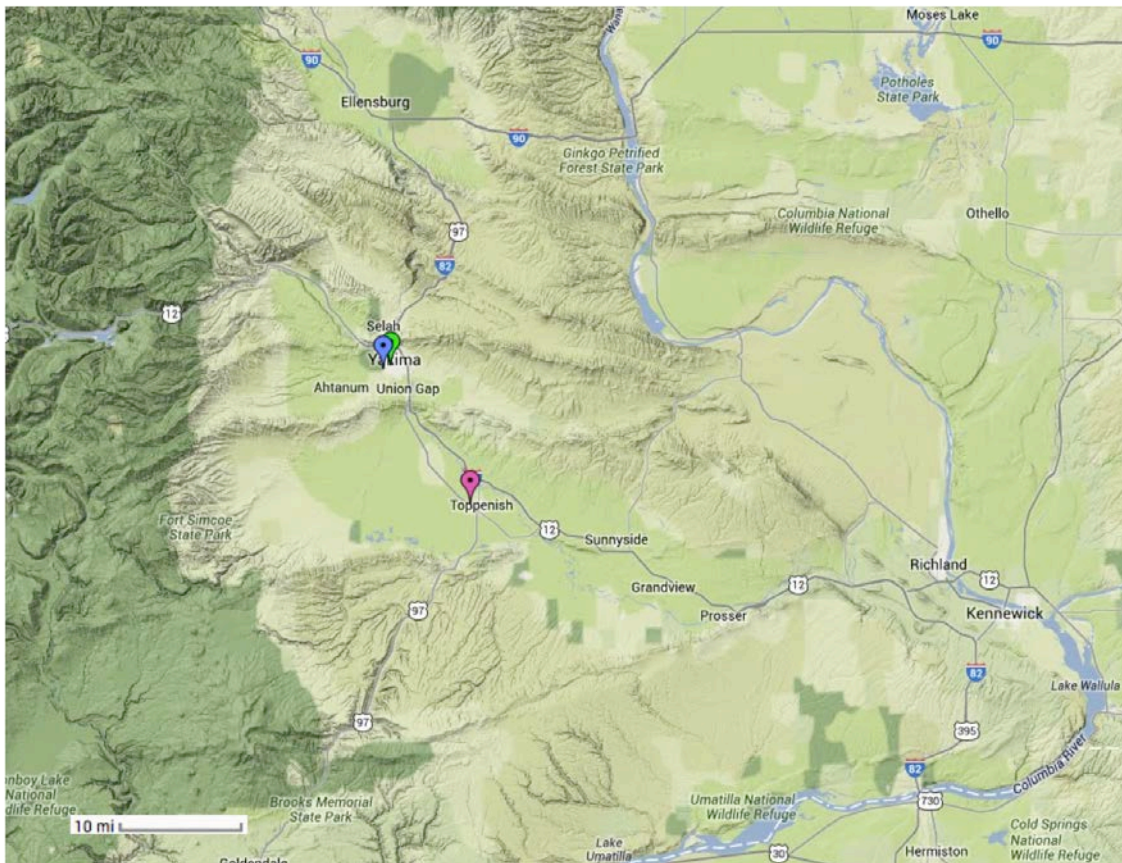


Figure 4.1: Terrain map of the YAWNS study region. The blue marker indicates the YAWNS primary site at Yakima, the pink marker indicates the YAWNS secondary site at Toppenish, and the green marker indicates the Yakima 4th Avenue monitoring site. Image courtesy Google Earth.

4.1.1. Yakima Site

The Washington State University Mobile Atmospheric Chemistry Laboratory (MACL) was deployed to the campus of Yakima Valley Community College (YVCC) (Lat: 46.58854, Lon: -120.5283, Elev. 327 m). The MACL is a 20-foot long climate-controlled trailer designed to facilitate field activities for atmospheric research. The

trailer includes instrument racks, sampling ports, and a 10-m tall crank-up tower for mounting instruments and inlets. In addition to the MACL, a 6-m tall flux-sampling tower with additional instruments was erected in the same open field approximately 20 m south of the MACL trailer. Pictures of the MACL trailer and the flux tower at the YVCC site are shown in Figure 4.2.



Figure 4.2. (left) The WSU Mobile Atmospheric Chemistry Lab (MACL) at the Yakima study site. (right) The flux tower at the Yakima site.

A satellite map showing the location of the MACL on the YVCC campus and the surrounding neighborhood is shown in Figure 4.3. The MACL was located in a baseball field about 40-m south of Arlington Road. This road was used primarily as a parking lot for YVCC students. To the immediate east and west were campus lawn and to the south the buildings of the YVCC campus. The site was far enough from busy roads that local roadway emissions were not a significant factor. There were major roads approximately 150 m west (South 16th Ave) and 400 m south of the site

(Nob Hill Rd). The site was in a medium-density mixed residential and commercial neighborhood approximately 1 km west of the Yakima urban center. There were significant wood smoke emissions from the residential areas around the sampling site due to the use of wood fuels for wintertime home heating.

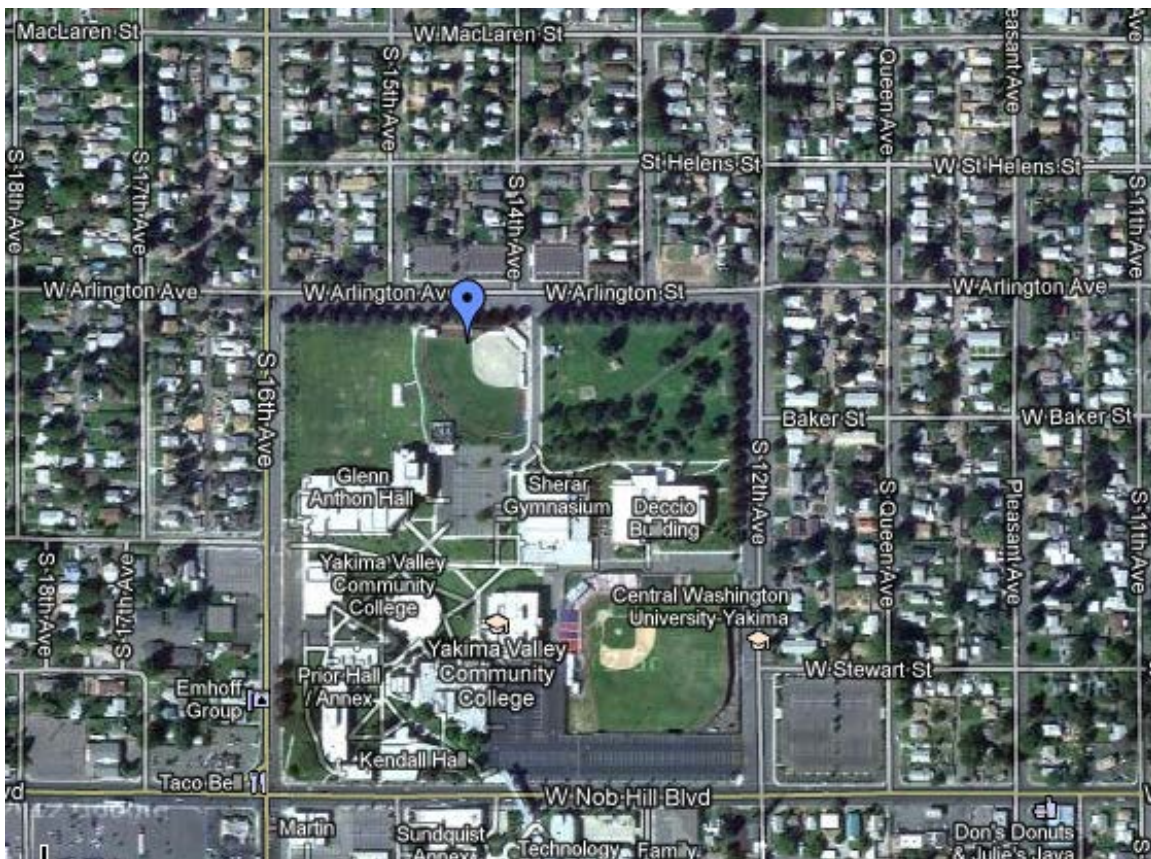


Figure 4.3: Satellite map of the neighborhood surrounding the primary YAWNS site in Yakima. Image courtesy of Google Earth.

4.1.2. Toppenish Site

Additional instruments were installed within the existing air monitoring station operated at Toppenish by the Yakama Nation (Lat: 46.38024, Lon: -120.33266, Elev. 216 m). The location of this site relative to Yakima can be seen in Figure 4.1, and a picture of the site is provided in Figure 4.4. The site is located in an

open field on the campus of Toppenish High School. A major highway, US 97, lies approximately 250 m to the southwest.



Figure 4.4. The air monitoring site at Toppenish operated by the Yakama Nation.

4.2. Atmospheric Conditions During YAWNS

Temperatures in Yakima during January 2013 were close to the long-term averages, with low temperatures during the month averaging 24.1 °F and highs averaging 37.4 °F (NOAA NOWData, 2013). The period was drier than is typical, with only 0.10” of precipitation reported for the month. The second half of the month was characterized by a mesoscale high-pressure event that resulted in strong upper level temperature inversions throughout the region, as confirmed by twice daily temperature soundings at Quillayute on the Washington coast and at Spokane, Washington. This mesoscale event began on 14 January and persisted until 23 January, though it affected different areas of the state in varying magnitudes at different times. In Yakima, the first part of the stagnation period occurred under

clear sky conditions, and the nighttime surface temperature inversions led to significant buildup of PM_{2.5}. Beginning on 16 January the area became cloudy and PM_{2.5} dropped significantly.

Figure 4.5 shows the Federal Equivalent Method (FEM) PM_{2.5} time series during January 2013 measured at the Yakima 4th Avenue monitoring station by the Yakima Regional Clean Air Agency (YRCAA) and at the Toppenish monitoring site operated by the Yakama Nation. Also shown are the periods during which burn bans were implemented in the area. During the month, the 24-hr PM_{2.5} standard (35 µg m⁻³) was exceeded on two occasions, on 15 and 16 January. It approached the standard on 25 January as well. The burn bans implemented during January 2013 reflected the air quality measured in Yakima during those periods. A brief Stage 2 ban was implemented on 7 January, but was removed the next day when a frontal passage cleaned out the valley. A Stage 1 burn ban was implemented on 14 January coinciding with the beginning of the stagnation period. The ban remained in effect until 29 January, changing between Stage 1 and Stage 2 depending on the concentration trend from day to day. The bans covered all areas overseen by YRCAA in the Upper and Lower Yakima Valleys.

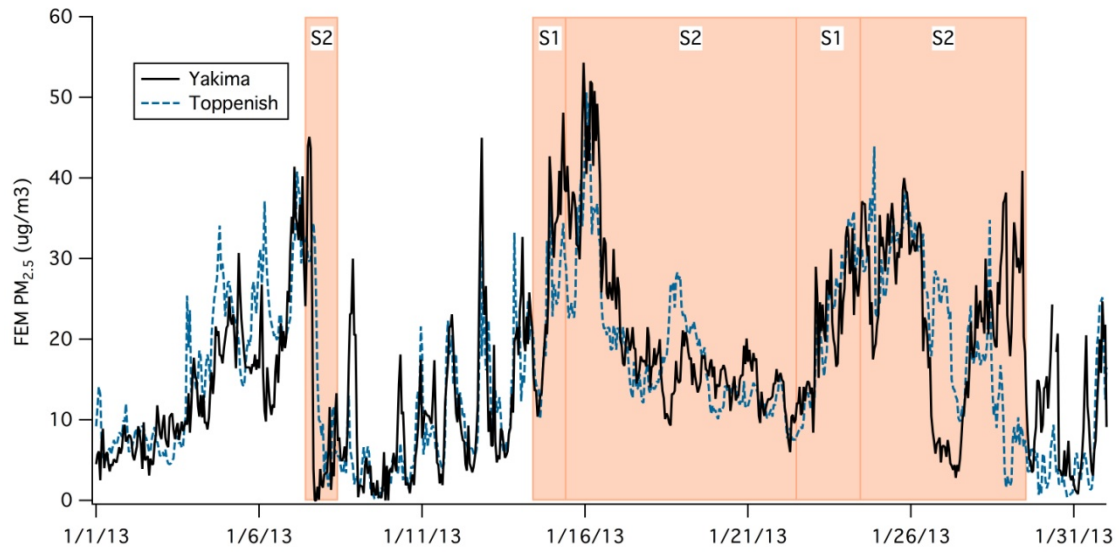


Figure 4.5. Hourly time series PM_{2.5} levels measured at the Yakima 4th Avenue and Toppenish monitoring sites during January 2013. Shaded areas indicate Stage 1 and Stage 2 burn bans, as labeled.

5. Instrumentation

The instruments deployed to Yakima and Toppenish during YAWNS are listed in Table 5.1 below. The table includes a brief description of the measurement, details on the instrument used, and the sampling period for the instrument.

Table 5.1. Summary of YAWNS measurements.

Primary Site in Yakima		
Measurement	Instrument	Sampling Period
NO _x & NO _y	Air Quality Designs dual-channel instrument (NO, NO ₂ , and NO _y)	1 min
NH ₃	Custom ammonia sampler w/ laboratory analysis	8 / 16 hrs
CO	AeroLaser Vacuum UV instrument	1 min
O ₃	Dasibi ozone monitor	1 min
Trace organic gases ⁽¹⁾	Proton Transfer Reaction – Mass Spectrometer (PTR-MS)	1 min
Aerosol number concentration	Condensation Particle Counter (CPC)	1 min
Aerosol composition	High Resolution Aerosol Mass Spectrometer (HR-AMS)	2 min
Aerosol black carbon content	Single Particle Soot Photometer (SP2)	1 min
Particle size distribution (0.020-0.700 μm)	Scanning Mobility Particle Sizer (SMPS)	5 min
PBL Height	Vaisala Ceilometer	30 min
Meteorological data	Vaisala WXT package	1 min
Satellite Site in Toppenish		
Measurement	Instrument	Sampling Period
NO _x	TECO 42 NO _x monitor	1 min
CO	TECO 48 CO monitor	1 min

⁽¹⁾ See Table 5.2 for the list of trace organic species measured.

5.1. Particle Instrumentation

5.1.1. *Aerosol Inlet*

Aerosols were sampled from approximately 7 m above ground level via an inlet mounted to the MACL crank-up tower. Air was pulled through this inlet at a total flow rate of approximately 4 liters per minute (lpm). The inlet line outside was a 0.5" outer diameter copper tube. This tube was hooked downward at the inlet to prevent precipitation from entering the inlet. The inlet line was also wrapped in heating tape and was thermostated to approximately 50 °F; this was done to prevent ice buildup within and around the inlet. Once inside the MACL trailer, the whole aerosol was passed through a Nafion dehumidifier (PermaPure Model MD-110-24S-4). This was done to dry the particles prior to sampling for easier intercomparisons of the different aerosol measurements.

5.1.2. *Condensation Particle Counter (CPC)*

The total particle number concentration (N_{tot}) was monitored using an Ultrafine CPC (Model 3776, TSI Inc., Shoreview, MN). The CPC operates by condensing butanol vapor onto particles such that they grow large enough to be detectable on a single particle basis by laser light scattering. The Model 3776 CPC used during YAWNS has a nominal size cutoff of 2.5 nm. Raw data from the CPC were stored at one-second time intervals via custom control software developed in LabView.

5.1.3. Scanning Mobility Particle Sizer (SMPS)

The particle number size distribution was measured using a custom-built SMPS assembled at WSU. Major components for the SMPS were purchased TSI, Inc. (Shoreview, MN). These included a differential mobility analyzer (DMA; TSI Model 308100) and a CPC (TSI Model 3775). Instrument control was via custom software developed using LabView (National Instruments, Austin, TX). Details on the operation and calibration of the SMPS system during YAWNS are provided in Appendix 11.1. The settings chosen for the study allowed the particle size distribution from 20-800 nm to be measured approximately every five minutes.

In addition to its use for ambient measurements during YAWNS, the SMPS also served as the primary calibration tool for the high-resolution aerosol mass spectrometer (HR-AMS) and the single particle soot photometer (SP2). For these calibrations, a nebulizer system was used to generate a fine mist from a solution or mixture of known composition. The water was next removed using a diffusion dryer, leaving a population of dry calibration particles of known composition. These particles were then size-selected with the DMA component of the SMPS and then split between the CPC component of the SMPS and the instrument to be calibrated. In this way the instrument being calibrated was provided a aerosol sample of known size, composition, and concentration. During these calibration periods, it was not possible to also measure the ambient particle size distribution.

5.1.4. *High-Resolution Aerosol Mass Spectrometer (HR-AMS)*

The composition of non-refractory submicron particulate material was measured using an Aerodyne high-resolution time-of-flight aerosol mass spectrometer (HR-AMS). The HR-AMS allows for the direct separation and measurement of most ions at the same nominal m/z , quantification of organic particulate mass and several inorganic species, and the determination of the size distribution of all ions. The AMS uses automated data analysis routines to classify the peaks in the mass spectrum into a finite number of classes of compounds, including organics, ammonium, sulfate, nitrate, and chloride. The instrument operates in two modes for ion transmission, referred to as V-mode and W-mode. V-mode is a single-reflection configuration allowing for higher sensitivity at somewhat lower resolution, while W-mode is a two-reflection configuration offering a lower sensitivity but higher resolution. In both modes, aerosol particles enter through a sampling inlet at a flow rate of approximately $1.5 \text{ cm}^3 \text{ s}^{-1}$ and are transmitted through an aerodynamic lens that first focuses particles into a narrow beam using six apertures of sequentially decreasing size. This focusing greatly concentrates the particles relative to the surrounding air.

The focused aerosol beam is finally accelerated in a supersonic expansion, caused by the difference in pressure between the sampling and sizing chambers. This acceleration also gives different velocities to aerosols of different sizes. After passing through the lens, the aerosols next pass through a mechanical chopper that can open or close to enter the particle-sizing chamber. At this point the instrument is typically alternated between two modes of operation- mass spectrum (MS) mode

and particle time-of-flight (PTOF) mode. Only MS-mode data are included in this report. In MS mode, particles travel unimpeded through the particle-sizing chamber until they impact onto a resistively-heated porous tungsten surface held at 600 °C where the volatile and semi-volatile portions of the aerosols are vaporized and immediately ionized using 70-eV electron impact ionization. The mass spectrometer detects the positive ion fragments generated by the electron impact ionization and determines the mass-to-charge (m/z) distribution of the particle beam. The HR-AMS detects non-refractory species that can evaporate rapidly at the vaporizer conditions (mostly volatile and semi-volatile components). These include sulfate, nitrate, ammonium, chloride, and total organic matter. Other non-volatile constituents, such as crustal oxides, sea salt, and black carbon, are not detectable. A more detailed description of the measurement approach for the HR-AMS and its operation and calibration during YAWNS is provided in Appendix 11.2.

5.1.5. Single-Particle Soot Photometer (SP2)

The black carbon (BC) mass in individual particles between ~80-650 nm was determined using a Single Particle Soot Photometer (SP2) (Schwarz et al., 2006). The SP2 was adjusted following the recommendations detailed in Laborde et al. (2012), and the incandescence signal was calibrated using fullerene soot particles (Alpha Aesar; #L20W054) that were size selected using a differential mobility analyser. Data analysis was conducted using the Paul Scherrer Institut Toolkit.

5.2. Trace Gas Instrumentation

5.2.1. *Gas Phase Instrumentation Inlet*

Air sample for the gas phase instrumentation was supplied by a common sample line. This sample line consisted of 0.5" outer diameter PFA tubing that was attached to the crank up meteorological tower with the inlet at a height of approximately 10 m, as seen in Figure 4.2. A funnel around the inlet protected the line from ingestion of snow and rain. The tube ran into the trailer and was attached to a diaphragm pump that pulled air through the tube at approximately 30 liters per minute. The gas phase instruments (PTR-MS, O₃, CO, CO₂) sub-sampled from this flow. Instruments were protected from particle contamination by in-line Teflon membrane filters. The NO_x/NO_y analyzer had its own inlet system enclosed in a NEMA enclosure mounted to the meteorological tower approximately 1 m below the aerosol inlet. The NO_x/NO_y inlet system contained a heated molybdenum oxide catalyst for NO_y conversion and a photolysis cell for NO₂ conversion. The sample inlet consisted of a short piece of heated 0.25" outer diameter PFA tubing that protruded approximately 1 inch from beneath the enclosure. The PFA tubing below and within the enclosure was resistively heated and thermostated to 30 °C to prevent loss of nitric acid.

5.2.2. *NO_x/NO_y Analyzer*

NO, NO₂, and NO_y were measured using a two-channel chemiluminescence NO detector (Air Quality Design). NO_y was measured continuously on one channel by conversion to NO with a molybdenum oxide catalytic converter. The other

channel measured NO for 30 seconds then NO_x (NO + NO₂) for 30 seconds in an alternating cycle. NO₂ was photolyzed to NO via a blue light converter. The difference between the measured NO_x and NO was reported as NO₂. NO_y is defined as NO_x plus the compounds that result from the oxidation of NO_x. This includes but is not limited to: NO₃, N₂O₅, HNO₃, HONO, PAN, organic nitrates, and particulate nitrate. The instrument response time to NO for both channels is less than 1 second. Data were recorded at 1 Hz and reported at 1-minute intervals. Instrument sensitivity was determined using an NO calibration gas of 500 ppmv ± 1%, NIST traceable, (Scott-Marrin, Inc.) diluted in dry zero air to provide a 250 ppbV NO calibration level. Calibration of the NO₂ converter efficiency was performed using gas phase titration of NO to NO₂. A detailed description of the measurement approach for the NO_x/NO_y analyzer and its operation and calibration during YAWNS is provided in Appendix 11.3.

5.2.3. Aerolaser Vacuum UV Carbon Monoxide Analyzer

Carbon monoxide (CO) was measured using a vacuum UV fluorescence instrument (Aerolaser GmbH, Germany). The instrument allows fast response and sensitive measurements of CO; the response time is approximately 1 second and the detection limit is approximately 50 pptv. The instrument was calibrated by standard addition whereby a low flow of a 101.6 ppmv ± 1% NIST traceable standard (Scott Marrin) was added to the sample air every 4 hours for approximately 1 minute to keep track of potential sensitivity drifts. Background response to zero air was determined by passing ambient air through a CO

destruction catalyst. Data were collected at 1 Hz and reported as 1 minute averages. A detailed description of the calibration and data reduction procedures for the CO measurement can be found in Appendix 11.4.

5.2.4. Proton Transfer Reaction Mass Spectrometer (PTR-MS)

VOC measurements were made using a PTR-MS instrument (Ionicon Analytik, GmbH, Austria). The PTR-MS continuously measures organics in air by chemical ionization using H_3O^+ as a proton transfer reagent ion. The method has been well described in literature (Lindinger et al., 1998). Organic compounds with proton affinities greater than that of water undergo fast proton transfer reactions with H_3O^+ :



where R is the organic compound and RH^+ is the product ion (M+1 ion). The ions were detected with a quadrupole mass spectrometer. Compounds of interest in urban atmospheres that can be measured with this approach include aromatic compounds such as benzene and toluene, simple alcohols (methanol and ethanol) and aldehydes (formaldehyde, acetaldehyde). The instrument is insensitive to small alkanes, acetylene, and ethylene. For monoaromatic compounds that have geometric isomers, such as the xylene isomers and ethylbenzene, the sum total of these compounds is reported.

The proton transfer reaction occurs in an ion drift tube that enhances the kinetic energy of the ions so that collisions with the bath gas (air) cause desolvation of hydrated ions. For many compounds, R5.1 is dissociative at the kinetic energies

required for efficient desolvation, resulting in the formation of fragment ions that complicate the interpretation of the PTR-MS mass spectrum as a simple M+1 mass spectrum. To mitigate this problem the PTR-MS was operated at a lower drift tube electric field, which requires sample drying. For the YAWNS field campaign, the sampled air was dehumidified to -30 °C using a cold trap, allowing for the operation of the PTR-MS drift tube at 80 Td (Jobson and McCoskey, 2010). Operation at 80 Td (drift pressure 2.08 mbar, drift temperature 65 °C, drift voltage 327 V) allowed for measurement of formaldehyde and significantly reduced fragmentation, improving accuracy in the measurement of aromatic compounds. The PTR-MS was calibrated by diluting a multi-component gas standard containing 13 compounds at 2 ppmv ± 5% (Scott Marrin) with humidified zero air to 19.8 ppbv. Formaldehyde sensitivity was calibrated using a permeation tube (KinTek). A more detailed discussion of the PTR-MS operation and calibration during YAWNS is presented in Appendix 11.5.

The PTR-MS performed full mass scans (m/z 31-150) 5-8 January. After 8 January, a suite of 45 organic ions was measured and data for 10 of these ions are reported. For these 10 ions, we have confidence in their compound attribution and PTR-MS sensitivity factors, and these data were well above compound detection limits. These compounds are listed in Table 5.2. The mass spectrometer measures each mass for a specified dwell time (1-5 seconds), and cycled through the list of 45 ions every minute. Data are thus reported every minute but should not be construed as 1-minute averages.

Table 5.2. Trace organic gases species measured by PTR-MS.

Ion Mass (m/z)	Compound Attribution	Notes
31	Formaldehyde	Air toxic / direct emissions / photoproduct
33	Methanol	Solvents
42	Acetonitrile	Wood smoke tracer
45	Acetaldehyde	Air toxic / photochemical product
47	Ethanol	Vehicle emissions
59	Acetone	Solvents
79	Benzene	Air toxic / vehicle emissions
93	Toluene	Vehicle emissions
107	C ₂ benzenes (C ₈ H ₁₀)	Vehicle emissions
121	C ₃ benzenes (C ₉ H ₁₂)	Vehicle emissions

After 10 January, the PTR-MS also performed grab sampling onto a Tenax trap for direct thermal desorption into the PTR-MS drift tube as described in Erickson et al. (2014). This sampling approach was an experiment to better measure higher molecular weight organic compounds associated with diesel engine exhaust. Every 30 minutes, the Tenax trap was desorbed for approximately 5 minutes. For this reason, data gaps exist in the VOC record when thermal desorption analysis was being performed. These thermal desorption data will not be reported for YAWNS as we are still learning how to interpret the measurements.

5.2.5. Ammonia (NH₃) Denuder Sampler

Ammonia was sampled using a ChemComb Speciation Sampling Cartridge (Thermo Scientific, Franklin, MA). Ammonia sampling began on 16 January and continued until the end of the study. There were some additional sampling gaps in that period due to unavailability of denuders. Prior to use, the 47 mm honeycomb denuders were prepared according to established procedures described in

Appendix 11.6. Briefly, the denuders were coated with 10 mL of a solution that contained 1% phosphoric acid and 10% methanol. Denuders were prepared in Pullman and then transported overnight to Yakima for use. Just prior to sampling, the denuders were placed in the cartridge samplers that were mounted on a fence approximately 10 m from the MACL trailer. Samples were collected by drawing air through the cartridge at a flow rate of 10 L per min. Typically two samples were collected per day– one 8-hr sample beginning at 09:00 and one 16-hr sample beginning at 17:00. After sampling, denuders were removed from the sampling cartridges and returned to Pullman for analysis. Analysis procedures are described in Appendix 11.7. Briefly, ammonia was eluted from the denuders with 10 mL of deionized water. Ammonia concentrations were then determined spectrophotometrically with the Nitrogen-Ammonia Reagent Set, TNT, AmVer™(Salicylate), Low Range kit (Hach Company, Loveland, CO) according to manufacturer's instructions. These solution concentrations the total mass collected per sample, which was then converted to a mean atmospheric concentration during the sample period. These concentrations were corrected to remove the small artifacts found on blank denuders analyzed as a control.

5.2.6. CO₂ and H₂O Analyzer

Carbon dioxide and water vapor were measured by a LiCor 840A analyzer. Factory response factors were used for the determination of CO₂ and water vapor mixing ratios. Instrument performance for CO₂ was verified by measuring a

calibration tank containing 390 ppmv CO₂ ± 1 % (Scott Marrin). Data were recorded at 1 Hz and one-minute averages were reported.

5.2.7. Ozone Monitor

Ozone was measured by UV absorption using a Daisibi 1008 monitor. This instrument was calibrated against a dedicated secondary O₃ standard instrument owned by WSU. One-minute averages were reported.

5.3. Meteorological Instruments

5.3.1. Ceilometer

Atmospheric planetary boundary layer (PBL) heights and cloud base heights were detected using a ceilometer (model CL31, Vaisala). This instrument measures the optical backscatter intensity of light emitted in the near-infrared (wavelength = 910 nm). During YAWNS, the ceilometer was set to report vertical profiles from zero to 4,500 m above ground level every 16 s, with a vertical resolution of 10 m.

Structures present in the backscatter retrieval (up to three cloud base heights and three PBL heights) were identified using the Vaisala PBL height algorithm (version 3.5), which is the default setting in Vaisala BL-VIEW software and is based on the gradient method (Vaisala, Inc., 2010). This method selects the maximum of the negative gradient of the backscatter coefficient to be the top of the PBL. Individual measurements were averaged over a 30-minute period for our analysis.

5.3.2. Weather Station

Two weather stations were deployed to the YAWNS site at Yakima. One, a model WXT510 (Vaisala, Inc.) was mounted at 10 m atop the MACL's crank-up tower. The other, a model WXT520 (Vaisala Inc), was mounted about 6 m above the ground on the flux-sampling tower. Both stations measured wind speed, wind direction, air temperature, relative humidity, and atmospheric pressure. Unless otherwise indicated, the weather data discussed in this report are from the WXT510 mounted on the MACL tower.

5.3.3. Flux Tower Measurements

Surface energy fluxes were measured using two eddy covariance systems installed at 2.12 and 4.17 m above ground level on a 6-m tall aluminum flux-sampling tower. Data from the flux tower were available beginning at 16:00 on 14 January and ending at 17:00 on 26 January. Each eddy covariance system consisted of a three-dimensional sonic anemometer (CSAT3, Campbell Scientific, Inc.) and an open-path carbon dioxide/water vapor (CO₂/H₂O) infrared gas analyzer (IRGA; model LI 7500a, LI-COR, Inc.). Sensor signals from the eddy covariance systems were recorded at 10 Hz using a datalogger (model CR5000, Campbell Scientific, Inc.). The 10 Hz raw time-series data collected in this study were processed and corrected to obtain eddy covariance fluxes by using a post-field data processing program. Briefly, the virtual air temperature was converted to air temperature following the procedure suggested by Campbell Scientific Inc.'s instruction manual (2006). The raw 10 Hz time series data were checked for noise using the criterion that data with

automatic gain control (AGC) values (output from the LICOR 7500 sensor) greater than 65 were removed. Data points were labeled as spikes when their magnitudes exceeded 4.5 times the standard deviation in a running 600-point window. If the number of continuous points meeting the spike criterion was less than four, then these values would be replaced through linear interpolation; longer duration events were not labeled as spikes. The planar fit method was used for coordinate system transformation. Fluxes were then computed using a block average method. Sensible and latent heat fluxes were obtained via 30-min mean covariance between vertical velocity and the respective air temperature and water vapor density fluctuations. Due to air density effects, latent heat flux was corrected according to the Webb Pearman and Leuning (WPL) corrections (Webb et al., 1980).

Besides the eddy covariance measurements, a variety of micrometeorological variables were measured as 30-minute averages of 1 s readings, including net radiation (model CNR1, Kipp & Zonen Inc.), temperature and relative humidity (model HMP45C, Vaisala Inc.), wind speed and direction (mode 03002, R.M. Young Inc.), and soil temperature (model 109SS-L, Campbell Scientific, Inc.).

5.4. Toppenish Measurements

Carbon monoxide and NO and NO_x were measured at the Toppenish site using a TECO 48 monitor for CO and a TECO 42 monitor for NO and NO_x. Instruments were calibrated using the same standard gases used for the Yakima site instruments before installation. Data was logged to a dedicated laptop as well as to the Washington Department of Ecology telemetry system. The CO instrument had an automatic zero cycle whereby ambient air was pulled through a destruction catalyst

(Sofnocat 514, Molecular Products). Air was sampled through a ¼” PFA Teflon sample line with the inlet approximately 12 feet above the ground.

5.5. Existing measurements in the area

The instruments described in Sections 5.1 through 5.4 were installed for the duration of the YAWNS study. Additionally, data from existing sites in the area were leveraged for this study as required (Table 5.3). In addition, there are several meteorological sites in the Yakima area operated by various entities.

Table 5.3. Routine monitoring in the YAWNS study region.

Sampler	South 4th Ave, Yakima	Toppenish (co-located w/ YAWNS site)	Sampling Frequency
Continuous PM _{2.5} Mass	FEM	Correlated Nephelometer	Hourly
PM _{2.5} Gravimetric Samplers	1-in-3 FRM & Aerosol Speciation	-	Daily (Every 3rd Day)
Meteorological Parameters	-	Wind speed, direction, & temperature	Hourly

6. Data

6.1. Data Quality

Each instrument described in Section 5 was evaluated separately for data quality assurance. After processing, the data were carefully scrutinized and compared against the instrument logs to ensure that data collected when instruments did not meet operational specifications were removed from the final results. Next, for ease of comparison, all data were average to a uniform 30-minute time series. These time series begin at 00:00 on 5 January and end at 12:00 on 27 January 2013. The time-averaged data have been provided directly to Washington Department of Ecology via a shared directory on a internet cloud storage site. Data in these series are provided as the 30-minute data average for each time step, the standard deviation, and a data flag. The standard deviation in the time series is primarily a reflection of the time variability of the measured parameter over an individual 30-minute period. Toppenish data are available for a longer time period, from 12:00 on 11 December 2012 to 10:00 on 28 January 2013.

Data in the averaged time series were flagged to indicate the data completeness within each 30-minute period. Periods with 5% data completion or less were flagged “Little or No Data”; periods with 5-50% data completeness were flagged as “Majority Missing Data”; periods with 50-95% completeness were flagged as “Some Missing Data”; and data with more the 95% is flagged as “Complete Data”. The completeness summary for all major parameters is presented in Table 6.1 below. There are two special cases for reporting data completion. For the ceilometer,

recorded data almost continuously for during the study, but only reported the boundary layer and cloud base heights when specific criteria were met in the instrument’s analysis software. The data completion statistics indicate how frequently these criteria were met so that results were reported. For the SMPS, evidence of a small system leak was discovered in the post-study data analysis. Only portions of the data set were affected. The leak had only a trivial effect on the particle number size distribution, but affected the volume distribution more strongly. The impacted periods are flagged separately in the archived data, but in Table 6.1 these periods are included in the “Complete Data” category.

Table 6.1. Data completion statistics for the YAWNS.

Measurement	Little or No Data	Majority Missing Data	Some Missing Data	Complete Data
CPC	6.9	0.6	3.1	89.2
SMPS	19.1	0.0	0.7	80.2*
HR-AMS	28.6	0.6	1.2	69.6
SP2	25.9	0.1	0.4	73.6
NO _x /NO _y	4.6	0.7	6.2	88.4
CO	3.6	0.4	14.7	81.3
PTR-MS	8.3	2.5	7.8	81.4
CO ₂	1.6	0.2	1.6	96.7
Ozone	7.1	0.3	0.8	91.8
WXT (MACL)	6.6	0.2	0.8	92.4
Ceilometer [#]				
-PBL Ht	35.9	10.3	9.1	44.6
-Cloud Base	25.0	4.7	4.8	65.5
Flux Tower ⁺	46.5	N/A	N/A	53.5
Toppenish CO	10.4	0.4	9.3	79.9
Toppenish NO _x	5.7	0.1	0.3	94.0

* This entry is the sum of two flag categories. 53.5% of the SMPS data passed all QA/QC checks. 26.7% of the data showed evidence of a small leak in the system. This leak did not significantly affect the number size distribution or total number concentration, but there was a significant impact on the volume distribution.

The ceilometer was operational and producing data for nearly the entire study. Here, the data completion statistics refer to the output of the instrument’s algorithm for calculating the boundary layer and cloud base heights.

+ The flux tower data are only reported when the analysis criteria are met for a given 30-minute period. Thus data are either complete or fully missing.

6.2. Time Series

Time series plots of the major parameters measured during YAWNS are shown in Figures 6.1 to 6.12 below. Analysis of the data follows in sections 7 and 8.

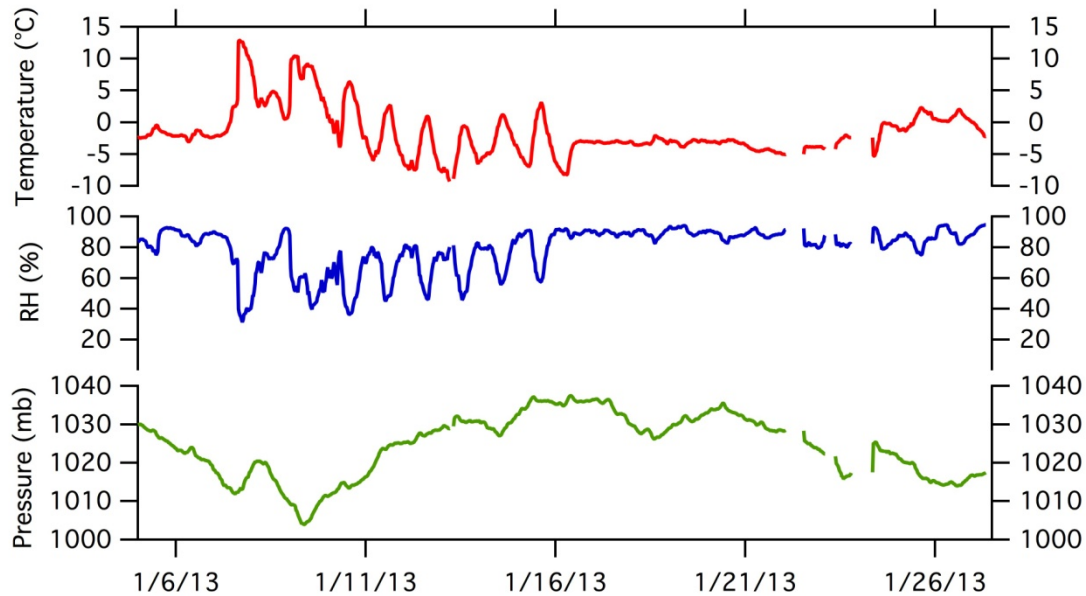


Figure 6.1. YAWNS time series for temperature, relative humidity, and pressure at Yakima. Pressure has been corrected to sea level equivalent.

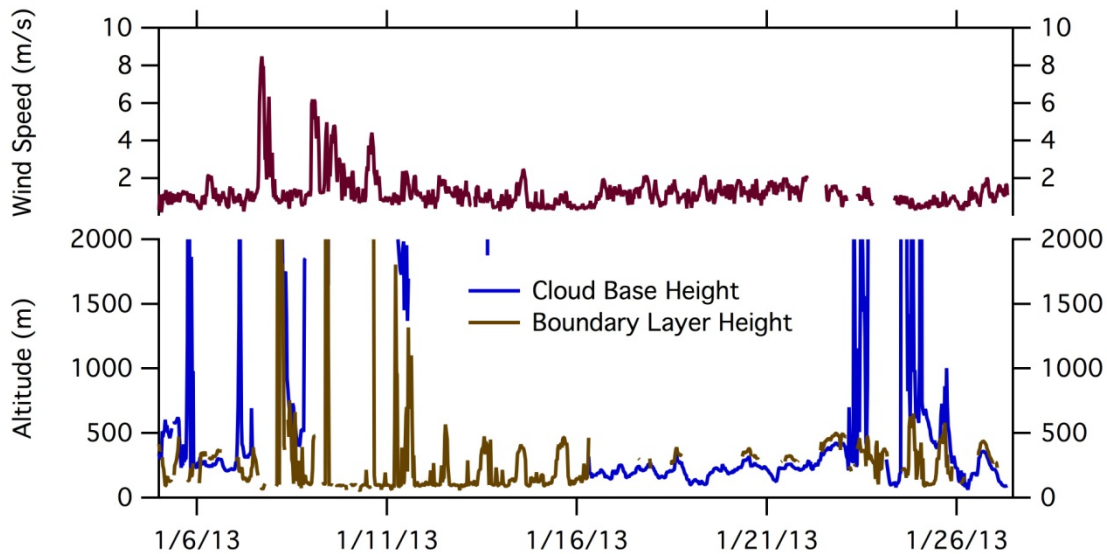


Figure 6.2. YAWNS time series for wind speed, boundary layer height, and cloud base height at Yakima.

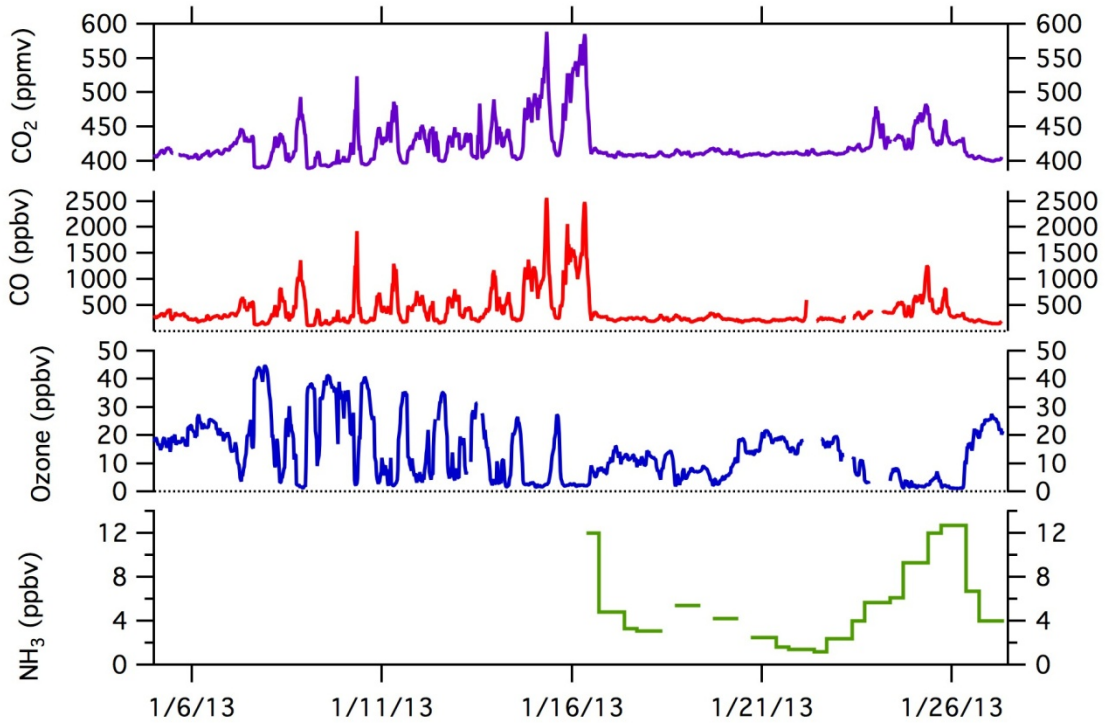


Figure 6.3. YAWNS time series for carbon dioxide, carbon monoxide, ozone, and ammonia at Yakima.

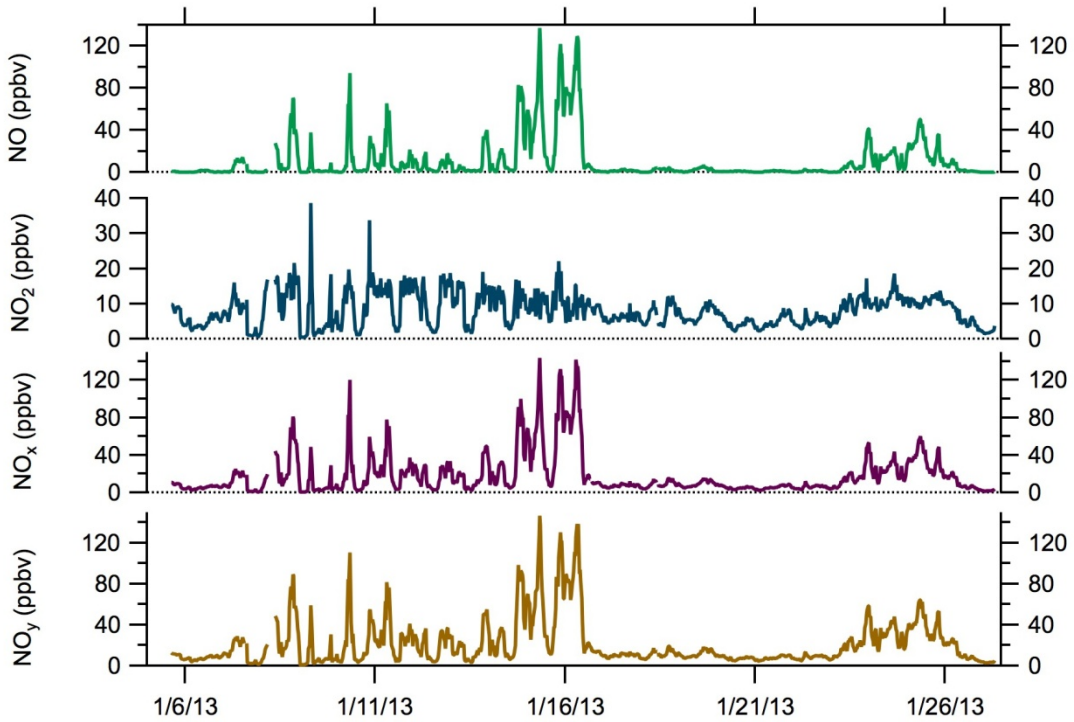


Figure 6.4. YAWNS time series for NO, NO₂, NO_x, and NO_y at Yakima.

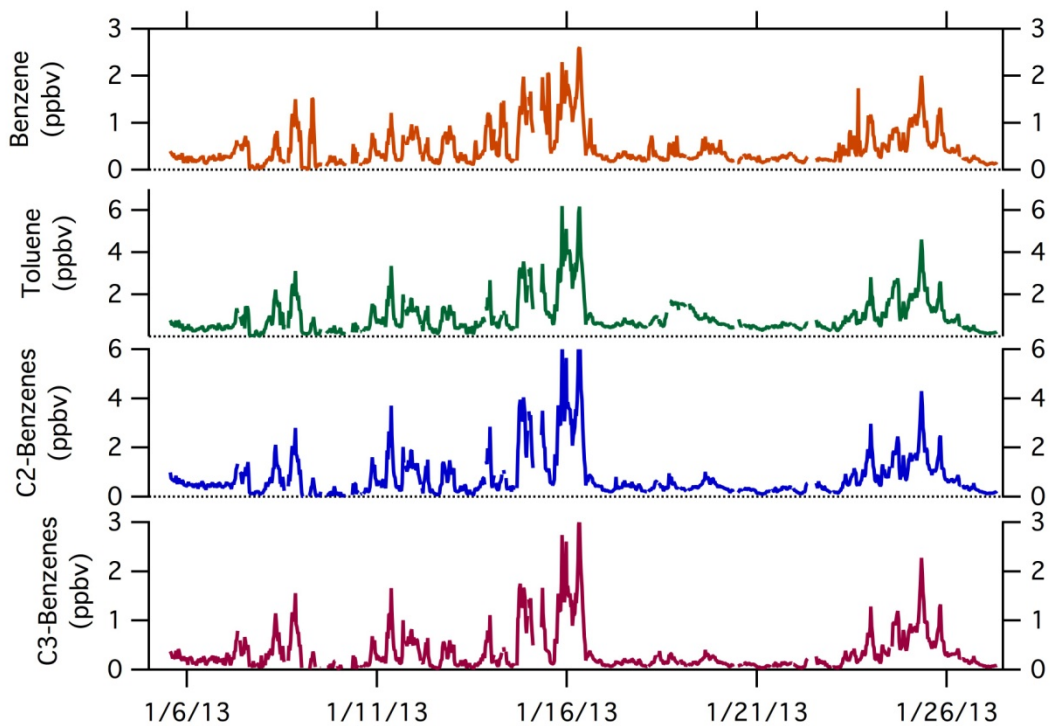


Figure 6.5. YAWNS time series of ion masses representing several aromatic compounds from the PTR-MS at Yakima. Not all ion masses are shown.

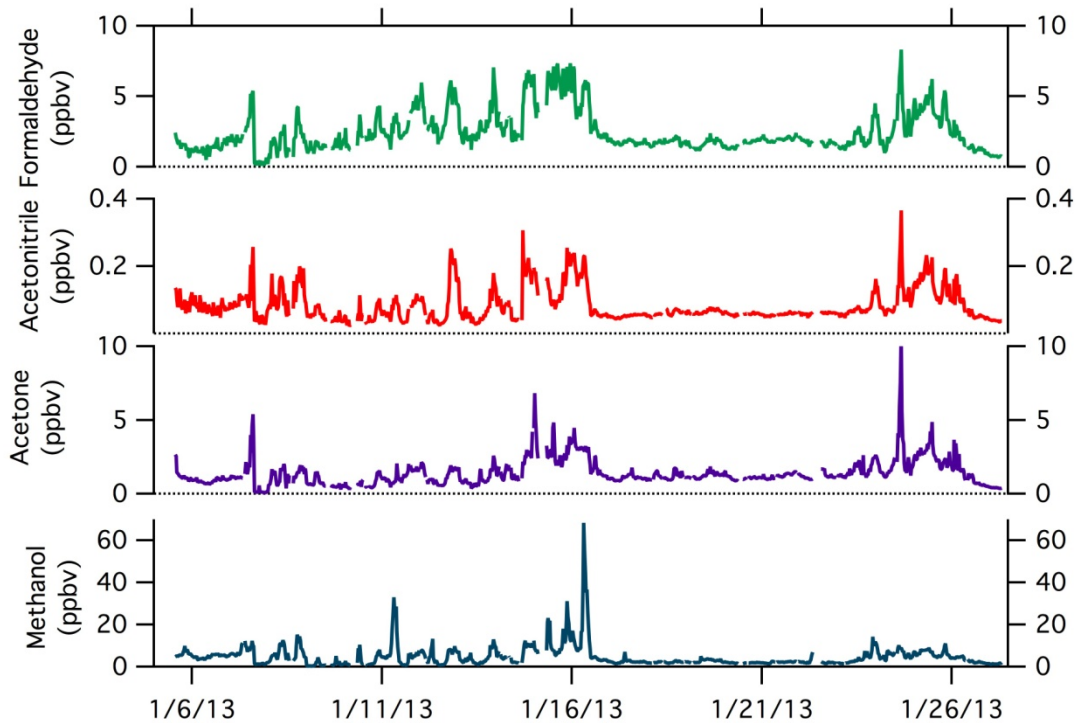


Figure 6.6. YAWNS time series of ion masses representing oxygen- or nitrogen-containing compounds from the PTR-MS at Yakima. Not all ion masses are shown.

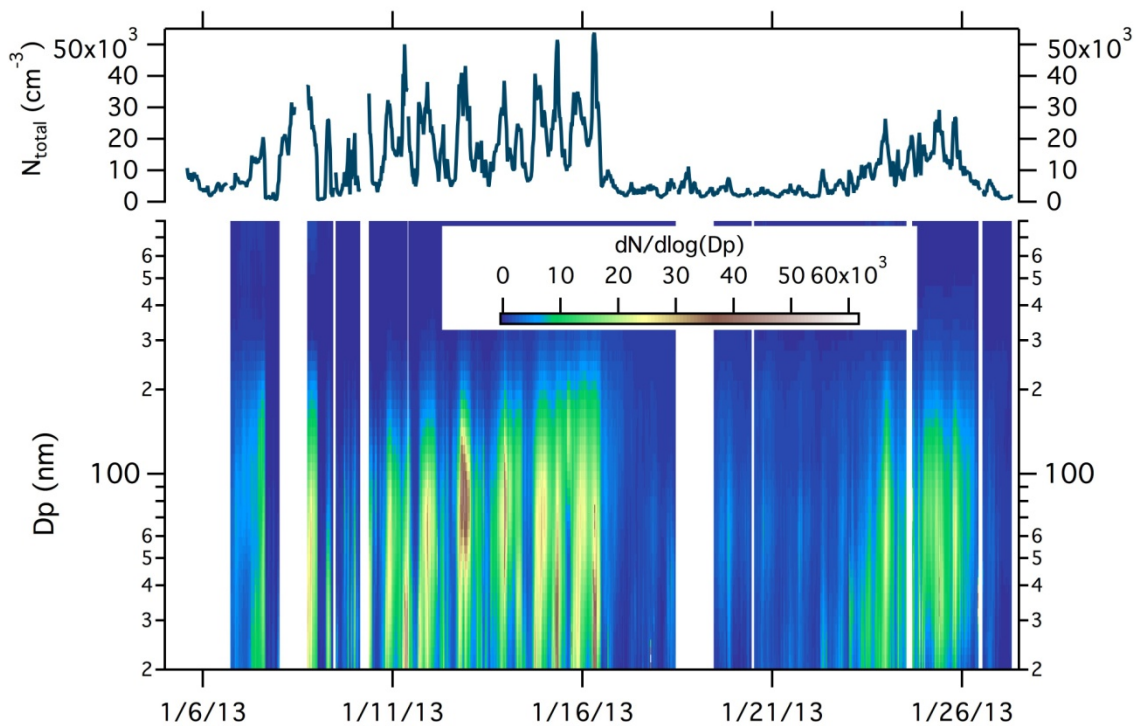


Figure 6.7. YAWNS time series of particle number concentration (from the CPC) and particle size distribution (from the SMPS) at Yakima.

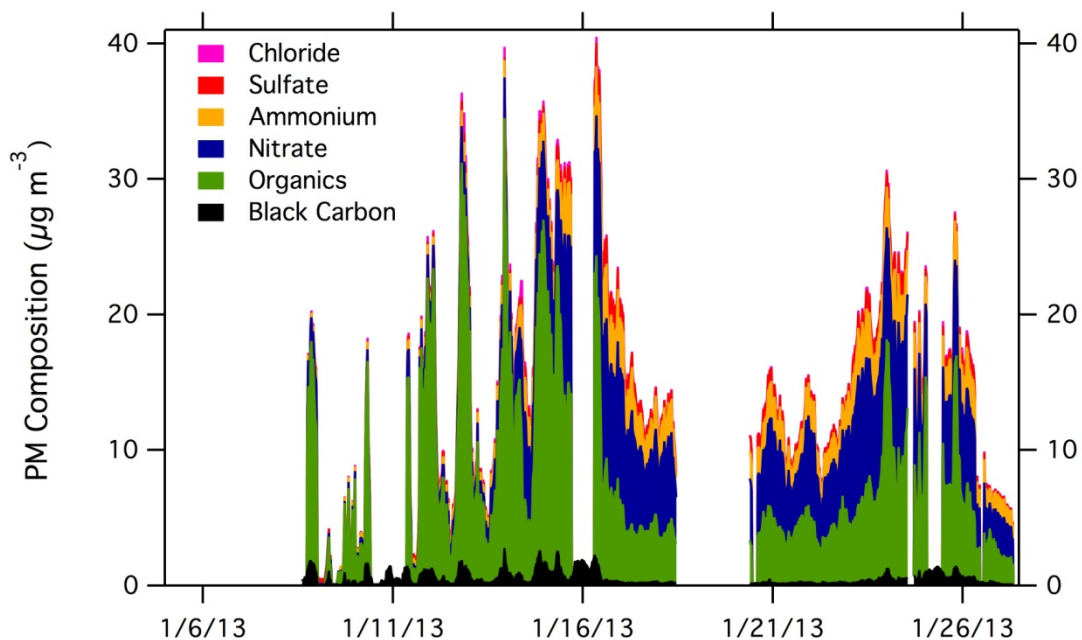


Figure 6.8. YAWNS time series of PM composition at Yakima. Components are stacked to indicate relative contribution to total PM loading. Black carbon is from the SP2; other data are from the AMS.

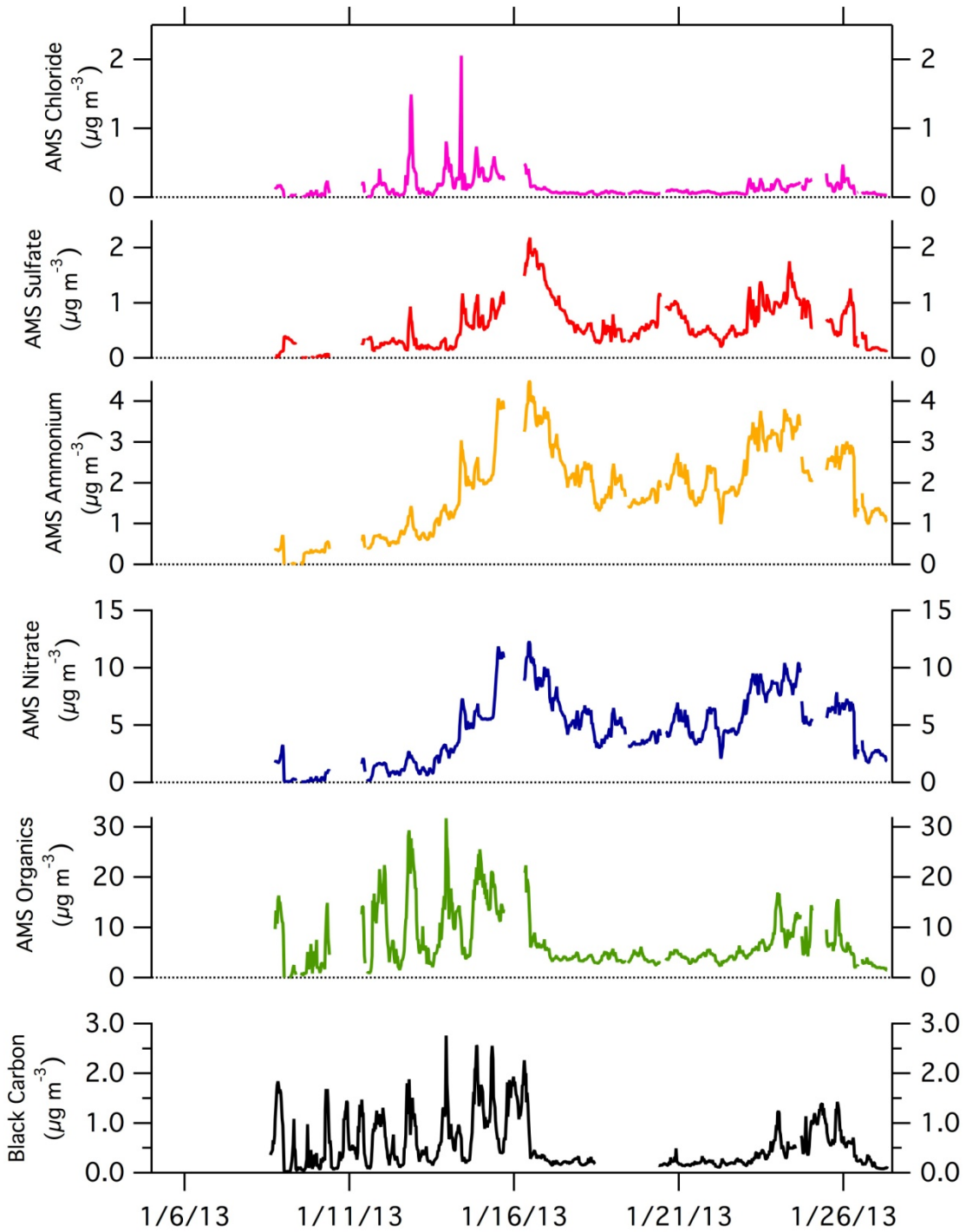


Figure 6.9. YAWNS time series of PM composition at Yakima. Components are shown here as individual traces to highlight temporal variability. Black carbon is from the SP2; other data are from the AMS.

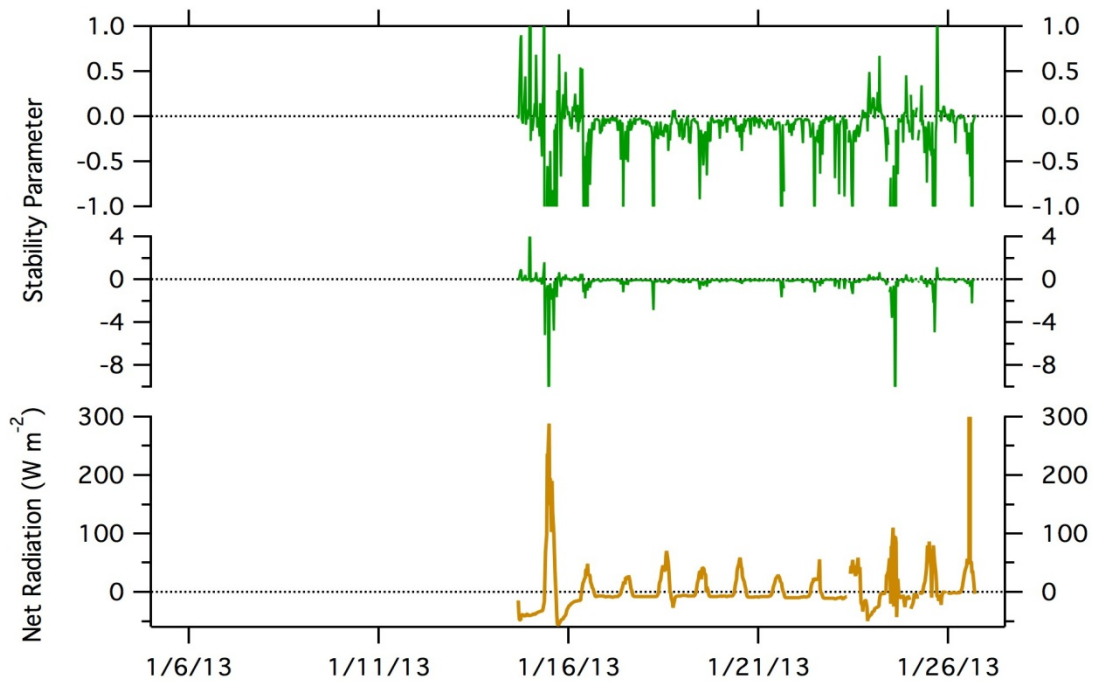


Figure 6.10. Results from the YAWNS flux tower measurements. Only a subset of measured parameters is shown, specifically the calculated net radiation and the calculated stability parameter. Stability parameter is shown twice of separate axes to highlight the near-zero variability during portions of the study.

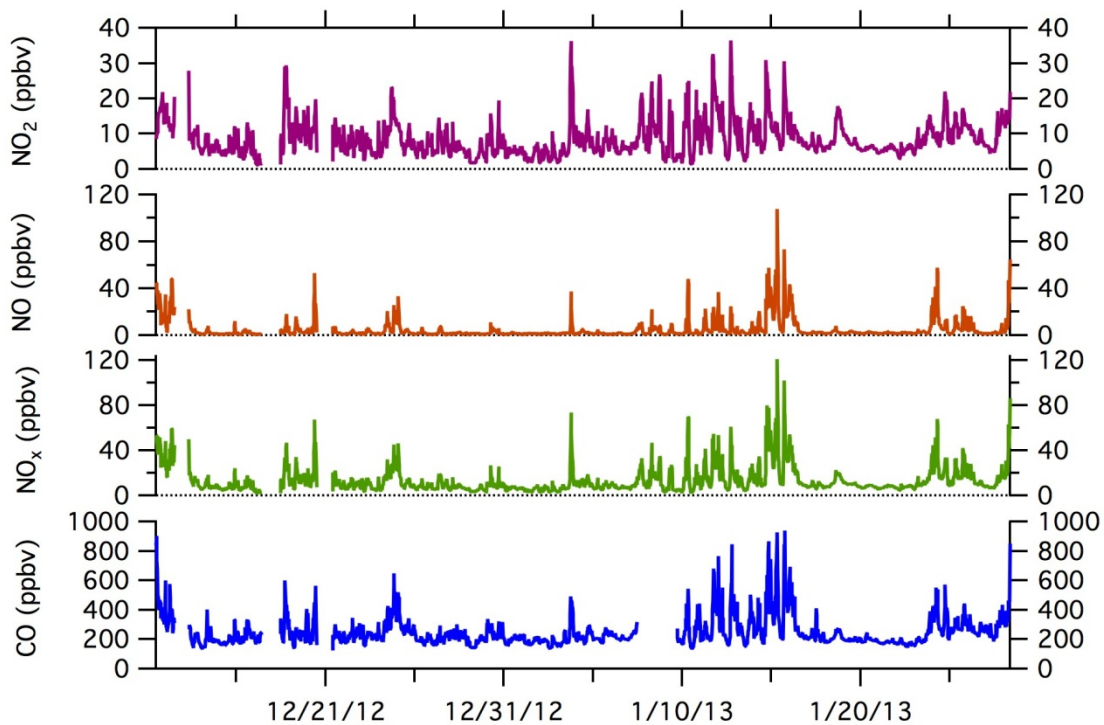


Figure 6.11. YAWNS time series of CO and NO_x at Toppenish. Note that the time axis on this figure differs from previous time series; data were available from Toppenish for longer periods.

7. Positive Matrix Factorization of PM Organic Composition

The initial analysis of the HR-AMS aerosol composition measurements reduces the data to produce times series of the major refractory aerosol components- nitrate, sulfate, ammonium, chloride, and organics. This is done in one of two ways, depending on whether the unit mass resolution (UMR) or high-resolution (HR) data are used. Both approaches yield very similar results; in this report the results presented are based on UMR data. With UMR data, the HR-AMS signal for each unit mass-to-charge ratio is initially lumped. This means that that different ions from different source molecules will initially be grouped based on their common unit mass-to-charge ratio. To separate these contributions, the signal is redistributed according to a study-specific fragmentation table. The result of this analysis is the desired first-order product: time series of nitrate, sulfate, ammonium, chloride, and organics. These results for YAWNS are shown in Figure 6.9.

For the inorganic components, these first-order categories each generally include the contributions from only one major PM constituent (e.g., nitrate, sulfate, and ammonium). In contrast, the organics category includes hundreds of compounds, derived from a variety of primary source types and secondary atmospheric processes. As such, the information content of the organics category is somewhat limited. Greater understanding of the organic aerosol can be derived by conducting a more detailed analysis of the time series of the HR-AMS mass spectral data within the organics component. The most common approach currently to accomplish this is via a positive matrix factorization (PMF) analysis on the organic

aerosol component of the AMS data (Zhang et al., 2011). Code has been developed specifically for conducting PMF analysis using HR-AMS organics data (Ulbrich et al., 2009). Using this code, we have conducted a PMF analysis of the organic aerosol observed during YAWNS to better understand the sources contributing to PM in Yakima during winter.

After a detailed evaluation of mass spectral profiles, time series, diurnal variations, and correlations with external tracers, we selected a four-factor solution as an appropriate UMR solution for the YAWNS study period. The mass spectra for the four factors are shown in Figure 7.1. Three of these spectra are consistent with factors that are regularly found in PMF analyses of HR-AMS data (e.g., Aiken et al., 2009, 2010; Hildebrandt et al., 2011; Zhang et al., 2011). These factors have been labeled oxidized organic aerosol (OOA), hydrocarbon-like organic aerosol (HOA), and biomass burning organic aerosol (BBOA). OOA is characterized mainly by the strength of the m/z 44 fragment (largely from CO_2^+), and is frequently treated as a proxy for secondary organic aerosol. HOA contains much more m/z 43 (from C_3H_7^+) than 44, and also shows strong signal at m/z 55 and 57 (largely C_4H_7^+ and C_4H_9^+ , respectively). The HOA factor is associated with fresh fossil fuel combustion aerosol. BBOA contains significant mass spectral contributions from m/z 60 and 73, ions that are derived from wood smoke ($\text{C}_2\text{H}_4\text{O}_2^+$ and $\text{C}_3\text{H}_5\text{O}_2^+$, respectively). This factor shows somewhat more variability in the literature, but its presence in the YAWNS data set is consistent with the prevalence of wood stove emissions in the Yakima airshed.

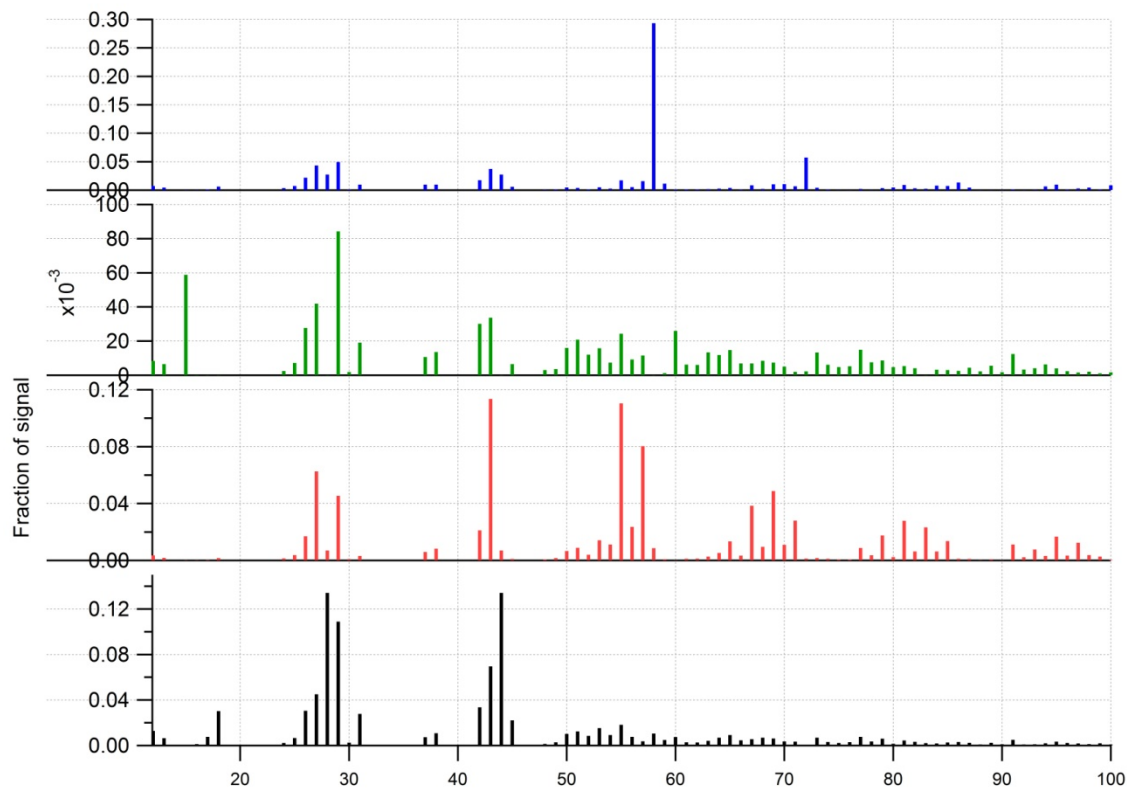


Figure 7.1. Mass spectra of organic aerosol composition factors produced by the PMF analysis of the AMS unit-mass resolution organics signal. The x-axis is mass-to-charge ratio (m/z). The four factors, from top to bottom, have been identified as amines, BBOA, HOA, and OOA.

The fourth factor revealed by the PMF analysis is one that is not frequently observed in ambient data. Based on a review of the limited available literature (e.g., Hildebrandt et al., 2011) and in consultation with other HR-AMS users, we have tentatively identified this factor as representative of amines. This identification is based on the dominance of m/z 58 and 72 in the factor, which are associated with amine ions ($C_3H_8N^+$ and $C_4H_{10}N^+$, respectively) and have been previously been found in unit mass resolution mass spectral signatures. An examination of the high-resolution mass spectral signal has confirmed that the ion contribution at these m/z numbers include significant amounts of the amine ions (Figure 7.2).

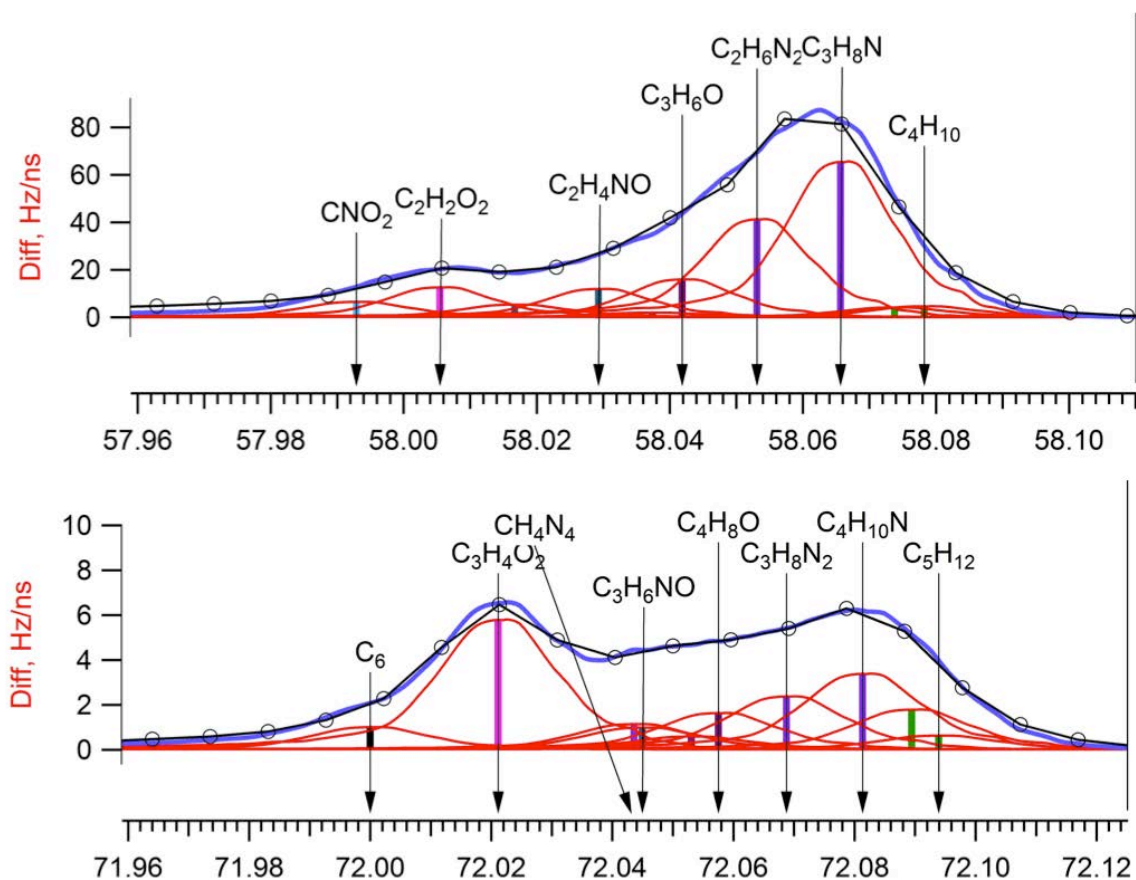


Figure 7.2. Evidence of amine contributions at m/z 58 (top panel) and m/z 72 (bottom panel) from the high resolution AMS data. In each plot, the black circles indicate the observed signal as a function of m/z . Red curves are fitted contribution from individual labeled ions, and the blue curves represent the sum of the fitted ions. In the top panel, the dominant contribution is from $C_3H_8N^+$ at m/z 58.066. In the bottom panel, $C_4H_{10}N^+$ (m/z 72.081) is one of several ions making significant contributions to the overall observed signal.

The time series of the four identified PMF factors are shown in Figure 7.3.

The contribution of the amine factor is limited to a small number of distinct events between 8 January and 13 January. The cause of these events is currently unknown but is being investigated. As such the amine factor is not discussed further in this report.

The other factors, those linked to HOA, BBOA, and OOA, contribute to the overall organic aerosol level in varying degrees throughout the study. Their

relationships with other PM constituents and trace gas species will be explored further in the next section.

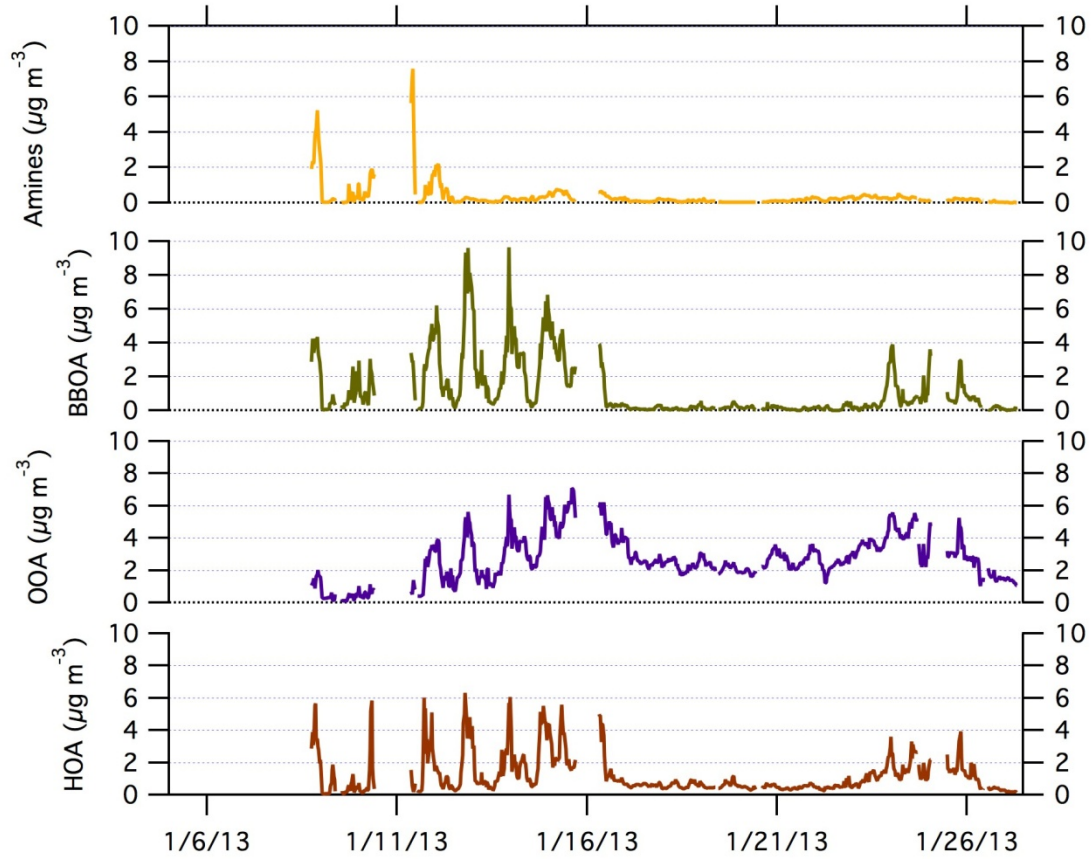


Figure 7.3. Time series of the four organic aerosol factors identified via PMF analysis. HOA is hydrocarbon-like organic aerosol; OOA is oxidized organic aerosol, and BBOA is biomass burning organic aerosol.

8. Meteorological and Chemical Drivers of PM Levels

8.1. Classification of Study Periods

Figure 8.1 shows time period classifications based upon observed meteorological conditions in Yakima. Frontal passages on 7 January and 9 January produced strong winds, elevated temperatures, and clean conditions; these events are noted in the figure. After 9 January, a high pressure condition developed, the skies cleared, and temperatures began to drop. Our analysis of the meteorological and chemical drivers of PM episodes in Yakima largely focuses on the contrast between this clear-sky period and a period the following week that was characterized by persistent low-level cloud. The beginning of the 'Clear Sky' focus period was chosen to be on the morning of 10 January (07:00). This extended period has essentially continuous clear skies, a strong diel cycle in temperature, and large day-to-night variations in boundary layer height that drove strong variations in day-to-night concentrations of primary pollutants. The end of the Clear Sky period was the morning of 16 January (07:00). Very soon after this time a cloud layer formed that persisted for a week; this second period is our 'Persistent Cloud' focus period. This condition was stable beginning at 12:00 on 16 January, and continued until 00:00 on 23 January. This period is notable for the low concentrations and absence of diel variations for primary pollutants. However, this period also still had elevated PM_{2.5} levels. Following the Persistent Cloud period, Yakima experienced a mixed meteorology condition characterized by broken cloud and somewhat higher temperatures. This Mixed Meteorology period from 23-26 January had higher

primary pollutant concentrations than the preceding Persistent Cloud period, and particulate nitrate remained elevated.

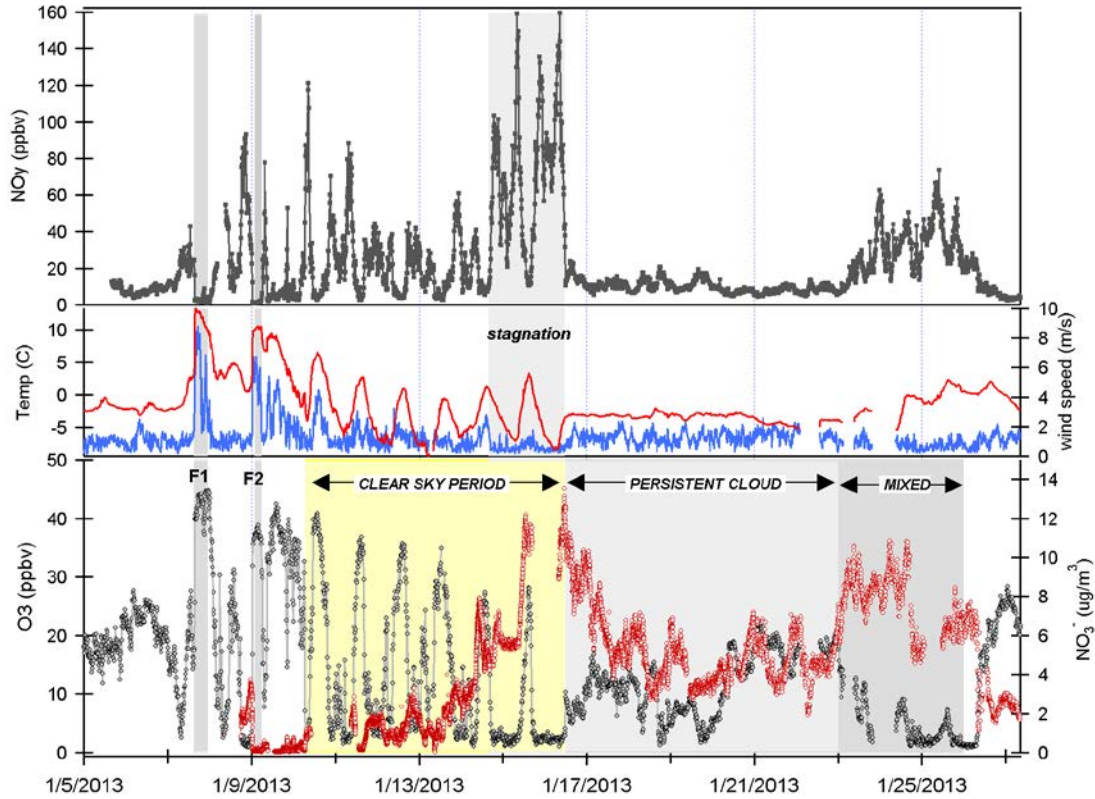


Figure 8.1. Time period classifications during YAWNS showing ozone (black), particulate nitrate (red), wind speed (blue), temperature at 10-m (red), and NO_y (grey). Time periods labeled F1 (7 January) and F2 (9 January) in grey shading indicate frontal passages. The Clear Sky period (10-16 January) is shown in yellow shading. During this period wind speeds on 14-16 January fell to low levels producing a Stagnation Pollution Episode highlighted in grey in the NO_y and temperature traces. The Persistent Cloud period (16-23 January) is shown in light grey shading. The Mixed Meteorology period (23-26 January) is shown in grey shading.

Part of the Clear Sky and all of the Persistent Cloud periods were impacted by a mesoscale stagnation condition. During the Clear Sky period, this led to very high PM levels on the nights of 14 January and 15 January. This Stagnation Pollution Episode has specific policy implications due to the high PM levels observed. Particulate nitrate is especially important during this episode, when it displayed

sharp increases in concentration. The Stagnation Pollution Episode begins on 14 January (16:00) and continues until the morning of 16 January (07:00). These focus periods are highlighted in Figure 8.1 to illustrate differences in the time series data, and the categories are summarized in Table 8.1.

Table 8.1. Categories for YAWNS time periods.

Category	Time Period
Clear Sky	10-Jan (07:00) to 16-Jan (07:00)
Persistent Cloud	16-Jan (12:00) to 23-Jan (00:00)
Stagnation Pollution Episode	14-Jan (16:00) to 16-Jan (07:00)
Mixed Meteorology	23-Jan (00:00) to 26-Jan (00:00)

8.2. Comparison of Clear Sky and Persistent Cloud Periods

Among the most noteworthy characteristics of the YAWNS study is the stark contrast between the observed atmospheric properties between the Clear Sky period and the Persistent Cloud period that immediately followed. The nighttime observations during the Clear Sky period had among the highest pollutant concentrations measured during the study, especially during the Stagnation Pollution Episode. On the other hand, during the Persistent Cloud period most pollutants were greatly reduced. Importantly, the mesoscale meteorological state was stable across much of both of these periods. Similar contrasts between clear and cloudy conditions during mesoscale stagnations have been observed previously in Idaho’s Treasure Valley (Mwaniki et al., 2014; Wallace et al., 2012) and have been reported anecdotally elsewhere (R. Elleman, personal communication). Still, the

phenomenon has not been thoroughly described. The YAWNS study provides the most comprehensive data set available to date to describe the impacts of persistent low-level cloud on surface air pollution during mesoscale stagnation conditions.

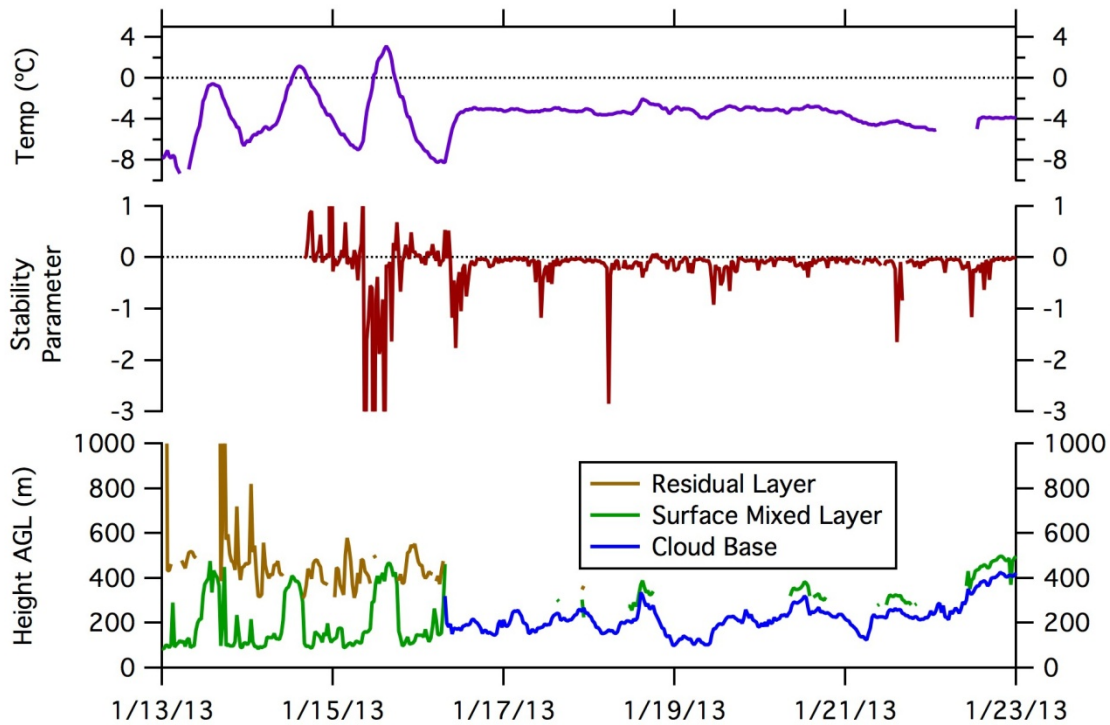


Figure 8.2. Meteorological parameters during the clear-sky stagnation and persistent cloud periods during YAWNS. For the stability parameter, negative values indicate unstable conditions, positive values are stable, and zero values are neutral.

The YAWNS observations suggest strongly that the transition from polluted to clean conditions observed mid-morning on 16 January was driven by dynamics accompanying the onset of low-level cloud. This is shown in Figure 8.2. During the Clear Sky period preceding the onset of cloud, the observed atmospheric conditions were consistent with the diurnal cycle typically associated with wintertime stagnation periods. During nighttime in this period, the surface mixed-layer height is very low, roughly 100 m, and conditions are strongly stable. This is consistent with a

surface-level temperature inversion inhibiting vertical mixing. A clearly defined residual layer is present above the surface mixed layer, at approximately 400 m. Pollutants emitted during this time are trapped in the inversion layer near the surface, causing concentrations to build up to unhealthy levels (Figure 8.3). In the morning, the inversion breaks as the surface heats, and surface mixed layer depth increases to the 400 m level. This dilutes the surface level concentrations of many pollutants by mixing relatively cleaner air from the residual layer down into the surface layer. After sunset, surface cooling reestablishes the low-level temperature inversion and the shallow near-surface mixed layer.

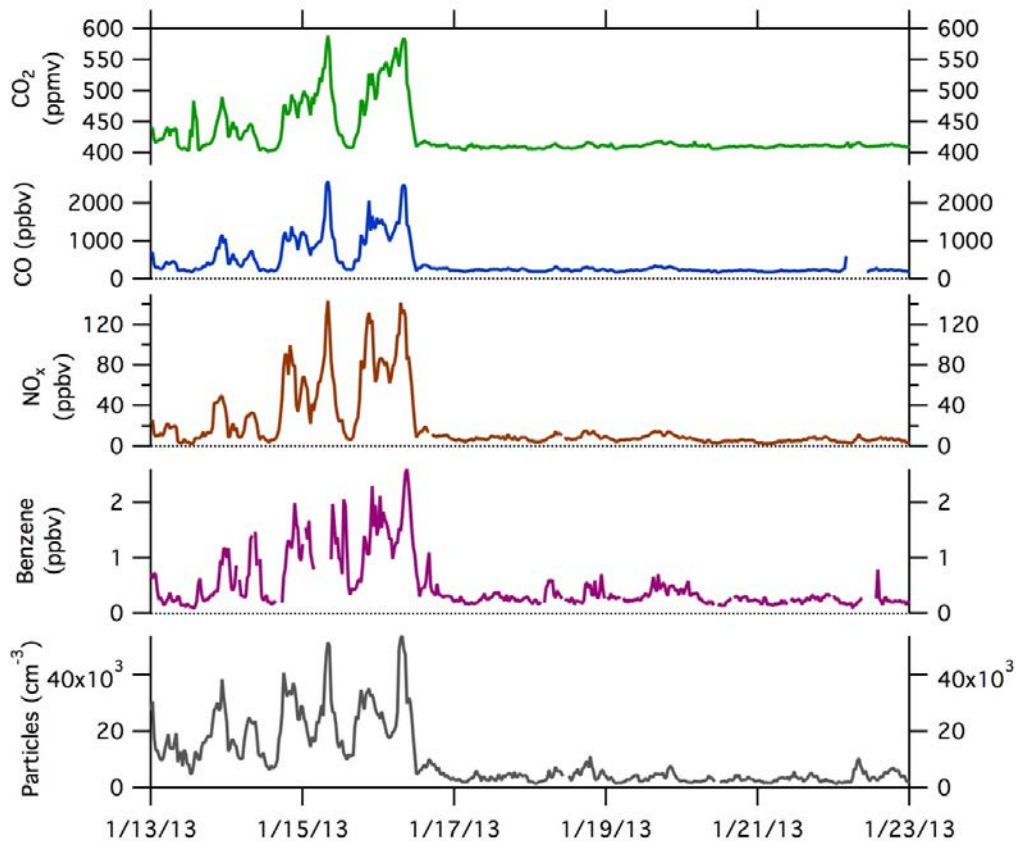


Figure 8.3. Select trace gas and particle number concentrations during the clear-sky stagnation and persistent cloud periods during YAWNS.

On the morning of 16 January during YAWNS, low-level cloud develops, and the diurnal pattern for both the boundary layer height and most pollutants is significantly affected. The beginning of this new condition is highlighted in Figure 8.2. At approximately 08:00, the cloud layer forms, as indicated by the change in the ceilometer response from a boundary layer detection to a cloud layer detection. The height of the cloud base is similar to the overnight boundary layer height, between 100 and 300 m. Because of the optical thickness of the cloud, the cloud top height cannot be determined from the ceilometer data. Over the course of the next few hours, the levels of most pollutants drop to low levels, similar to concentrations observed during afternoons when a relatively deep, well-mixed boundary layer is present. This is shown for several trace-gas pollutants in Figure 8.3, and the same pattern was observed for additional VOC species not shown. The change in pollutant levels is not simultaneous with the cloud layer development. The pollutant concentration decreases begin later and occur over a longer time period compared with the cloud development. The cloudy period and the accompanying changes in pollution levels persist, day and night, for several days until the cloud dissipates on 23 January. Meteorological parameters are remarkably stable throughout this period, with almost no variability in cloud base height, temperature, RH, or wind speed. Figure 8.4 contrasts the diel variation of temperature and other meteorological metrics between the Clear Sky and Persistent Cloud periods. Figure 8.5 shows how the diel variability in CO₂, CO, and O₃ differs between the two periods.

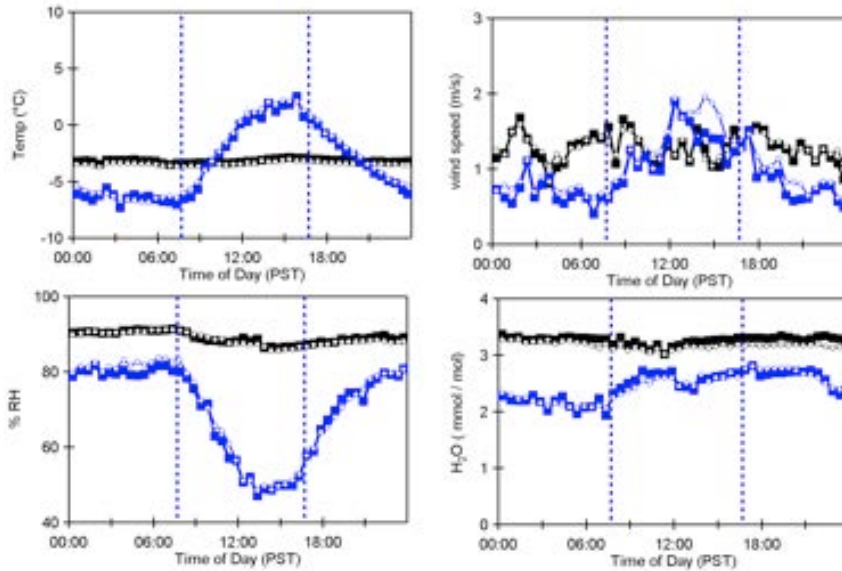


Figure 8.4. Diel variation of temperature, wind speed, relative humidity, and water vapor mixing ratios showing 30-minute averages (open circles) and medians (solid squares) for the Clear Sky period (blue trace) and Persistent Cloud period (black trace).

In contrast to particle number concentrations and primary pollutant concentrations, the $PM_{2.5}$ mass concentration measured by YRCAA in central Yakima did not exhibit dramatic declines on the morning of 16 January, nor did the particulate mass measured by the aerosol mass spectrometer. Particulate mass concentration did begin to decrease at this time, but much more gradually, over the course of a few days. From the $PM_{2.5}$ results alone it would not be possible to determine why the temporal trend in particulates is different from other pollutants.

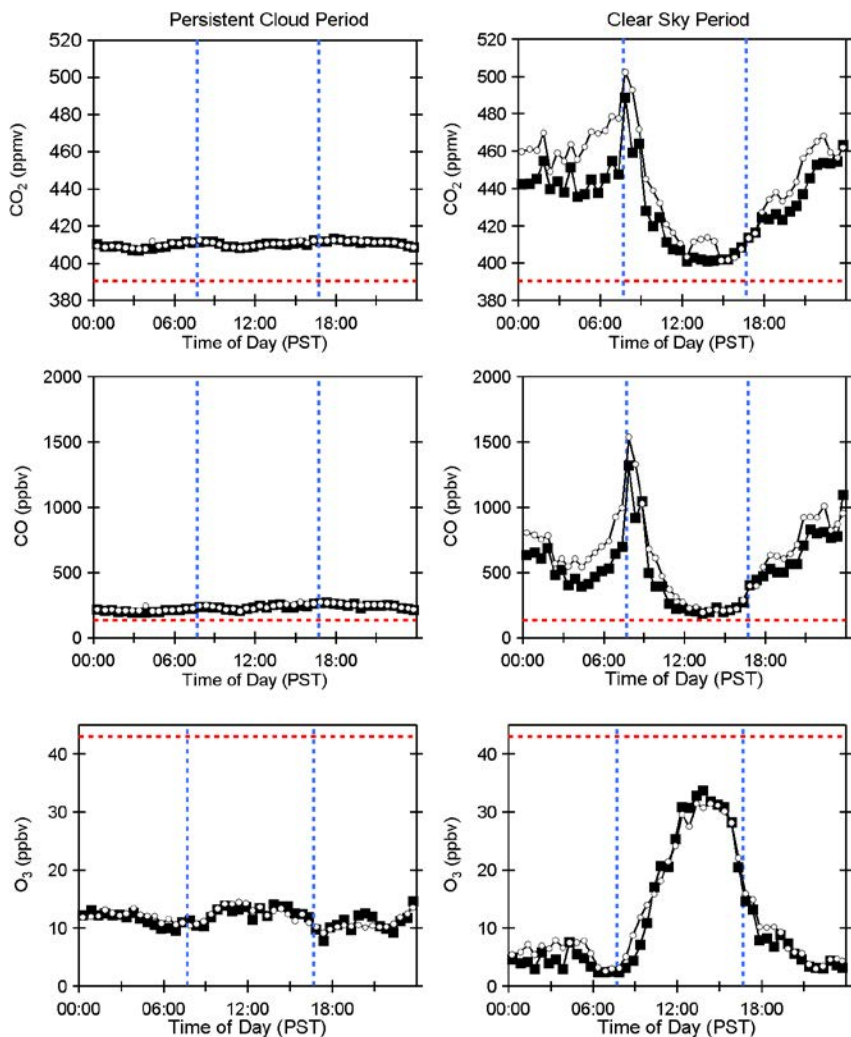


Figure 8.5. Diel variation of CO_2 , CO and ozone contrasting the Persistent Cloud period data on the left hand side with the Clear Sky period on the right hand side. Open circles represent the 30-minute averages and black solid squares the median values. Red dashed line indicates the regional background values as measured during a high wind period associated with a frontal passage on 7 January. Vertical blue dashed lines represent sunrise and sunset.

An examination of the aerosol composition across this transitional period reveals the apparent source for this contrast (Figure 8.6). The black carbon concentration did in fact decline dramatically at the same time as the other primary species. The HOA and BBOA factors from the PMF analysis of the HR-AMS organics data showed similar declines over the same time period. These particulate components are associated with local, fresh emissions and thus their transition is

consistent with those of the primary trace gases. On the other hand, the inorganic species do not change as dramatically on the morning of the 16 January. Particulate nitrate, ammonium, and sulfate all begin to decline gradually at this time, but still remain significantly above their background levels. The OOA factor from the PMF analysis of the HR-AMS organics data behaves similarly. These particulate components, nitrate, sulfate, ammonium, and OOA, are all secondary products that result from atmospheric processing. In summary, the onset of persistent low-level cloud caused primary pollutant concentrations to be consistently low day and night but secondary PM components such as nitrate and OOA remained elevated. The effects of these changes on the apparent source contributions to the particulate organic material is shown in Figure 8.7.

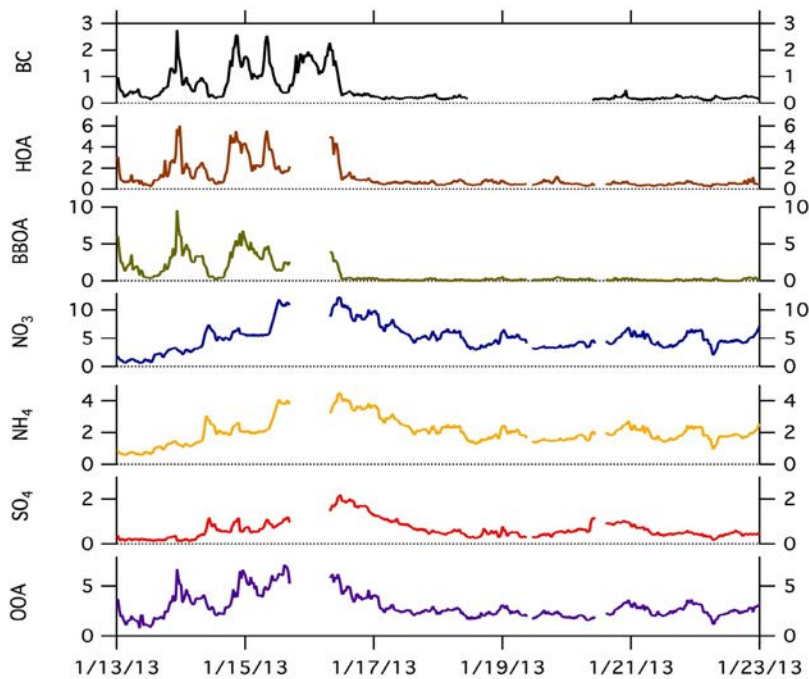


Figure 8.6. Trends in aerosol components during the Clear Sky and Persistent Cloud periods. The y-axes for all plots have units $\mu\text{g m}^{-3}$. BC is the black carbon measurement; HOA, BBOA, and OOA are the hydrocarbon-like, biomass burning, and oxidized organic aerosol factors, respectively, from the PMF analysis. NO_3 , NH_4 , and SO_4 are particulate nitrate, ammonium, and sulfate, respectively.

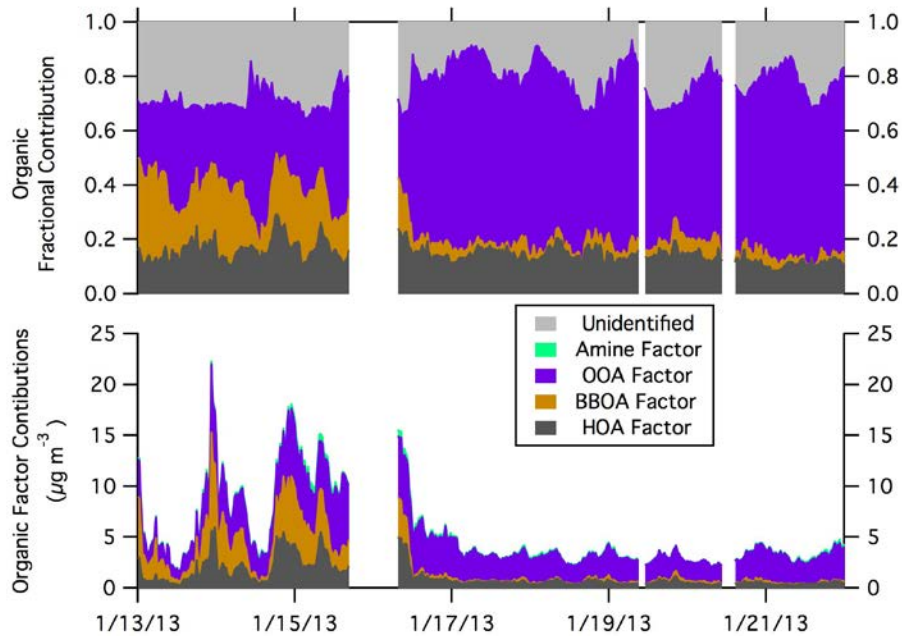


Figure 8.7. Contributions of PMF-derived factors during the YAWNS Clear Sky and Persistent Cloud periods.

The dynamics of the cloud-topped boundary layer in Yakima may be similar to a marine stratocumulus cloud (Figure 8.8). The dynamics of this mechanism have been reviewed recently by Wood (2012). In marine stratocumulus, the boundary layer is effectively mixed from the surface up to the cloud top, driven by latent heating and evaporative cooling within the cloud. At cloud top, mixing is reduced but there is some entrainment of (typically cleaner) air from the free troposphere driven by evaporation and solar heating.

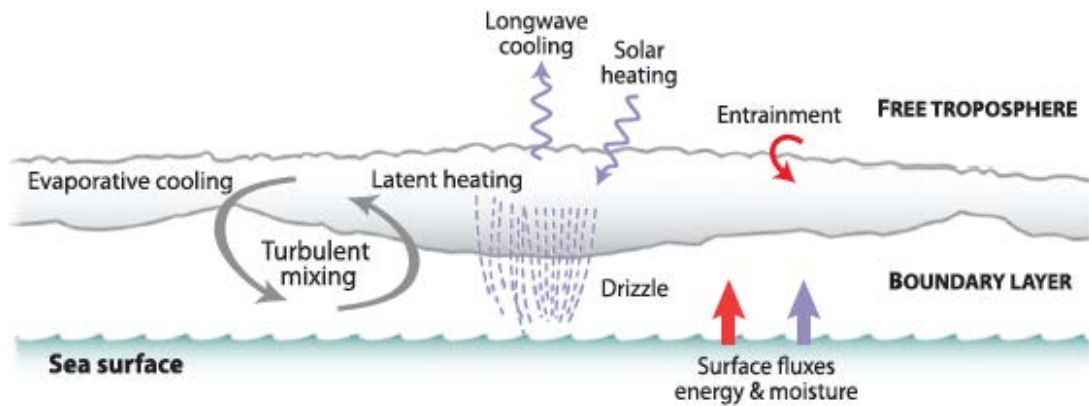


Figure 8.8. Schematic showing the key process occurring in the marine stratocumulus-topped boundary layer. Schematic from Wood (2012).

Cloud-top data are not available for YAWNS, so it is not possible to determine whether this proposed mechanism is fully consistent with the observed behavior. Based on what data are available, it is a reasonable model. The observations for most primary pollutants (e.g., CO₂, CO, black carbon) during the Persistent Cloud period were approximately the same as were observed in the late afternoons during the Clear Sky conditions, implying similar mixed layer heights. Afternoon boundary layer heights during the Clear Sky period were measured by the ceilometer to be approximately 400 m. During the Persistent Cloud period, the measured cloud base height varied between 100 and 300 m; this is at least consistent with cloud tops at approximately the same height as the afternoon boundary-layer height during clear-sky conditions. The calculated stability parameters based on the flux tower data are also consistent with this proposed model. Flux tower data are not available for much of the Clear Sky period, but are available for the Stagnation Pollution Event starting on the afternoon of 14 January. During this period, the turbulence parameter indicated unstable conditions during the day, but stable conditions at night (middle panel, Figure 8.2). During the Persistent Cloud period, in contrast, the turbulence

parameters consistently indicated neutral or unstable conditions. This is additional evidence that during the Persistent Cloud period the boundary layer was well mixed throughout the diel cycle.

The impact of the changed near-surface dynamics from the Clear Sky to the Persistent Cloud period is further revealed by examining the local atmospheric ventilation. There are several approaches to quantifying the effectiveness of pollutant dispersion away from its source region; here we will use the venting index used and described by the British Columbia Ministry of Environment (BC Air Quality, 2014). The venting index is based on the raw venting, the product of the mixing height (in meters) and the mean surface layer wind speed (in meters per second):

$$V_{raw} = H_{mixing} \times WS_{avg} \quad [\text{Eq 8.1}].$$

The raw venting is then adjusted using a polynomial expression to obtain the venting index:

$$VI = 9 + 0.02V_{raw} - 1.7 \cdot 10^{-6}V_{raw}^2 + 6.8 \cdot 10^{-11}V_{raw}^3 \quad [\text{Eq 8.2}].$$

The venting index is scaled so that low numbers (0-33) represent poor mixing conditions, mid-range numbers (34-54) represent fair mixing, and larger number (>54) represent good mixing.

To estimate the venting index for YAWNS, we used the 30-min average wind speeds measured at 10m from the MACL instrument mast and the 30-minute average boundary layer heights measured by the ceilometer. When no boundary layer height estimate was available from the ceilometer, we used 400 m as a best estimate. This assumed value was applied to nearly all of the Persistent Cloud

period. The raw venting and calculated venting index for the Stagnation Pollution Episode and Persistent Cloud periods are shown in Figure 8.9.

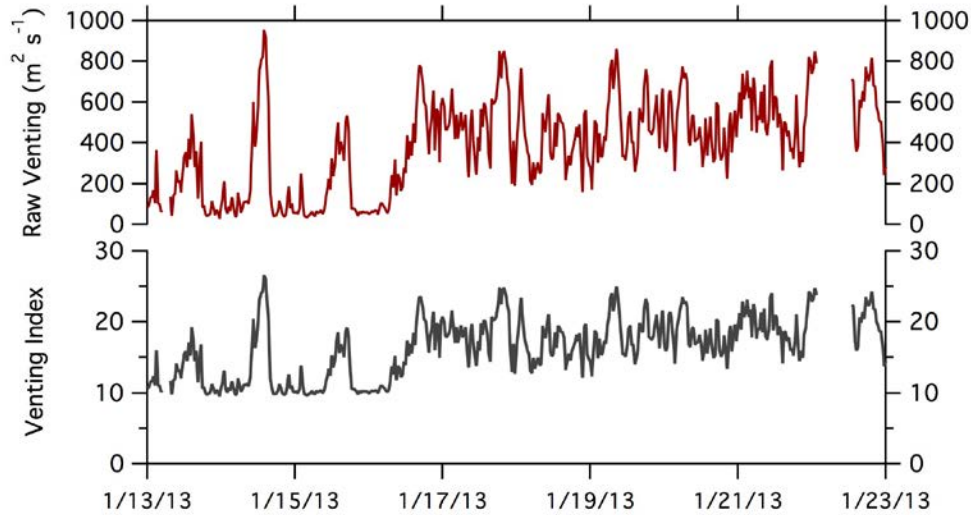


Figure 8.9. Raw venting and venting index for the Stagnation Pollution Episode and Persistent Cloud periods during YAWNS. During the persistent cloud, a constant mixing layer height of 400m was assumed.

The calculated venting index during these periods of YAWNS indicates that mixing would always be classified as ‘poor’. However, there were still clear differences in ventilation. On the nights of 13-15 January, during the Stagnation Pollution period, the venting index was consistently low, approximately 10. During the days in the Stagnation Pollution period, the venting index increased to values between 15 and 25. The Persistent Cloud period had variable venting, but values were always greater than 12, and usually between 15 and 25. This supports the argument that mixing during the Persistent Cloud period was similar to what was observed during daytime conditions in the Clear Sky period.

The persistence of elevated levels of particulate nitrate and other secondary species during the Persistent Cloud period while primary pollutant concentrations

decline is not readily explained. This persistence could be a result of enhanced secondary pollutant production during the cloudy period, or could arise from less effective ventilation of secondary species. Possible mechanisms for these observed phenomena are discussed in the following sections.

8.3. Neutralization State of Major Particulate Inorganic Ions

The amount of nitrate in the particle phase depends in large part on the amount of ammonium available to neutralize nitric acid. However, ammonium reacts preferentially to neutralize sulfate species first, and so the amount of sulfate available must also be considered to determine how much ammonium remains to react with nitrate. In most cases, if there is sufficient ammonium to neutralize any available sulfate, then overall full neutralization would be expected. After sulfate neutralization, any remaining ammonium would generally co-condense with nitrate (and vice versa), yielding a neutralized particle phase. However, in cases of cold temperatures and/or high humidity, it is possible for some unneutralized ammonia or nitric acid to condense to produce a basic or acidic aerosol (Mwaniki et al., 2014).

To evaluate the degree of neutralization of these major inorganic aerosol species during YAWNS, we compared the amounts of ammonium, nitrate, and sulfate on a molar basis. The mass-based composition data from the HR-AMS were first converted to molar concentrations using the ionic masses: 18.04, 62.01, and 96.07 $\mu\text{g}/\mu\text{mol}$ for ammonium, nitrate, and sulfate, respectively. The results are shown in the bottom panel of Figure 8.10. As expected, nitrate and ammonium dominate the inorganic composition on a molar basis, both being approximately an order of magnitude greater than the sulfate concentration. We then used the sulfate

and nitrate concentrations to determine the stoichiometric equivalent ammonium concentration required for full neutralization. This was done according to this relationship:

$$[\text{NH}_4^+]_{eq} = 2 * [\text{SO}_4^{2-}] + [\text{NO}_3^-] \quad [\text{Eq 8.3}].$$

The time series of the calculated equivalent ammonium is plotted against the measured ammonium in the middle panel of Figure 8.10. The difference between them is in the top panel of the same figure.

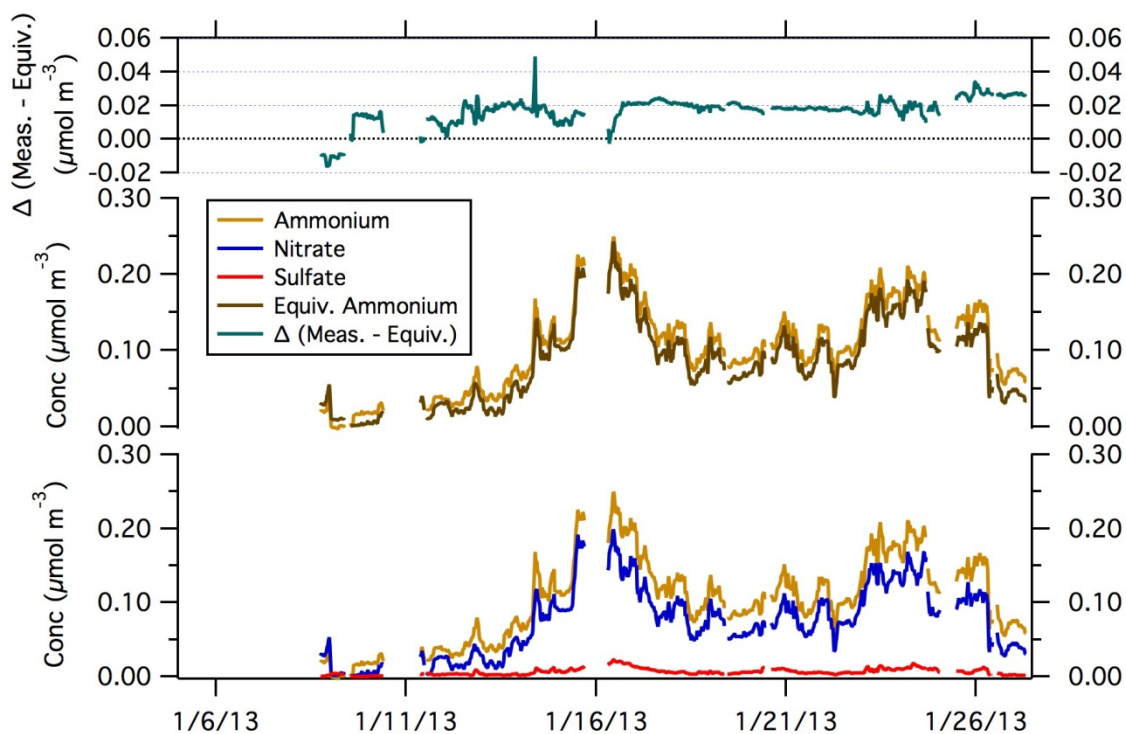


Figure 8.10. Time series of major inorganic ions measured at Yakima by the HR-AMS, on a molar basis. Bottom panel shows the time series. Middle panel show the relationship between the measured ammonium and the equivalent ammonium based on full neutralization of nitrate and sulfate. Top panel shows the difference between the measured and calculated equivalent ammonium.

The results of the neutralization calculation reveal a small but persistent bias between the calculated equivalent ammonium and the measured concentration,

with the measured concentration typically being larger. This is apparent in the time series (top two panels, Figure 8.10) as well as in the scatter plot presented in Figure 8.11. As the latter figure shows, there is overall a very strong correlation between the measured ammonium and the calculated equivalent ammonium ($r^2 = 0.98$). However, the slope between the two is $\sim 5.6\%$ less than unity. There are several possible causes for this offset. One likely factor is the composition-dependent collection efficiency for the HR-AMS. It could also be that there are additional anion species, perhaps organic, that contribute to the ion balance but are not accounted for in this analysis. In any event, the magnitude of this artifact is small, and overall the analysis shows strong agreement in the ammonium/nitrate/sulfate ion balance. It is reasonable to treat this aerosol as fully neutralized.

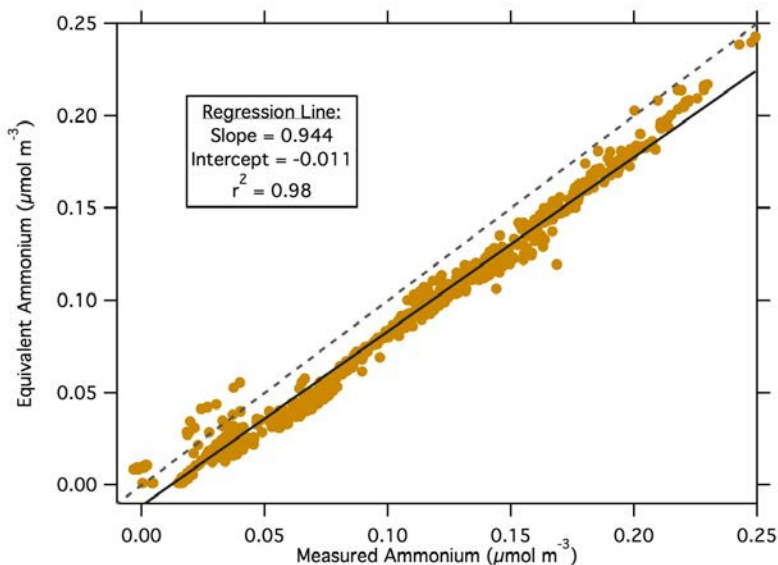


Figure 8.11. Scatter plot of the calculated equivalent ammonium versus the measured amount. Results indicate that $\sim 94\%$ of the measured ammonium is neutralized by sulfate or nitrate. The remaining amount may be due to unmeasured anionic species or due to a small measurement bias. The grey dashed line is the 1:1 relationship.

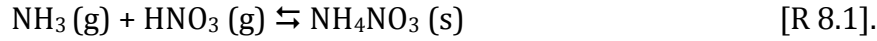
8.4. Potential Causes of Observed Particulate Nitrate Levels at Yakima

The major motivation of the YAWNS study was to need to understand the causes of the observed particulate nitrate levels during wintertime in the upper Yakima Valley. Fundamentally, particulate nitrate loads are always driven primarily by three factors: meteorology, and the availability of ammonia and nitrate precursors. How these factors interrelate and the influence of additional secondary factors can vary and are the focus of this discussion.

The role of meteorology in influencing particulate nitrate formation cannot be ignored. Particulate ammonium nitrate exists in chemical equilibrium with ammonia and nitric acid in the gas phase. In summer, when temperatures are warm, the equilibrium is shifted toward the gas phase, and there is little nitrate present in particulate form. However, at the cold temperatures present in Yakima during winter, the gas-particle equilibrium is heavily shifted toward the particle phase. While that basic concept is straightforward, the full details of the ammonium nitrate equilibrium relationship are complex. In addition to temperature, there are dependencies on relative humidity and the full aerosol composition. Additionally, the levels of nitric acid and ammonia in the atmosphere depend strongly on the gas-phase chemistry of these species, which have additional meteorological dependencies. A full analysis of this system is beyond the scope of this project, but simplified conceptual model can inform our understanding of the situation in Yakima during winter.

In an idealized system consisting only of ammonia and nitric acid in dry air, the equilibrium between the gas and particle phase can be described by reaction

8.1:



The dissociation expression associated with this reaction is:

$$K_p(T) = p_{\text{NH}_3} p_{\text{HNO}_3} \quad [\text{Eqn. } 8.4],$$

where p_{NH_3} and p_{HNO_3} are the partial pressures of ammonia and nitric acid, respectively, expressed in units of ppbv (at sea-level pressure). The value of the equilibrium dissociation constant, $K_p(T)$, is a strong function of temperature (Seinfeld & Pandis, 2006):

$$\ln K_p = 84.6 - \frac{24220}{T} - 6.1 \ln \left(\frac{T}{298} \right) \quad [\text{Eqn. } 8.5].$$

Here, temperature (T) is in Kelvin. The value of $K_p(T)$ for YAWNS is provided in Figure 8.12. During the warmest part of the study it reaches a maximum value of 1.2 ppb², but during Clear Sky period it was 0.1 or below, and during the Persistent Cloudy period its value was approximately 0.01. These values should be treated as the maximum gas phase product for NH₃ and HNO₃ at any given time, since the presence of other substances, including water, would tend to force more of the ammonia and nitric acid into the condensed phase.

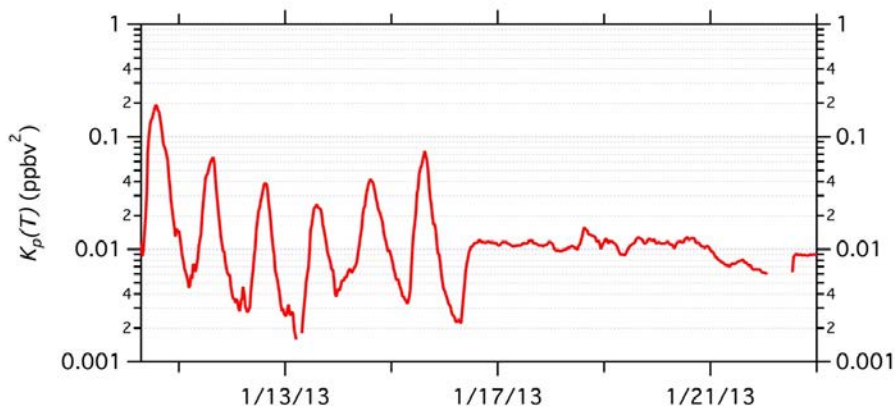


Figure 8.12. Calculated value of the ammonium nitrate equilibrium dissociation constant.

The low values of the ammonium nitrate dissociation constant throughout YAWNS place a strong constraint on how much NH_3 and HNO_3 can be present in the gas-phase. For example, if equal amounts of each compound were present, then maximum gas phase concentrations for NH_3 and HNO_3 would be 1 ppbv each for $K_p(T) = 1.0 \text{ ppbv}^2$, while if $K_p(T) = 0.01 \text{ ppbv}^2$, then only 0.1 ppbv of each component could exist in the gas phase. This phase partitioning constraint can inform our understanding of the factors influencing particulate nitrate loads in Yakima. Direct measurements of HNO_3 were not available during YAWNS. Ammonia observations were only available during the second half of the study, and ranged from 1.2 to 12.7 ppbv. During this same period, the dissociation constant did not exceed 0.06. From the measured NH_3 and the calculated dissociation constant, the maximum possible gas-phase HNO_3 concentrations can be inferred for the second half of YAWNS, shown in Figure 8.13. These concentrations are negligible, not exceeding 7 pptv, which corresponds to approximately $0.02 \mu\text{g m}^{-3}$ of nitrate aerosol. Thus the large excess amount of gas-phase ammonia implies that that essentially all of the available nitric acid is converted to particulate nitrate, and that the availability of HNO_3 is the

limiting factor in determining the particulate nitrate concentration. It follows from this that for the part of the YAWNS during which ammonia data are available, which included most of the period where elevated particulate nitrate was present, the nitrate concentration would be expected to be largely insensitive to atmospheric ammonia levels. While this presented model is greatly simplified relative to the real atmosphere, most complicating factors (e.g., relative humidity) would lead to even greater particulate nitrate formation.

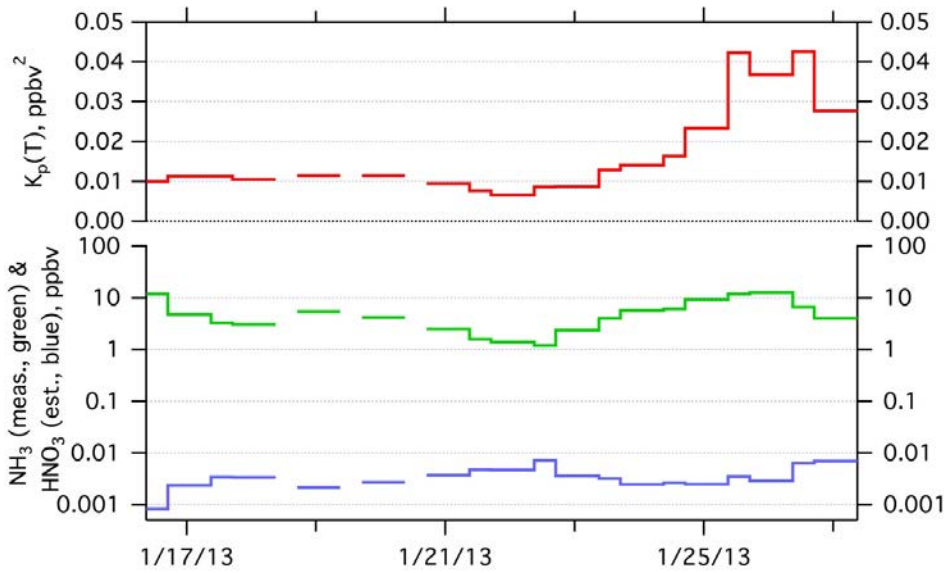


Figure 8.13. Estimated maximum gas-phase nitric acid concentrations during YAWNS, for the portion of the study during which ammonia data are available. Gas-phase nitric acid is estimated using the ammonium nitrate equilibrium partitioning constant and the measured ammonia concentrations.

If the availability of nitric acid is the limiting factor in determining the amount of particulate nitrate present, then for Yakima the particulate nitrate is ultimately determined by how effectively NO_x emissions can be converted to HNO_3 . The portion of NO_y that is not NO_x is denoted NO_z (i.e., $\text{NO}_z = \text{NO}_y - (\text{NO} + \text{NO}_2)$). NO_z arguably represents a good metric for the pool of potential particulate nitrate, since

it consists primarily of material that has already undergone some atmospheric aging and includes the particulate nitrate itself as well as three of its key gas-phase precursors- nitric acid, NO_3 , and N_2O_5 . Figure 8.14 shows the time series of NO_z along with that of particulate nitrate. The NO_z has been converted to nitrate-equivalent mass for ease of comparison, using this equation:

$$[\text{NO}_z]_{\text{mass}} = [\text{NO}_z]_{\text{ppbv}} * 10^{-9} * \frac{p}{RT} * 62.005 * 10^6 \quad [\text{Eqn. 8.6}].$$

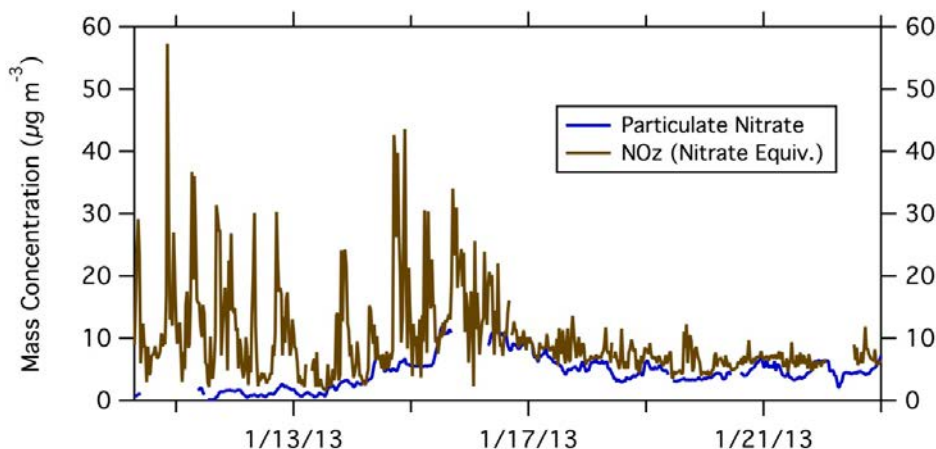


Figure 8.14. Comparison of NO_z , based on the NO_x and NO_y measurements with particulate nitrate during the Clear Sky and Persistent Cloud periods.

The time series shows that there are periods where most of the NO_z present at Yakima is in the form of particulate nitrate. This is especially so during the Persistent Cloud period. Though highly variable for much of the study, there was always sufficient NO_z present to form several $\mu\text{g m}^{-3}$ of nitrate aerosol, if the NO_z had been in the right chemical form. Because of the low temperatures and high ammonia loadings, virtually none of the NO_z would have been gas-phase nitric acid. The particulate nitrate episodes were not solely a result of a greater pool of reactive nitrogen and excess gaseous ammonia being present, but also the result of chemical

and environmental conditions that allowed for nitric acid and particulate nitrate to form more efficiently relative to other compounds.

8.5. Particulate Nitrate Formation Mechanisms

In daytime during summer the major pathway for converting NO_x into particulate nitrate is oxidation of NO_2 by HO radical as illustrated in Figure 8.15.

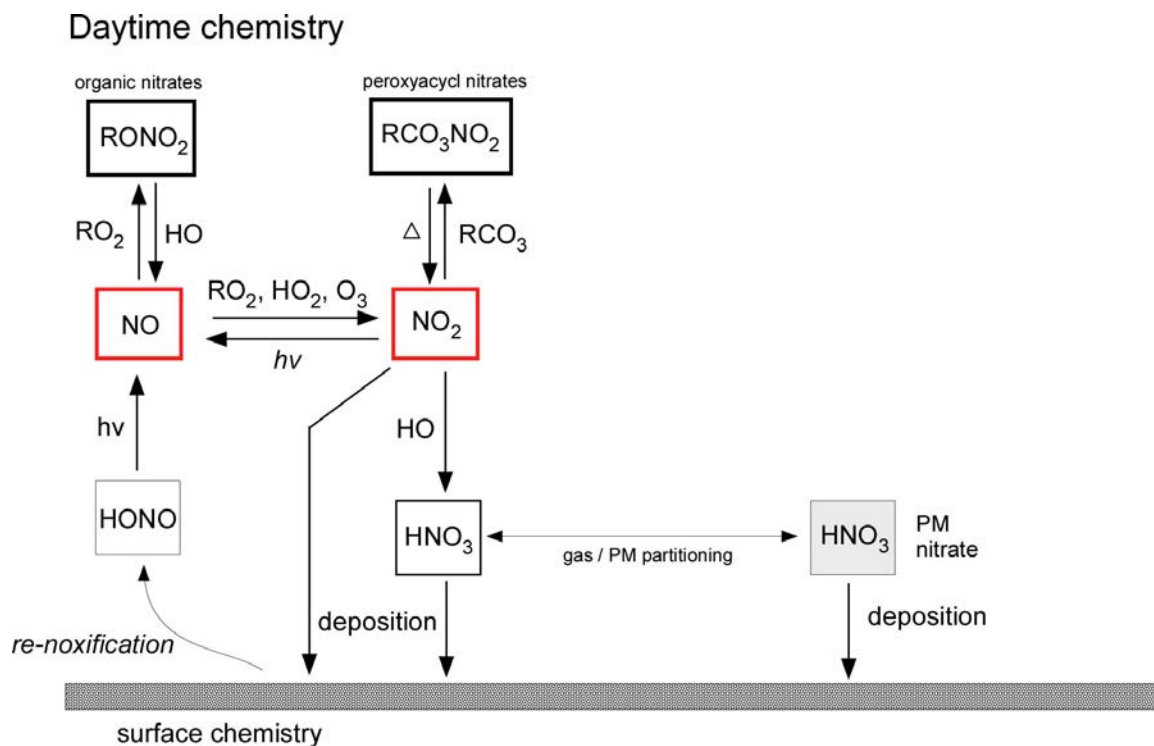


Figure 8.15. Block diagram of major reactions that convert emissions of NO into particulate nitrate during the day: reactive oxides of nitrogen shown by red box and longer lived reservoir species shown by dark black box (organic nitrates, peroxyacyl nitrates).

This rate is expected to be slow since daytime HO radical formation rates will be low owing to low wintertime photolysis rates. The concentration of HO radical will be strongly dependent on light conditions (i.e., the occurrence of cloud, and snow cover) and the concentrations of photolabile HO_x precursor compounds, especially nitrous acid (HONO) and primary aldehyde compounds (glyoxal and formaldehyde).

The Clear Sky period was the sunniest time period and thus the most likely period for daytime oxidation of NO_2 to be significant.

Nighttime chemistry

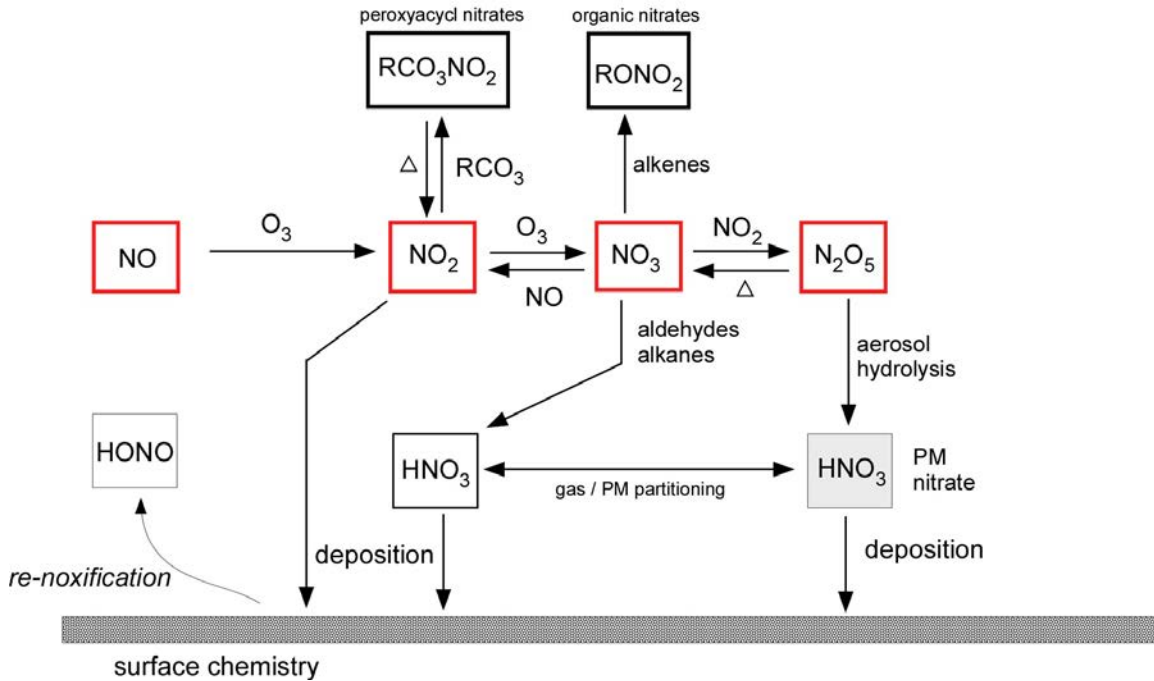


Figure 8.16. Block diagram of major reactions that convert emissions of NO into particulate nitrate during the night: reactive oxides of nitrogen shown by red box (NO , NO_2 , NO_3 , N_2O_5) and longer lived reservoir species shown by dark black box (organic nitrates, peroxyacyl nitrates).

At night two other formation mechanisms of particulate nitrate are possible as shown in Figure 8.16. One mechanism is the hydrolysis of N_2O_5 on particles; the other is reaction of NO_3 radical with aldehydes such as formaldehyde, acetaldehyde and other aldehydes emitted by gasoline and diesel engine exhaust. N_2O_5 is in thermal equilibrium with NO_2 and NO_3 ; lower temperatures shift the equilibrium in favor of N_2O_5 . Significant concentrations of NO_3 don't exist in the daytime due to its rapid photolysis rate in sunlight; the atmospheric lifetime at noon under clear sky conditions during YAWNS is approximately eight seconds. Thus NO_3 chemistry is

only significant at night. The NO_3 radical is rapidly converted back to NO_2 by reaction with NO and significant nighttime concentrations of NO_3 and N_2O_5 are not possible when NO is elevated.

Differences in the meteorological conditions between the Clear Sky and Persistent Cloudy periods likely impacted nighttime concentrations of NO_3 and N_2O_5 . During the Clear Sky period, significant day and night differences in surface heating resulted in strongly varying mixed layer heights that significantly impacted mixing ratios of NO_x and VOCs throughout the day as shown in Figures 8.17 and 8.18. A morning rush hour “peak” is evident in the Clear Sky data; lowest mixing ratios occurred in the afternoon and increased at night. Daytime mixed layer heights discerned by the ceilometer were 400 m on average in the afternoons of 13-15 January, while nighttime heights for this period averaged 135 m. The shallow mixed layer heights at night and early morning led to elevated levels of NO which would inhibit NO_3 concentrations and the N_2O_5 hydrolysis pathway for particulate nitrate formation. During the Persistent Cloud period, there was marked absence of strong diel variations in primary pollutants.

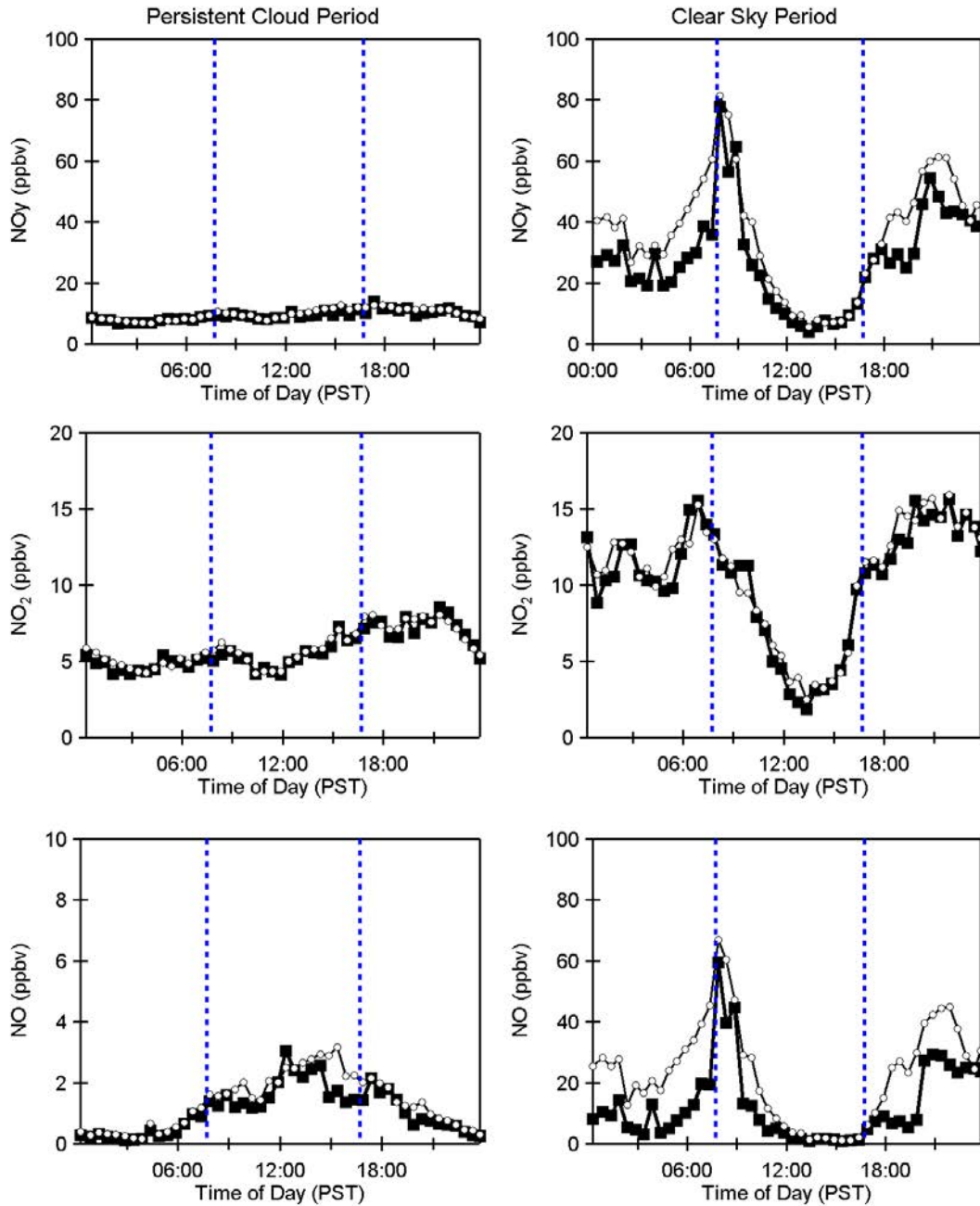


Figure 8.17. Diel variation of NO_y, NO and NO₂, contrasting the Persistent Cloud period on the left hand side with the Clear Sky period on the right hand side. Open circles represent the 30-minute averages and black solid squares the median values. Vertical blue dashed lines represent sunrise and sunset.

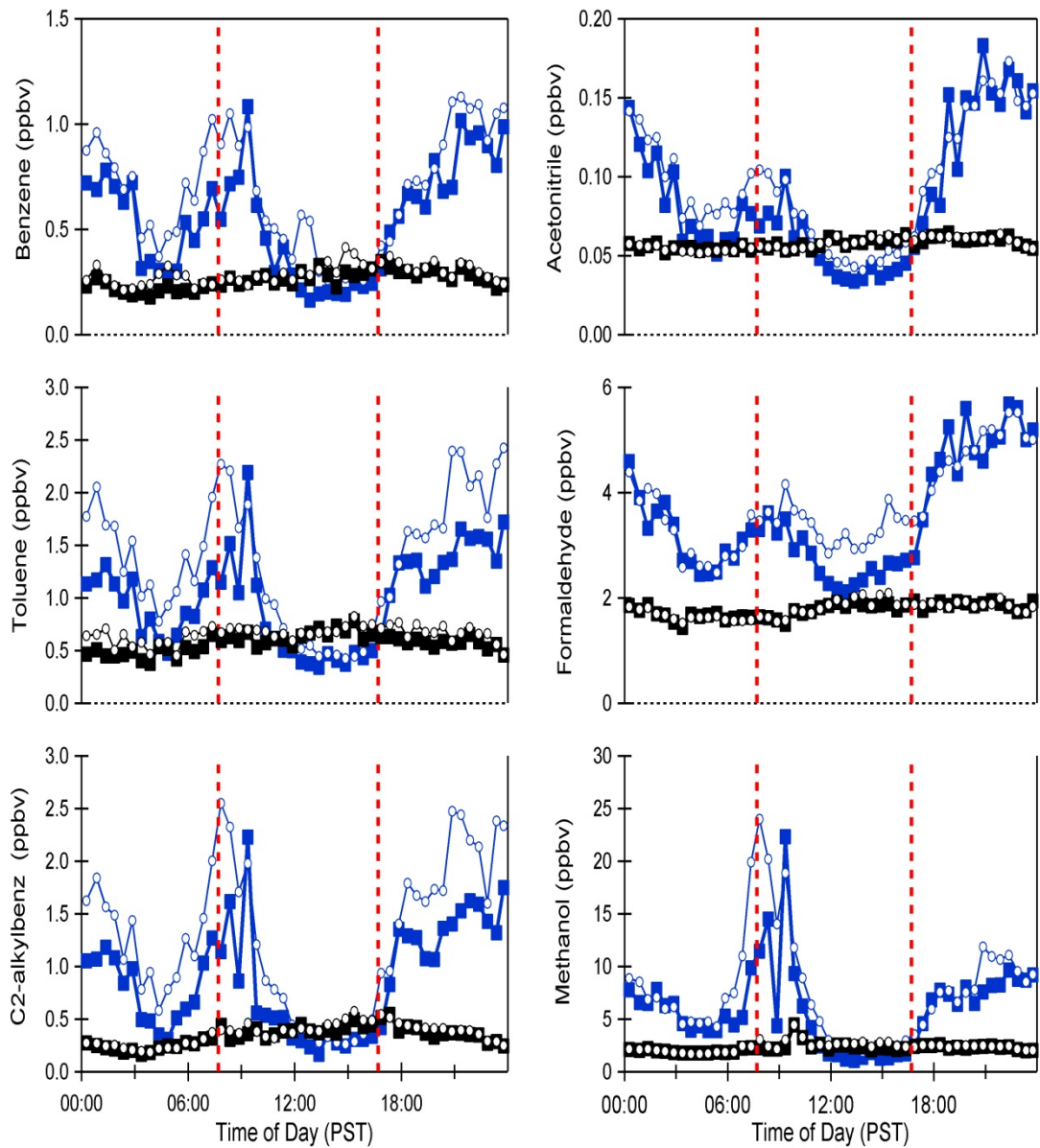


Figure 8.18. Diel variation of selected VOCs, contrasting the Persistent Cloud period in black with the Clear Sky period in blue. Open circles represent the 30-minute averages and solid squares the median values. Vertical red dashed lines represent sunrise and sunset.

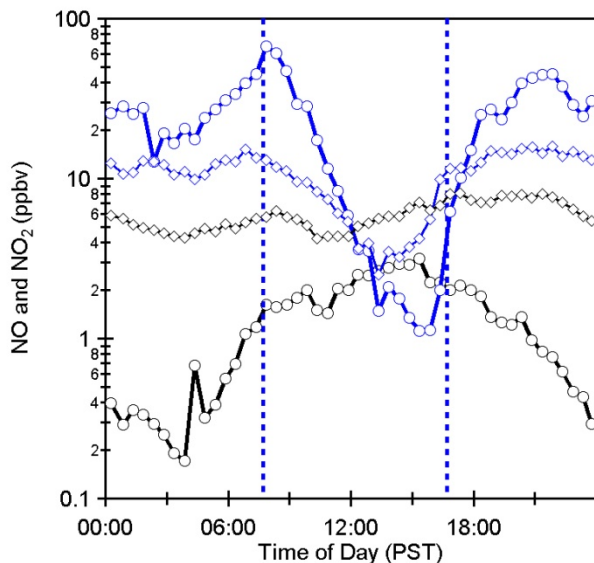


Figure 8.19. Diel variation of 30-minute averages of NO (circles) and NO₂ (diamonds), contrasting the Clear Sky period (blue traces) with the Persistent Cloudy period (black trace). Vertical blue dashed lines indicate sunrise and sunset.

In particular, a very different diel trend was observed for NO. NO mixing ratios were typically less than 1 ppbv at night and slightly greater than 1 ppbv during the day. These nighttime NO mixing ratios were as much as a factor of 100 lower than during the Clear Sky period. In Figure 8.19, NO and NO₂ diel trends for these periods are shown on a log scale to better visualize the large differences in NO mixing ratios observed. The effects of the enhanced nighttime dilution during the Persistent Cloud period can be seen. Additionally, the higher ozone levels during the cloudy period seem to provide an effective oxidation pathway from NO to NO₂. Low nighttime NO mixing ratios and significant NO₂ and O₃ mixing ratios at night in turn likely resulted in higher NO₃ concentrations and formation of nitrate through either N₂O₅ hydrolysis or NO₃ reaction with aldehydes such as formaldehyde.

The diel patterns of PM constituent compounds are consistent with a greater nitrate production during the Persistent Cloud period due to nighttime NO₃ radical

chemistry. Figure 8.20. shows the diel variation of particulate organics, nitrate, ammonium, and sulfate contrasting the Clear Sky period with the Persistent Cloudy period. Median concentrations of nitrate and ammonium were a factor of 2-3 greater throughout the day and night during the Persistent Cloud period while sulfate concentrations were a factor of two greater. Median nitrate concentrations were higher at night and lower in the day for the cloudy period while a clear diel variation pattern was not evident in the clear sky data.

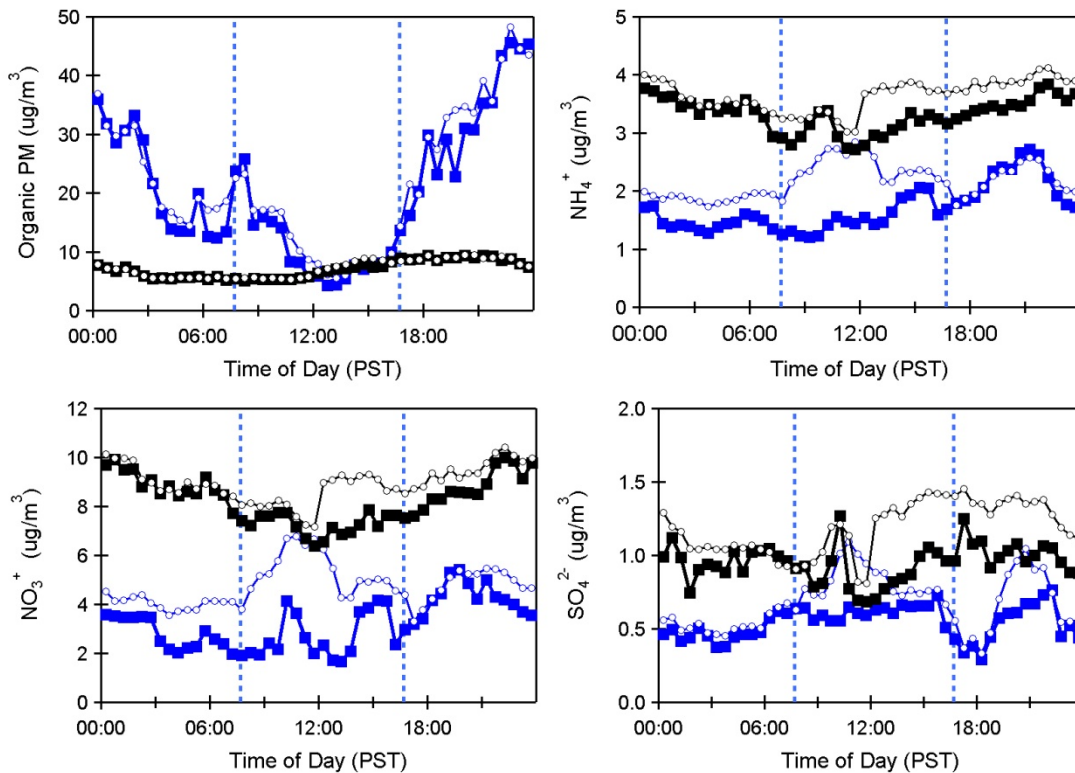


Figure 8.20. Diel variation of organic PM, nitrate, ammonium, and sulfate showing 30-minute averages (open circles) and medians (solid squares) for the Clear Sky (blue trace) and Persistent Cloudy periods (black trace). Vertical blue dashed lines indicate sunrise and sunset.

Organic PM concentrations at night were much higher during the Clear Sky period. Figure 8.21 shows the diel variation of the source factors derived from the

PMF analysis of the HR-AMS organics data. The pattern for OOA looks similar to that of nitrate for the Persistent Cloud period, and there is relatively little difference in OOA between the Clear Sky and Persistent Cloud periods. The observed reduction in organic PM during the Persistent Cloud period was due to a drop in the HOA and BBOA factors. HOA and BBOA show similar patterns as other primary pollutants during the Clear Sky period, with much higher levels overnight when the mixing layer was shallow, and increased dilution during the day. There is clear evidence of a morning peak in HOA during Clear Sky conditions, and a smaller increase in BBOA. During the cloudy period, both HOA and BBOA were low throughout the diel cycle.

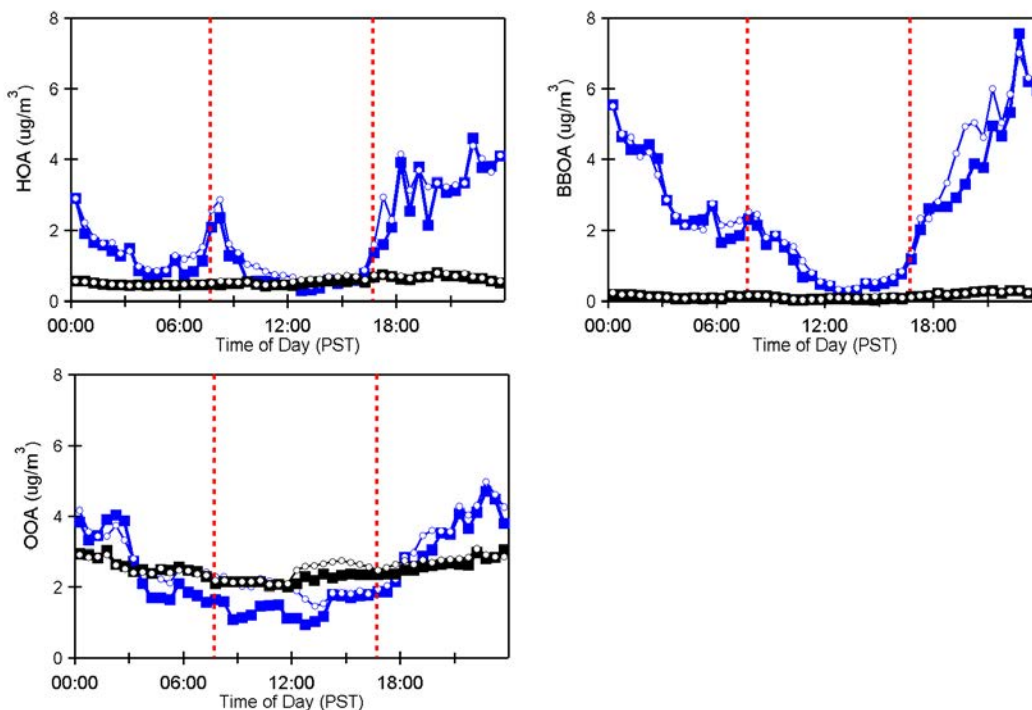


Figure 8.21. Diel variation of source factors derived from the PMF analysis of the AMS organics data. organic Shown are 30-minute averages (open circles) and medians (solid squares) for the Clear Sky (blue trace) and Persistent Cloudy periods (black trace). Vertical red dashed lines indicate sunrise and sunset.

Another interesting feature in the particulate nitrate data occurred during the Stagnation Pollution Episode period, when rapid increases in concentration

occurred after sunrise on the mornings of 14 and 15 January. These are shown in Figure 8.22. Rapid gas-phase production of HNO_3 would not be expected during the early morning hours, yet particulate nitrate concentrations doubled between sunrise and noon. One interpretation of this increase would be that particulate nitrate is increasing due to mixing down from above as the surface inversion breaks. This implies high particulate nitrate concentrations in the residual layer, presumably due to enhanced overnight NO_3 production. The onset of the morning increase in nitrate matches well the increase in surface temperature and odd oxygen ($\text{NO}_2 + \text{O}_3$) and decrease in CO and other primary pollutants.

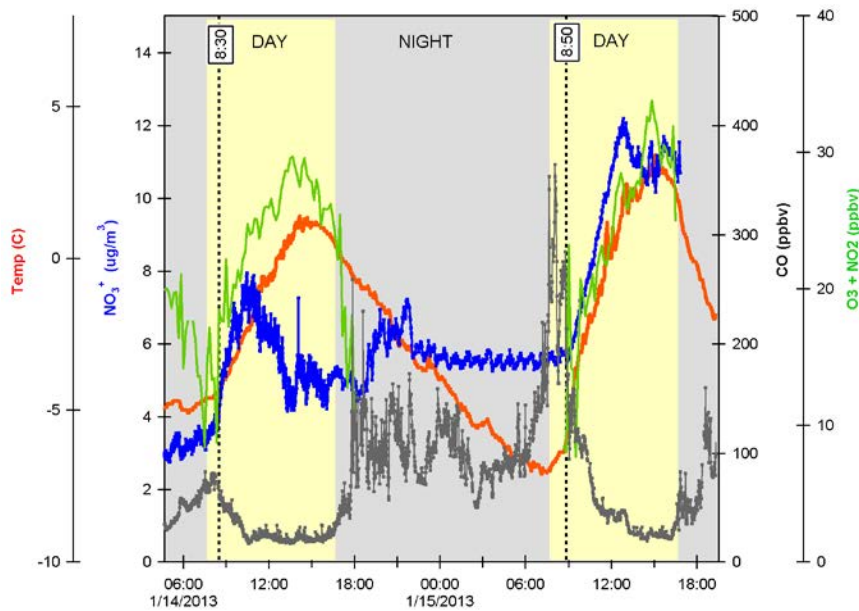


Figure 8.22. Time series of PM nitrate (blue), 10-m temperature (red), CO (black), and odd oxygen ($\text{O}_3 + \text{NO}_2$) for 14-15 January. Yellow shading indicates daylight period between sunrise and sunset. Sudden increase in nitrate in the morning (indicated by dashed lines) coincides with increase in surface temperature, decrease in CO, and increase in odd oxygen ($\text{O}_3 + \text{NO}_2$), suggesting the rapid increase in nitrate in the early day was due to mixing of residual layer air containing elevated levels of PM nitrate to the surface as the surface inversion breaks up in the morning.

8.6. Mixed Meteorology Period

The previous sections highlighted the contrasts between the Clear Sky and Persistent Cloud periods of the YAWNS study. These periods had well-defined meteorological conditions, which allowed some clarity in describing the connections between the meteorological and chemical conditions in the atmosphere as they relate to particulate nitrate formation. However, the atmosphere does not usually conform to such clean patterns. Periods of varying meteorology make pollution events less predictable, and challenge the ability of air quality modelers to forecast pollution events. Even if these events are more difficult to predict, it is worthwhile to describe them when possible to add to the understanding of air quality managers.

One such Mixed Meteorology period followed the Persistent Cloud period during YAWNS. When the low-level cloud layer broke up on 23 January, a period of variable meteorology ensued that was accompanied by elevated $PM_{2.5}$ concentrations until mid-day on 26 January. The time series of major meteorological variables during this period are presented in Figure 8.23. Time series for selected trace gases and the particle number concentration are in Figure 8.24. Time series for the major PM chemical components and the source factors from the PMF analysis of the HR-AMS organics data are shown in Figures 8.25 and 8.26, respectively.

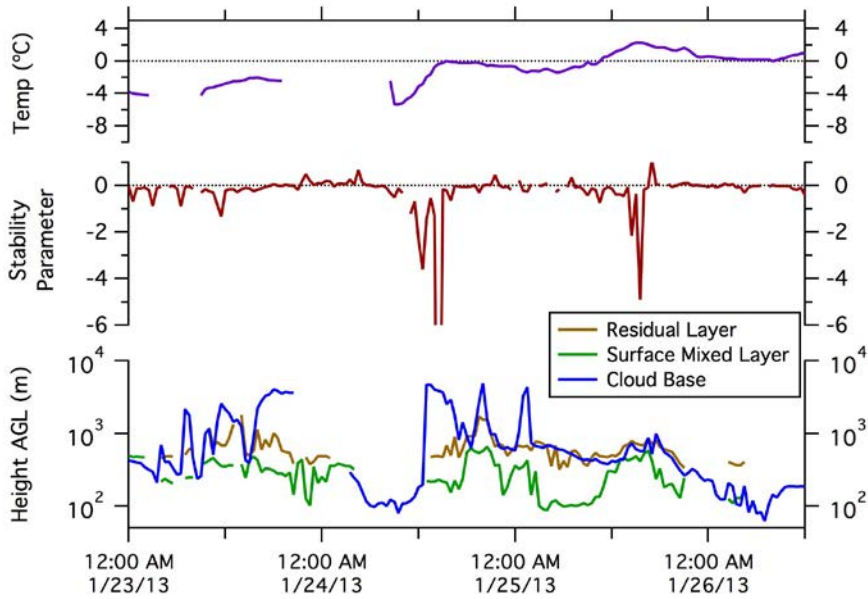


Figure 8.23. Meteorological conditions during the Mixed Meteorology period from 23-26 January. Note that the y-axis on the bottom panel is on a log scale.

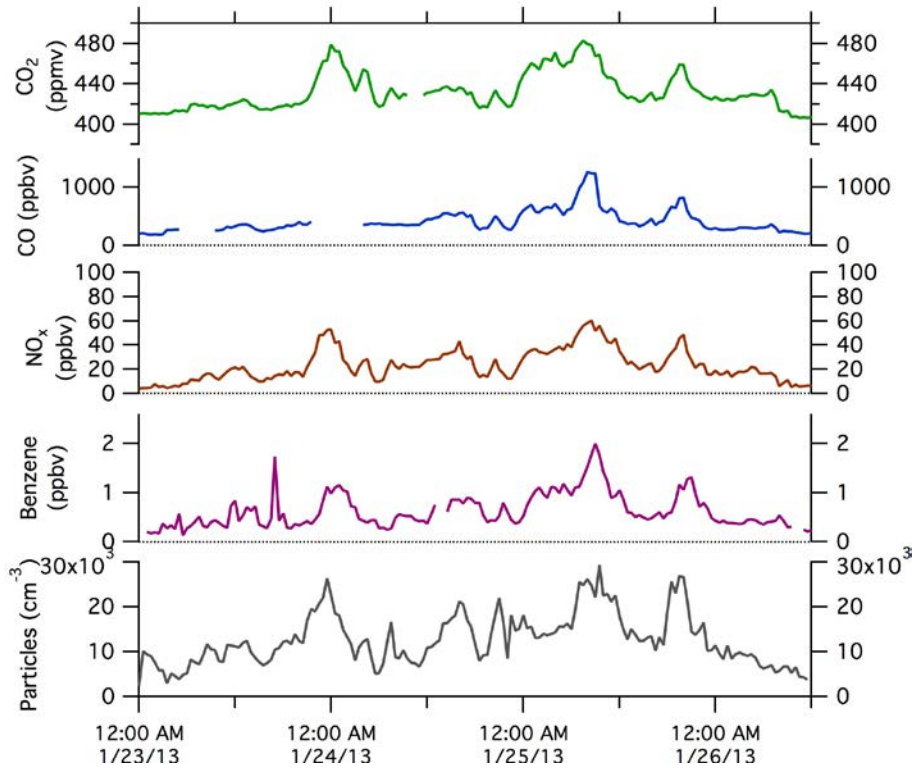


Figure 8.24. Selected trace gas and particle number concentrations during the Mixed Meteorology period.

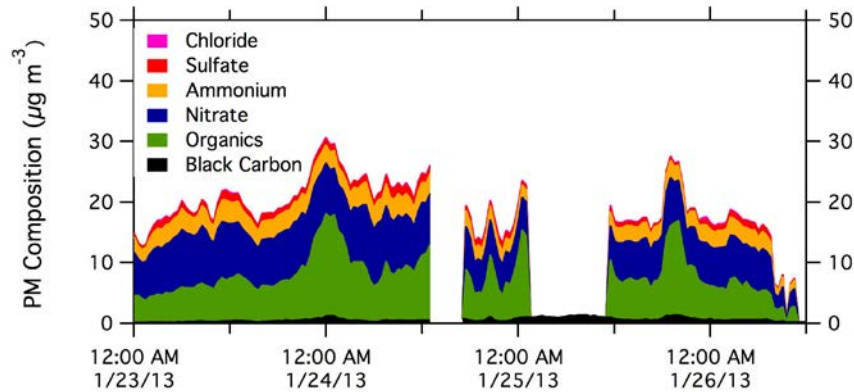


Figure 8.25. Aerosol composition during the Mixed Meteorology period.

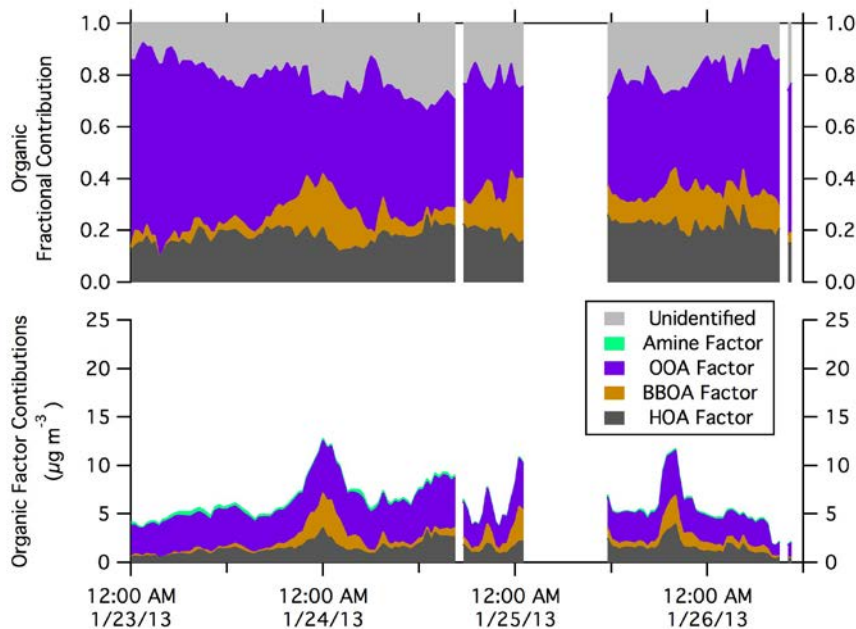


Figure 8.26. Source factors from the PMF analysis of the AMS organics data during the Mixed Meteorology period.

The temperature record for this period shows a gradual warming trend, and mixed upper and lower level clouds. The surface layer was typically neutral or slightly stable during nighttime, with better mixing during the day. The height of the surface mixed layer and the residual layer were more variable, ranging from less than 100 m to more than 1000 m based on the ceilometer output. Unlike during the Clear Sky period, the lowest mixed layer heights did not typically occur overnight

during this Mixed Meteorology period. Consistent with the meteorology, the trace gas and particle number concentrations were highly variable during this period, but did not exhibit a clear diel trend. Concentrations tended to be high when the surface mixed layer was shallow, and vice versa.

The PM concentrations during the Mixed Meteorology period were generally high, and secondary species were dominant. The total measured mass ranged between 10 and 30 $\mu\text{g m}^{-3}$, and followed the same general temporal trends as the trace gas species. Inorganic constituents (nitrate, sulfate, and ammonium) comprised roughly half of the observed PM, and organics and black carbon comprised the other measured half. From the PMF analysis of the organic PM, it was found that most was oxidized organic aerosol (presumably SOA). HOA comprised ~20% of the organic aerosol. BBOA made only a small contribution in the mornings and early afternoons during this period, but had greater contributions during evening and at night.

8.7. Sources of NO_x

Yakima County emits approximately 1800 total tons of NO_x during the winter season (December, January and February), or 20 tons per day (Washington Department of Ecology, 2014). The breakdown of these emissions by source type is summarized in Figure 8.27. In winter, 80% of the total NO_x emissions are from on-road vehicles, with 2/3 of that amount from gasoline vehicles and the other 1/3 from diesel vehicles. Residential burning accounts for 5% of the NO_x emissions in Yakima County, but only 1% of the total NO_x emissions are from wood stoves.

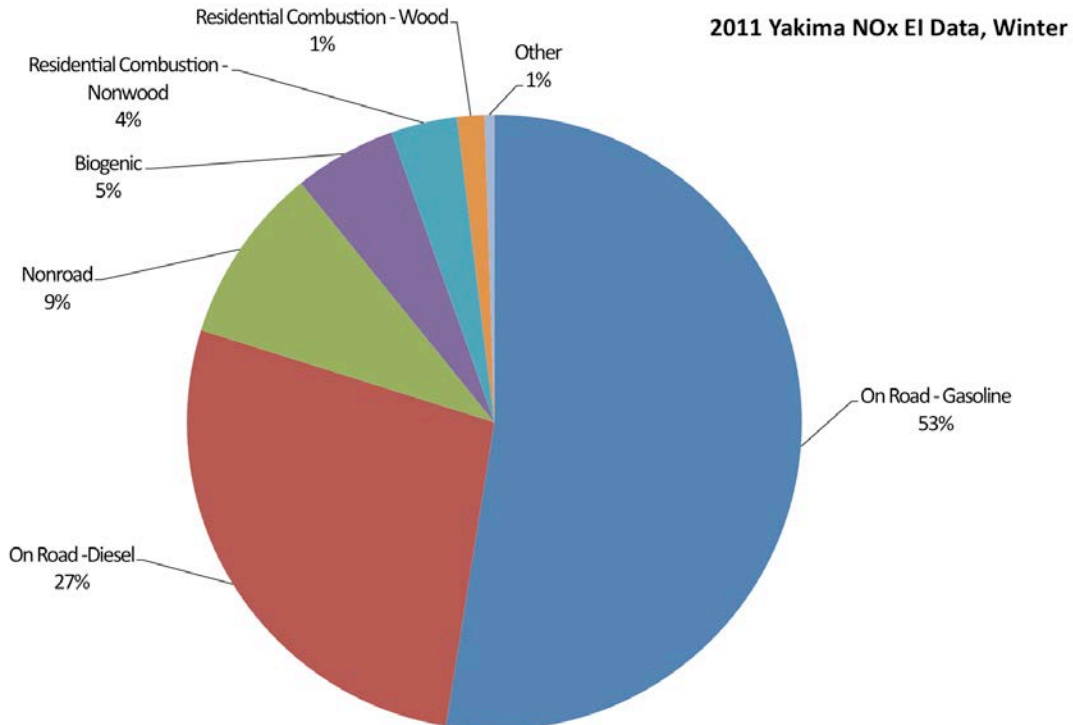


Figure 8.27. Winter season NO_x emissions contributions by source for Yakima County, from the 2011 Washington Comprehensive Emissions Inventory.

On-road vehicle emissions were estimated in the inventory using EPA's Motor Vehicle Emission Simulator (MOVES) model. MOVES was developed to provide an accurate estimate of emissions from mobile sources under a wide range of user-defined conditions. The MOVES model includes a default database that defines vehicle and fuel characteristics, emissions control programs, meteorological information, and other parameters that affect vehicle emissions. Default data may be replaced by local data. The Washington Department of Ecology used Washington and Yakima County data to replace several of the parameters, thus improving the estimates for Yakima County. Local data were used for fleet age and composition, vehicle counts, fuel characteristics, amount of miles traveled by vehicle and roadway type, and Washington's adoption of California vehicle engine standards.

Non-road emissions were calculated with EPA's NONROAD model. NONROAD is much simpler than MOVES, requiring few user inputs. Local fuel parameters and temperatures were used in calculating emissions for Yakima County. Locomotive emissions were included in the non-road inventory. Locomotive emissions were calculated using information from the rail companies and EPA. Biogenics data was taken directly from EPA calculations. Although still in draft format, detailed information on the biogenics calculations may be found in the 2011 National Emissions Inventory Technical Support Document (US EPA, 2013a). Several residential burning categories that excluded wood burning were estimated. These include household waste, leaf, and brush burning. The calculations used local population data paired with EPA emission factors to estimate emissions in Yakima County.

8.8. Sources of Ammonia

The Washington State 2011 Comprehensive Emissions Inventory reports that the total emissions of ammonia in Yakima County during winter (December, January and February) are approximately 1500 tons, or 16.7 tons per day (Washington Department of Ecology, 2014). The breakdown of these emissions by source category is shown in Figure 8.28. The great majority of the ammonia emissions, 97%, are associated with agricultural activities. Livestock, primarily for dairy production, accounts for 94% of the total emissions and fertilizer use an additional 3%. The emissions from these activities are the major cause of the elevated ammonia concentrations observed in Yakima during winter.

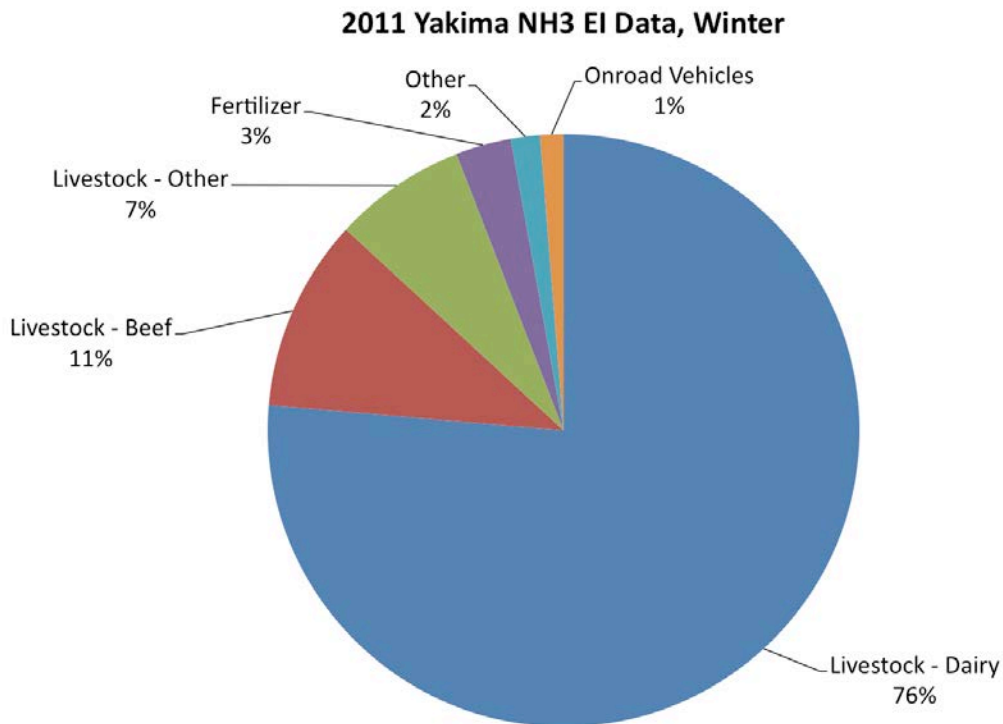


Figure 8.28. Winter season NH₃ emissions contributions by source for Yakima County, from the 2011 Washington Comprehensive Emissions Inventory.

In the emissions inventory, local cattle population data from the Washington State Department of Agriculture (WSDA) and US Department of Agriculture (USDA) were used with emission factors from the Carnegie Mellon University (CMU) Ammonia Model v.3.6 to estimate emissions from dairy and beef cattle (Pinder et al., 2004). An EPA seasonal profile used in their Clean Air Interstate Rule modeling platform was used to allocate emissions to each season: 13% of emissions to winter, 33% spring, 27% summer, and 28% fall. Other livestock emissions were taken from version 1 of EPA's 2011 National Emissions Inventory (US EPA, 2013a). Fertilizer emissions were calculated using WSDA's annual fertilizer tonnage report and emission factors from the CMU Ammonia Model v.3.6. It is noted that a study done by WSU at the Knott Dairy farm at WSU measured ammonia under different

meteorological conditions (Rumburg et al., 2005). Temperature, precipitation, and wind speed influenced observed emissions. Generally, emissions were higher than those calculated with the CMU model.

The possibility of additional ammonia contributions from leakage from large-scale industrial chillers in Yakima was also investigated. Large amounts of ammonia are typically stored onsite at chilling facilities for use as a refrigerant. To evaluate whether leakage from chiller operations could contribute significantly to ambient ammonia concentrations in Yakima, the Emergency Planning and Community Right-to-know Act (EPCRA) database was consulted to locate all of the large chiller facilities in Yakima. Fifty-four such facilities were found with Yakima addresses. Since particulate ammonium nitrate is a secondary pollutant that forms over relatively long time scales, the main question with respect to these chiller facilities was whether they might cumulatively be contributing substantially to ambient NH_3 concentrations in the Yakima area.

To investigate this, the US EPA AERSCREEN model (US EPA, 2013c) was used to determine how possible leaks from a single facility would disperse downwind under stagnant conditions. AERSCREEN produces worst case hourly concentrations from a single source, by making very conservative assumptions about pollutant dispersion. NH_3 leakage was modeled as a non-buoyant (-30 °C) ground level point source with negligible vertical velocity. Surrounding terrain was assumed to be flat and located in an urban area.

There is no record of persistent complaints of ammonia odors from the communities near these chiller facilities. From this, it was assumed that the maximum ammonia concentrations –if any substantial leaks do occur- must be below the human odor threshold of 5 ppmv (US EPA, 2001). The emission rate fed into AERSCREEN was adjusted until the highest downwind concentration predicted by AERSCREEN was just below 5 ppmv. Figure 8.29 shows how downwind NH₃ concentration decreases with distance from the facility.

The chiller located nearest to the YAWNS site was approximately 2.6 km away. At this distance downwind of the leak source, ambient NH₃ is predicted to be 0.018 ppbv. Although other chillers are further away and thus likely to impact the YAWNS site even less, if we conservatively assume that each chiller operation contributes 0.018 ppbv NH₃ at the YAWNS site- most likely a gross overestimate- then the 54 facilities would collectively contribute 0.97 ppbv total to the ambient ammonia mixing ratio. Considering that on high ammonia days 12 ppbv of ammonia was measured during the YAWNS campaign, it is highly unlikely that ammonia leaks from chiller facilities are a significant source of ammonia during stagnation episodes, even under a worst-case scenario.

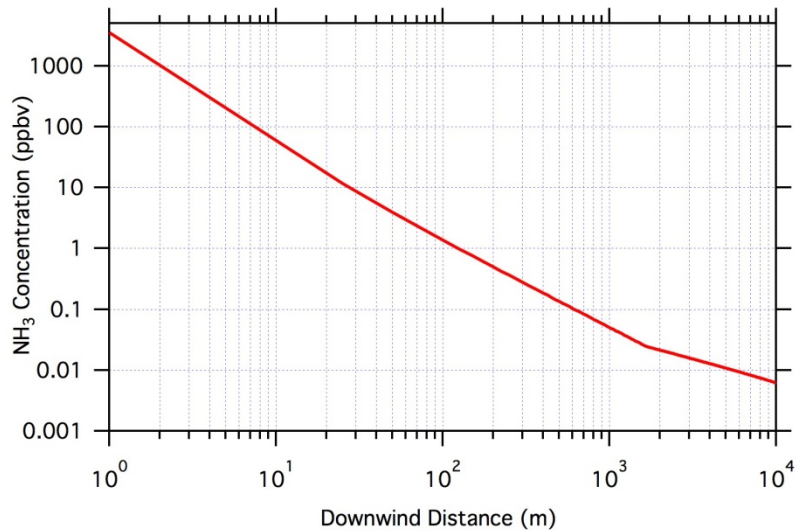


Figure 8.29. AERSCREEN modeled downwind dispersion of fugitive emissions from large-scale industrial coolers. Axes are in log scale. Source strength was scaled such that the maximum concentration was below the olfactory limit.

8.9. Intervalley Pollution Transport

Another possible cause of the PM pollution in the Yakima area is transport of polluted air from the Tri-Cities area via the lower Yakima Valley. The secondary YAWNS measurement site in Toppenish was established to investigate this possible connection; if polluted air was being transported toward Yakima via the lower Yakima Valley, that air would pass over Toppenish en route.

The paired time series for PM_{2.5} at Yakima and Toppenish were shown in Figure 4.5, and are presented again here (Figure 8.30). Particulate mass concentrations were similar at the two sites for much of the YAWNS study period, though after 26 January the trends at the two sites diverged. The Clear Sky and Persistent Cloud periods identified at Yakima seem to have been present at Toppenish as well. There is no indication that changes to particulate levels at Toppenish preceded increases at Yakima as would be expected if lower-to-upper

valley transport were a major influence. A scatter plot of the simultaneous $PM_{2.5}$ concentrations for the two sites is shown in Figure 8.31. A linear fit between the data sets shows a moderately strong correlation ($r^2 = 0.51$).

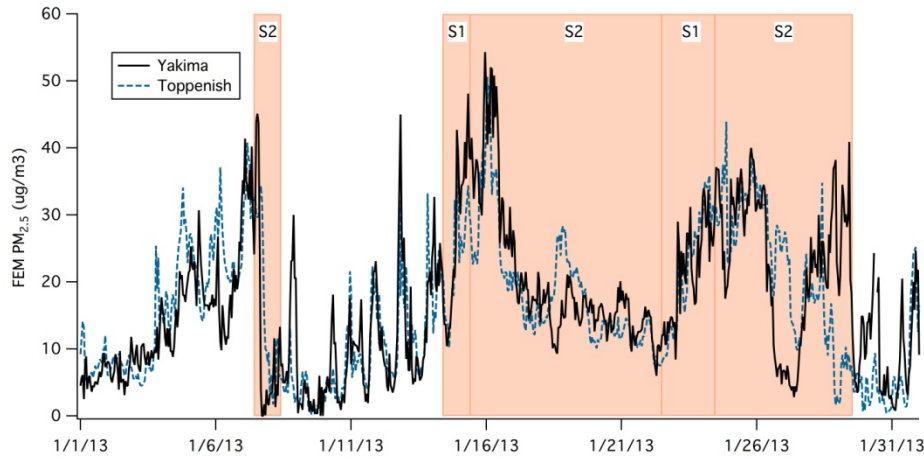


Figure 8.30. Time series of $PM_{2.5}$ concentrations during January 2013 at Yakima (black solid line) and Toppenish (blue dashed line).

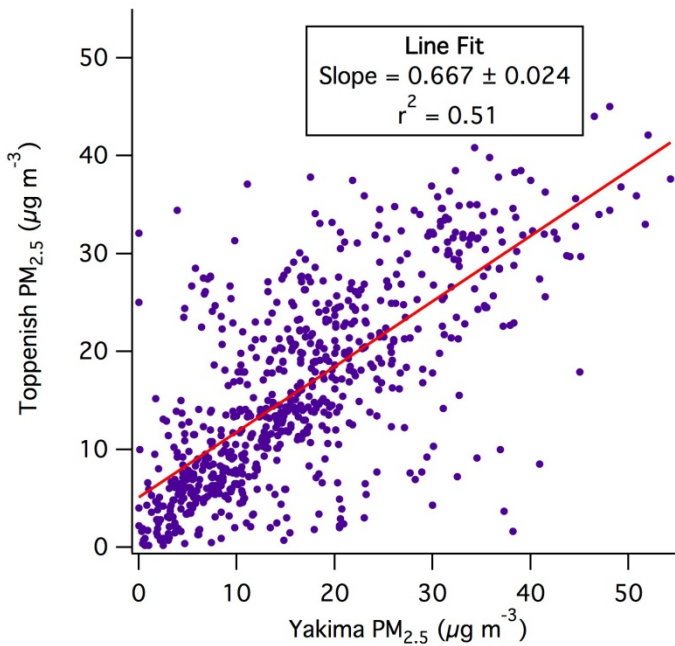


Figure 8.31. Scatterplot of the hourly $PM_{2.5}$ concentrations at Yakima and Toppenish in January 2013.

The correlation between the particulate mass concentrations at Yakima and Toppenish suggest that the same regional meteorological and chemical conditions

are influencing both sites, but there is not strong evidence that the conditions are a result of pollutant transport between the two sites. At Union Gap, one of the few gateways for surface transport between the two valleys, winds did not exhibit flow patterns consistent with intervalley transport in either direction in the hours preceding any PM_{2.5} pollution episodes. The CO and NO_x data sets for the two sites provide further evidence for this conclusion. Scatterplots for these species at Yakima and Toppenish during YAWNS are presented in Figures 8.32 and 8.33 for CO and NO_x, respectively. Correlations for these species were somewhat lower than for PM_{2.5}, suggesting less regional influence on their concentrations (and thus more local influence). The slopes for these comparisons (Toppenish/Yakima) are also significantly less than one, indicating that Yakima consistently had higher NO_x and CO concentrations than did Toppenish. This implies that little of the NO_x and CO observed at Yakima was the result of intervalley transport.

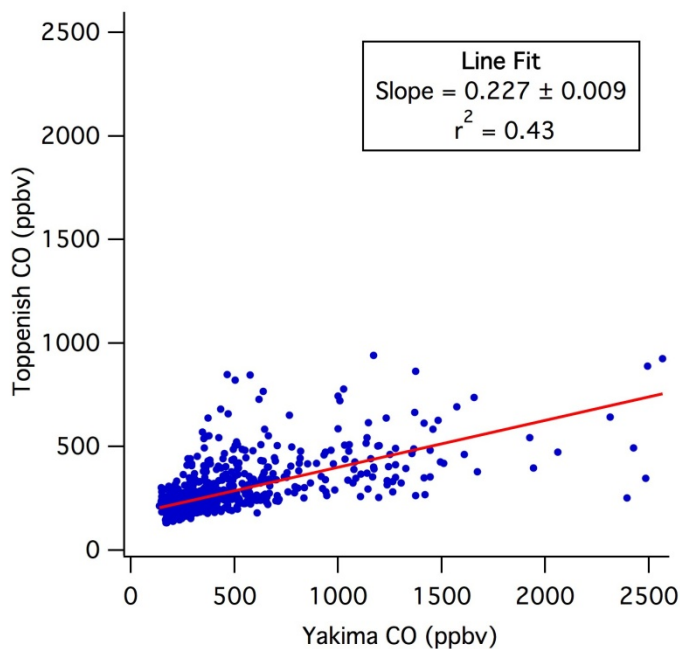


Figure 8.32. Scatter plot of CO concentrations at Yakima and Toppenish during the YAWNS study period. Each marker represents a pair of 30-min averaged concentration measurements.

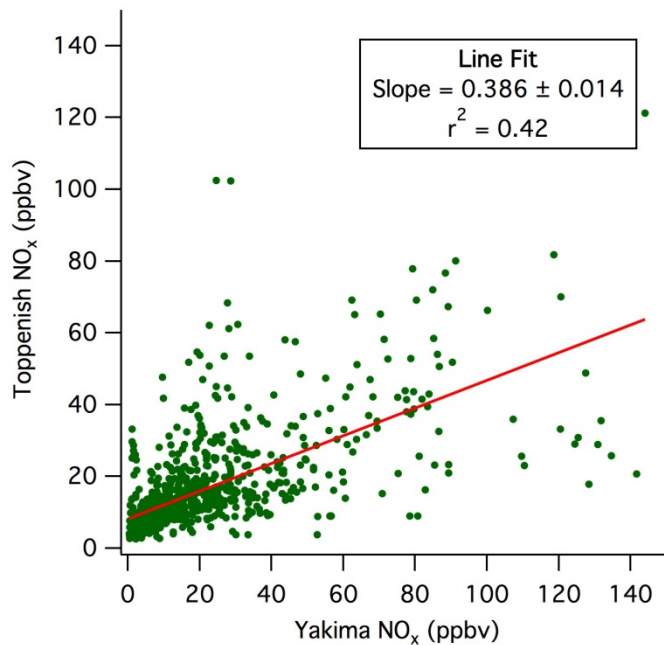


Figure 8.33. Scatter plot of NO_x concentrations at Yakima and Toppenish during the YAWNS study period. Each marker represents a pair of 30-min averaged concentration measurements.

The CO/NO_x ratios observed at Yakima (Figure 8.34) and Toppenish (Figure 8.35) provide additional evidence that intervalley pollution transport is relatively unimportant. CO and NO_x concentrations were higher in Yakima than in Toppenish, but the ratio of CO/NO_x was also much larger. The study-average ratio for Yakima was 14.2 ($r^2 = 0.92$) and for Toppenish it was 7.5 ($r^2 = 0.78$). As discussed by Wallace et al. (2012), lower ratios are more consistent with vehicle running emissions; the observed ratio is likely influenced by vehicle emissions from the major roadways near the Toppenish site. Wood stove emissions and vehicle cold-start emissions have higher CO/NO_x ratios; these sources appear to have a greater influence on local air pollutant concentrations in Yakima. Again, the implication is that the atmospheric environment at Yakima is not heavily influenced by intervalley transport.

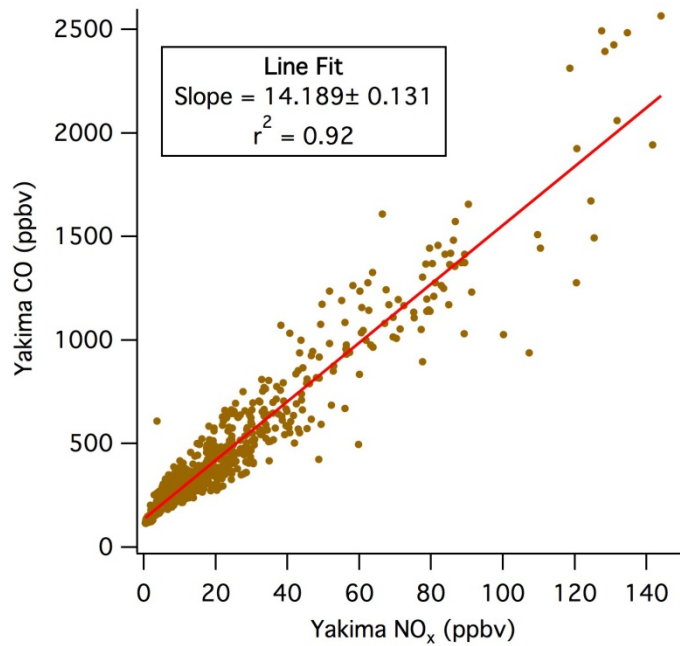


Figure 8.34. Scatter plot of CO and NO_x at Yakima, based on 30-minute averaged data. Results indicate an average CO/NO_x ratio of 14.2.

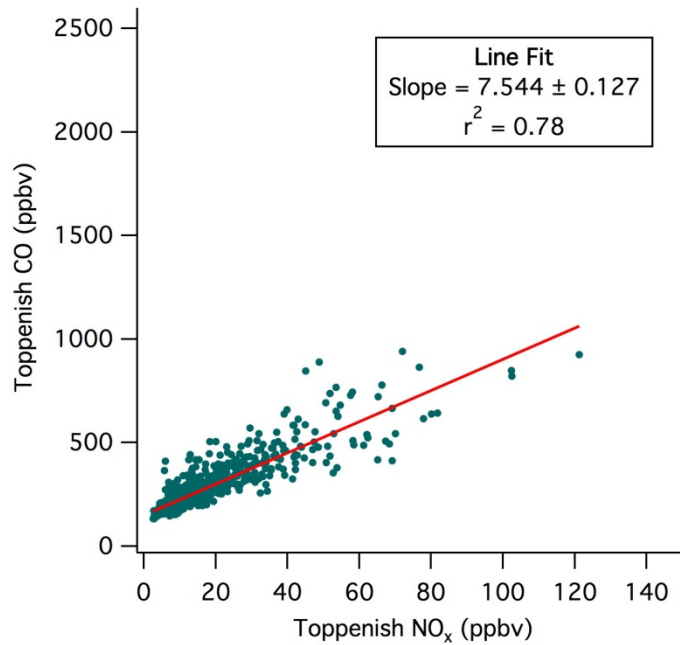


Figure 8.35. Scatter plot of CO and NO_x at Toppenish, based on 30-minute averaged data. Results indicate an average CO/NO_x ratio of 7.5.

8.10. Representativeness of Results

The particulate pollution levels observed during YAWNS are broadly consistent with the patterns measured at the location in previous years, both in terms of the total $PM_{2.5}$ (Figure 8.36) and its compositional split (Figure 8.37). The latter data are consistent in spite of being collected with different sampling and analytical methods.

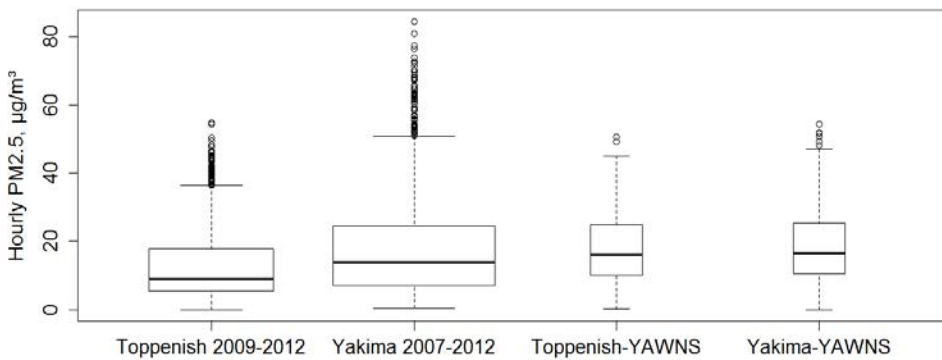


Figure 8.36. Comparison of hourly $PM_{2.5}$ data during YAWNS and the last several Januarys. Box widths are proportional to the number of data points.

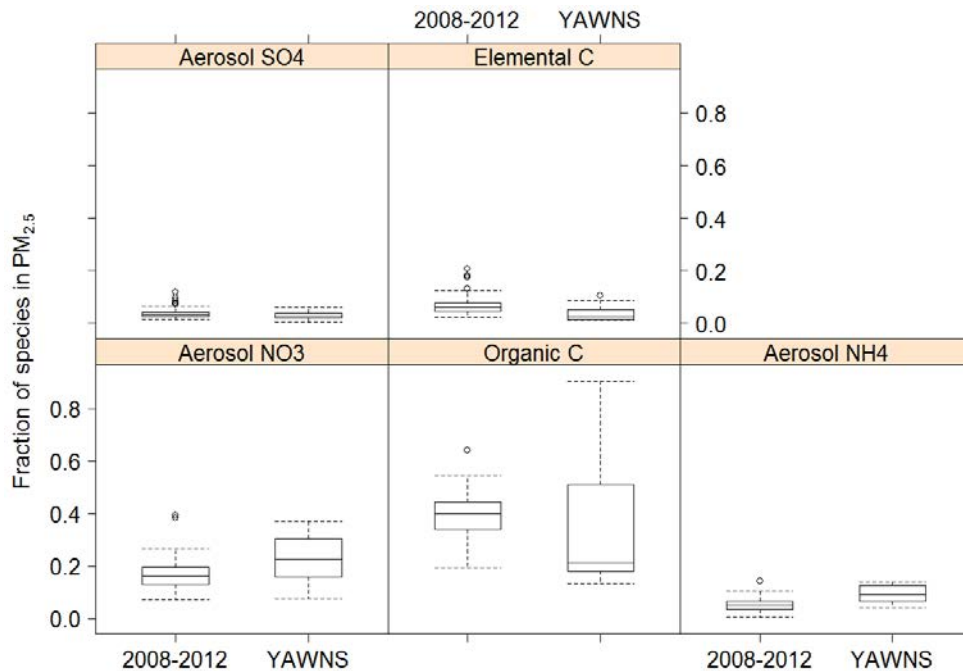


Figure 8.37. Comparison of $PM_{2.5}$ composition during YAWNS and the last several Januarys. YAWNS data were averaged over 24 hours to compare with previous speciation data.

The period of persistent cloud during YAWNS was not a rare meteorological occurrence. An examination of historical meteorological data collected at the Yakima airport shows that similar multi-day episodes occur intermittently. Table 8.2 lists periods of persistent wintertime cloud since 2000. Events are included when the 48-hour running relative standard deviation of relative humidity and temperature were each less than 5% for at least four consecutive days. These days also coincided with times when cloud bases were at their lowest. There were several additional instances when the same criteria were met for two or three successive days. Simultaneous PM_{2.5} and CO data were available for one of these episodes; these data are shown in Figure 8.38.

Table 8.2. Periods of persistent wintertime cloud in Yakima since 2000.

Month	Duration, days
December 2000	8
November 2002	6
January 2003	4
January 2004	8
December 2004	4
November 2005	4
January 2009	4
December 2009	4
November 2012	4
January 2013 (during YAWNS)	6

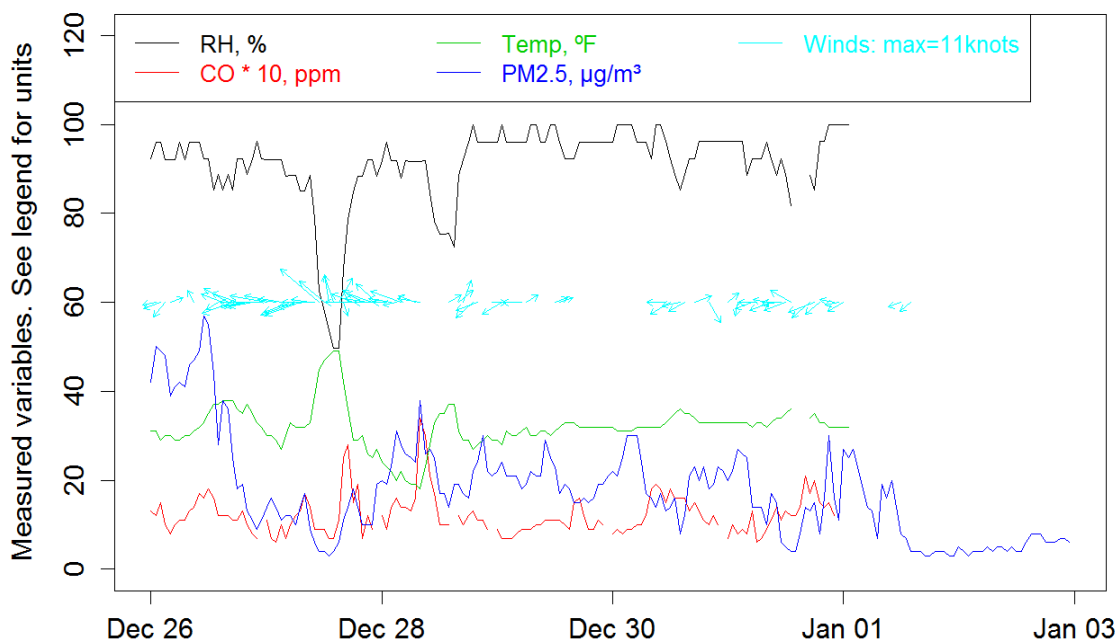


Figure 8.38. Persistent cloud in Yakima between 28 December 2004 and 1 January 2005.

The CO monitor was situated at an intersection for monitoring traffic emissions, and does not necessarily represent ambient CO concentrations at the PM_{2.5} monitor. Still, nighttime median CO concentrations during these days (when there is low traffic influence) were about 0.5 ppm lower than the overall December 2004 nighttime medians. Similarly, PM_{2.5} levels in Yakima remain slightly elevated for about two days during this episode. Winds meander, and temperature and RH show little diurnal variation for approximately three days. This pattern is similar to that observed during the Persistent Cloud period of YAWNS.

Overall, PM_{2.5}, speciation and meteorological data suggest that measurements made during YAWNS were representative of conditions encountered in the past several winters in the Yakima area. It is more difficult to assess whether the PM composition found in Yakima is representative of other parts of eastern Washington. PM_{2.5} speciation data in the region are somewhat sparse. Data from the

IMPROVE network monitor at Wishram, Washington shows elevated particulate nitrate fractions in wintertime $PM_{2.5}$. IMPROVE data from White Pass, Snoqualmie Pass, Pasayten, the Spokane Tribe, all in Washington, do not. Neither do historical speciation data from Spokane, Washington and La Grande, Oregon. A recent source apportionment study for urban areas in the Pacific Northwest (US EPA Region 10, 2013) highlights Boise and Salt Lake City as two other cities with significant particulate nitrate concentrations during winter. These cities are larger, but are located in valley topographies like Yakima; in each city nitrate comprises nearly 50% of the $PM_{2.5}$ during wintertime pollution events, with organic material making up much of the rest. Also like Yakima, Boise and Salt Lake City each have significant sources of ammonia nearby. The parallels between these cities suggest that comparative studies may be a fruitful approach for understanding how chemical and meteorological processes interact to produce elevated PM levels in each region.

9. Summary and Future Plans

Episodes of elevated particulate nitrate in the Yakima Valley during winter result from a combination of factors. The wintertime meteorology of the region drives gas-particle equilibrium of ammonium nitrate strongly toward the particle phase, and high relative humidity enhances this effect. High ammonia emissions from agricultural sources in the area lead to elevated atmospheric concentrations of the pollutant. This excess ammonia drives virtually all available nitric acid into the particulate phase, forming particulate nitrate, and leads to a condition where any additional nitric acid production would lead directly to greater particulate nitrate levels. The production of particulate nitrate precursors is complicated and sensitive to the varying meteorological and chemical conditions in the valley. Given the backdrop of excess gaseous ammonia, there is usually sufficient reactive nitrogen in the valley to produce elevated levels of particulate nitrate if the right meteorological conditions take hold.

Two distinct meteorology conditions were observed where nitrate levels were elevated. Under clear sky conditions, rapid increases of particulate nitrate in the morning after sunrise on 14 and 15 January suggest that particulate nitrate had formed in the residual layer and was being mixed down to the surface. During the period where a persistent cloud-capped boundary layer was present, particulate nitrate remained moderately elevated through the day and night. In this case it appears likely that surface emissions are mixed through the depth of the cloud-capped boundary layer day and night, with the boundary layer height determined by

cloud top height. This condition facilitates particulate nitrate formation by keeping nighttime NO mixing ratios low, which promotes formation of NO₃ radical at night. Particulate nitrate could then be formed either from the uptake of N₂O₅ and subsequent hydrolysis onto existing particles or from partitioning of gas-phase nitric acid produced from NO₃ + aldehyde reactions. Given the measured abundance of NH₃ and cold temperatures, gas-phase HNO₃ mixing ratios are expected to be low and the formation of particulate nitrate is limited by the availability of HNO₃.

Little evidence was found that pollution in Yakima is significantly impacted from regional transport via the Lower Yakima Valley. While meteorological conditions and PM_{2.5} levels were typically similar at Yakima and Toppenish, the levels of NO_x and CO indicated clearly that Yakima air quality was dominated by local sources. Additionally, it was found that the YAWNS study period was broadly representative of the typical wintertime meteorology and air quality conditions at Yakima. While not previously described in detail, persistent cloudy periods occur occasionally and have a clear impact on local air quality. Furthermore, the air quality in Yakima itself is consistent with other regional cities with a similar mix of emissions sources. In general, when elevated ammonia concentrations from agriculture mix with urban NO_x emissions in winter, elevated particulate nitrate is common.

9.1. Air Quality Management Implications

- Ammonia emissions reductions are unlikely to result in significant reductions in wintertime particulate nitrate unless order-of-magnitude reductions are viable. As it stands, the ammonia levels in winter are high enough that all available nitric acid is driven to particulate nitrate.
- The pathway to reducing the available nitric acid / particulate nitrate pool is not obvious. Particulate nitrate is the major atmospheric endpoint for NO_x , so ultimately NO_x reduction would reduce the potential particulate nitrate pool. However, NO also inhibits the formation of particulate nitrate by destroying the nitrate radical, which is an important intermediate species. Therefore it is entirely possible that a local NO_x reduction would skew the local atmospheric chemistry toward more local particulate nitrate production. A numerical modeling effort is required to determine the specific system behavior.
- During the persistent cloud conditions, mixing occurs throughout the cloud layer and perhaps beyond, resulting in reduced levels of some pollutants, including primary PM. While a reduction in the relative contribution wood smoke to organic PM is apparent during burn bans, calling or continuing burn bans during persistent cloud conditions might be less critical than during clear sky stagnation events. However, in addition to reducing exposure to the direct wood smoke emissions, burn bans may also reduce exposure to secondary organic aerosol. SOA in Yakima is thought to originate, in part, from the processing of wood smoke PM throughout the mixed layer.

- The cloud-capped condition is linked to elevated secondary PM levels. Thus the onset of cloud shifts the type of PM present, but elevated concentrations would still be expected to be associated with the meteorological condition.
- During YAWNS, burn bans appear to have been called at the correct times in Yakima, especially during clear sky and mixed meteorological conditions. The potential for elevated pollution was anticipated for the clear-sky stagnation period. During mixed-meteorology periods, forecasting remains a challenge. It may be possible to adjust responses to anticipate the likely increased mixing associated with persistent low-level cloud. While meteorological models do not reliably predict such cloudy periods, once they set in they are clearly identifiable. It may be possible to relax policy responses more confidently when persistent cloud is accompanied by slight reductions in the observed PM_{2.5} levels.

9.2. Recommendations for Additional Study

- One key question arising from this work is the frequency of persistent cloud episodes in the valleys of Washington State, and whether this meteorological condition consistently results in enhanced dilution of primary pollutants. The meteorological question could be explored using a data mining approach with the extensive meteorological sensor networks available in the state. The air quality link is more challenging; to study this would likely require the deployment of a network of reliable low-cost sensors for a representative primary pollutant such as CO.

- The chemical processing within the Yakima Valley that leads to enhanced particulate nitrate formation under certain conditions remains unclear and should be explored further. The vertical profiles of key species for both daytime and nighttime, and clear and cloudy conditions is key. This effort could be initiated using a 1-D vertical chemical model where the appropriate meteorology is proscribed. The study would be greatly enhanced by the availability of additional surface and vertical profile measurements of the key chemical species, including HNO_3 and N_2O_5 .
- The YAWNS data set provides an invaluable basis for evaluating the AIRPACT-4 modeling framework under wintertime conditions. It is anticipated that air quality predictability will prove poor during the Persistent Cloud period due to inadequate performance of WRF, the underlying meteorological model. The model performance test would be more appropriate during other portions of the study. An AIRPACT-4 study could also examine the potential effectiveness of various particulate nitrate reduction strategies. The sensitivity of particulate nitrate levels to ammonia versus NO_x control could be evaluated in this manner.
- Effectively forecasting air quality during clear sky stagnation and low-level cloud conditions requires accurate modeling of the surface mixing layer. WRF at a 4-km resolution is currently unable to adequately represent persistent cold air pools, making reliable air quality forecasts challenging. There are ongoing research studies in the intermountain west to better understand the meteorology of persistent cold air pools. Progress would be

significantly enhanced if the parallel meteorology and air quality research efforts could be merged.

10. References

Aiken, A. C., de Foy, B., Wiedinmyer, C., DeCarlo, P. F., Ulbrich, I. M., Wehrli, M. N., Szidat, S., Prevot, A. S. H., Noda, J., Wacker, L., Volkamer, R., et al.: Mexico city aerosol analysis during MILAGRO using high resolution aerosol mass spectrometry at the urban supersite (T0) – Part 2: Analysis of the biomass burning contribution and the non-fossil carbon fraction, *Atmos Chem Phys*, 10(12), 5315–5341, doi:10.5194/acp-10-5315-2010, 2010.

Aiken, A. C., Salcedo, D., Cubison, M. J., Huffman, J. A., DeCarlo, P. F., Ulbrich, I. M., Docherty, K. S., Sueper, D., Kimmel, J. R., Worsnop, D. R., Trimborn, A., et al.: Mexico City aerosol analysis during MILAGRO using high resolution aerosol mass spectrometry at the urban supersite (T0) – Part 1: Fine particle composition and organic source apportionment, *Atmos Chem Phys*, 9(17), 6633–6653, doi:10.5194/acp-9-6633-2009, 2009.

Allan, J. D., Delia, A. E., Coe, H., Bower, K. N., Alfarra, M. R., Jimenez, J. L., Middlebrook, A. M., Drewnick, F., Onasch, T. B., Canagaratna, M. R., Jayne, J. T., et al.: A generalised method for the extraction of chemically resolved mass spectra from Aerodyne aerosol mass spectrometer data, *J. Aerosol Sci.*, 35(7), 909–922, doi:10.1016/j.jaerosci.2004.02.007, 2004.

BC Air Quality: Venting Index, Venting Index [online] Available from: <http://www.bcairquality.ca/readings/ventilation-index.html> (Accessed 24 January 2014), 2014.

Campbell Scientific, Inc.: Instruction Manual: CSAT3 three-dimensional sonic anemometer, Logan, Utah, USA., 2006.

Chazette, P., Couvert, P., Randriamiarisoa, H., Sanak, J., Bonsang, B., Moral, P., Berthier, S., Salanave, S. and Toussaint, F.: Three-Dimensional Survey of Pollution During Winter in French Alps Valleys, *Atmos. Environ.*, 39(6), 1035–1047, doi:10.1016/j.atmosenv.2004.10.014, 2005.

DeCarlo, P. F., Kimmel, J. R., Trimborn, A., Northway, M. J., Jayne, J. T., Aiken, A. C., Gonin, M., Fuhrer, K., Horvath, T., Docherty, K. S., Worsnop, D. R., et al.: Field-Deployable, High-Resolution, Time-of-Flight Aerosol Mass Spectrometer, *Anal Chem*, 78(24), 8281–8289, doi:10.1021/ac061249n, 2006.

Erickson, M. H., Gueneron, M. and Jobson, B. T.: Measuring long chain alkanes in diesel engine exhaust by thermal desorption PTR-MS, *Atmospheric Meas. Tech.*, 7(1), 225–239, doi:10.5194/amt-7-225-2014, 2014.

Hildebrandt, L., Kostenidou, E., Lanz, V. A., Prevot, A. S. H., Baltensperger, U., Mihalopoulos, N., Laaksonen, A., Donahue, N. M. and Pandis, S. N.: Sources and

atmospheric processing of organic aerosol in the Mediterranean: insights from aerosol mass spectrometer factor analysis, *Atmos Chem Phys*, 11(23), 12499–12515, doi:10.5194/acp-11-12499-2011, 2011.

Jayne, J. T., Leard, D. C., Zhang, X., Davidovits, P., Smith, K. A., Kolb, C. E. and Worsnop, D. R.: Development of an Aerosol Mass Spectrometer for Size and Composition Analysis of Submicron Particles, *Aerosol Sci. Technol.*, 33(1-2), 49–70, doi:10.1080/027868200410840, 2000.

Jimenez Group Wiki: ToF-AMS Main, [online] Available from: http://cires.colorado.edu/jimenez-group/wiki/index.php?title=ToF-AMS_Main, 2013.

Jobson, B. T. and McCoskey, J. K.: Sample drying to improve HCHO measurements by PTR-MS instruments: laboratory and field measurements, *Atmospheric Chem. Phys.*, 10(4), 1821–1835, doi:10.5194/acp-10-1821-2010, 2010.

Kuhns, H., Bohdan, V., Chow, J., Etyemezian, V., Green, M., Herlocker, D., Kohl, S., McGown, M., Ramsdell, J., Stockwell, W., Toole, M., et al.: The Treasure Valley secondary aerosol study I: measurements and equilibrium modeling of inorganic secondary aerosols and precursors for southwestern Idaho, *Atmos. Environ.*, 37(4), 511–524, 2003.

Laborde, M., Schnaiter, M., Linke, C., Saathoff, H., Naumann, K.-H., Moehler, O., Berlenz, S., Wagner, U., Taylor, J. W., Liu, D., Flynn, M., et al.: Single Particle Soot Photometer intercomparison at the AIDA chamber, *Atmospheric Meas. Tech.*, 5(12), 3077–3097, doi:10.5194/amt-5-3077-2012, 2012.

Lim, S. S., Vos, T., Flaxman, A. D., Danaei, G., Shibuya, K., Adair-Rohani, H., AlMazroa, M. A., Amann, M., Anderson, H. R., Andrews, K. G., Aryee, M., et al.: A comparative risk assessment of burden of disease and injury attributable to 67 risk factors and risk factor clusters in 21 regions, 1990–2010: a systematic analysis for the Global Burden of Disease Study 2010, *The Lancet*, 380(9859), 2224–2260, doi:10.1016/S0140-6736(12)61766-8, 2012.

Lindinger, W., Hansel, A. and A. Jordan: On-line monitoring of volatile organic compounds at pptv levels by means of Proton-Transfer-Reaction Mass Spectrometry (PTR-MS) Medical applications, food control and environmental research, *Int. J. Mass Spectrom.*, 173, 191–241, 1998.

Mwaniki, G. R., Rosenkrance, C., Wallace, H. W., Jobson, B. T., Erickson, M. H., Lamb, B. K., Zalakeviciute, R. and VanReken, T. M.: Factors Contributing to Elevated Concentrations of PM_{2.5} during Wintertime near Boise, Idaho, *Atmospheric Pollut. Res.*, in press, 2014.

NOAA NOWData: Yakima Area climatic data, [online] Available from: <http://www.nws.noaa.gov/climate/xmacis.php?wfo=pdt>, 2013.

Pinder, R. W., Strader, R., Davidson, C. I. and Adams, P. J.: A temporally and spatially resolved ammonia emission inventory for dairy cows in the United States, *Atmos. Environ.*, 38(23), 3747–3756, doi:10.1016/j.atmosenv.2004.04.008, 2004.

Pope, C., Burnett, R., Thun, M., Calle, E., Krewski, D., Ito, K. and Thurston, G.: Lung Cancer, Cardiopulmonary Mortality, and Long-Term Exposure to Fine Particulate Air Pollution, *J Amer Med Assoc*, 287(9), 1132–1141, 2002.

RCW, 70.94.473: Limitations on burning wood for heat — First and second stage burn bans — Report on second stage burn ban., Revis. Code Wash., n.d.

Rumburg, B., Chen, J., Mount, G. and Lamb, B.: Washington State Dairy Ammonia emissions Model - Final Report, Washington State University, Laboratory for Atmospheric Research, Department of Civil & Environmental Engineering, Pullman, Washington., 2005.

Schwarz, J. P., Gao, R. S., Fahey, D. W., Thomson, D. S., Watts, L. A., Wilson, J. C., Reeves, J. M., Darbeheshti, M., Baumgardner, D. G., Kok, G. L., Chung, S. H., et al.: Single-particle measurements of midlatitude black carbon and light-scattering aerosols from the boundary layer to the lower stratosphere, *J. Geophys. Res.- Atmospheres*, 111(D16), doi:10.1029/2006JD007076, 2006.

Seinfeld, J. H. and Pandis, S. N.: *Atmospheric Chemistry and Physics: From Air Pollution to Climate Change*, 2nd ed., Wiley-Interscience., 2006.

Silva, P., Vawdrey, E., Corbett, M. and Erupe, M.: Fine particle concentrations and composition during wintertime inversions in Logan, Utah, USA, *Atmos. Environ.*, 41(26), 5410–5422, doi:10.1016/j.atmosenv.2007.02.016, 2007.

Stockwell, W., Kuhns, H., Etyemezian, V., Green, M., Chow, J. and Watson, J.: The Treasure Valley secondary aerosol study II: modeling of the formation of inorganic secondary aerosols and precursors for southwestern Idaho, *Atmos. Environ.*, 37(4), 525–534, doi:10.1016/S1352-2310(02)00895-6, 2003.

Ulbrich, I. M., Canagaratna, M. R., Zhang, Q., Worsnop, D. R. and Jimenez, J. L.: Interpretation of organic components from Positive Matrix Factorization of aerosol mass spectrometric data, *Atmos Chem Phys*, 9(9), 2891–2918, doi:10.5194/acp-9-2891-2009, 2009.

US EPA: Hazards of Ammonia Releases at Ammonia Refrigeration Facilities (Update). [online] Available from: <http://www.epa.gov/oem/docs/chem/ammonia.pdf> (Accessed 8 February 2014), 2001.

US EPA: 2011 National Emissions Inventory, version 1: Technical Support Document, Draft. [online] Available from: http://www.epa.gov/ttn/chief/net/2011nei/2011_neiv1_tsd_draft.pdf, 2013a.

US EPA: National Ambient Air Quality Standards (NAAQS), [online] Available from: <http://www.epa.gov/air/criteria.html> (Accessed 19 December 2013b), 2013.

US EPA: Screening Models | TTN - Support Center for Regulatory Atmospheric Modeling | US EPA, [online] Available from: http://www.epa.gov/scram001/dispersion_screening.htm (Accessed 27 January 2014c), 2013.

US EPA Region 10: Source apportionment modeling for multiple urban PM_{2.5} chemical speciation sites within the Pacific Northwest., 2013.

Vaisala, Inc.: User's guide: Vaisala boundary layer view software BL-VIEW., 2010.

Wallace, H. W., Jobson, B. T., Erickson, M. H., McCoskey, J. K., VanReken, T. M., Lamb, B. K., Vaughan, J. K., Hardy, R. J., Cole, J. L., Strachan, S. M. and Zhang, W.: Comparison of wintertime CO to NO_x ratios to MOVES and MOBILE6.2 on-road emissions inventories, *Atmos. Env.*, 63, 289–297, doi:10.1016/j.atmosenv.2012.08.062, 2012.

Washington Department of Ecology: An Evaluation of Two-Stage Burn Bans in Washington: Report to the Legislature. [online] Available from: <https://fortress.wa.gov/ecy/publications/publications/1102021.pdf>, 2011.

Washington Department of Ecology: Washington State 2011 Comprehensive Emissions Inventory, Air Quality Program, Washington State Department of Ecology. Draft Report and datasets., 2014.

Webb, E. K., Pearman, G. I. and Leuning, R.: Correction of flux measurements for density effects due to heat and water-vapor transfer, *Q. J. R. Meteorol. Soc.*, 106(447), 85–100, 1980.

Wood, R.: Stratocumulus Clouds, *Mon. Weather Rev.*, 140(8), 2373–2423, doi:10.1175/MWR-D-11-00121.1, 2012.

Zhang, Q., Jimenez, J. L., Canagaratna, M. R., Ulbrich, I. M., Ng, N. L., Worsnop, D. R. and Sun, Y.: Understanding atmospheric organic aerosols via factor analysis of aerosol mass spectrometry: a review, *Anal. Bioanal. Chem.*, doi:10.1007/s00216-011-5355-y [online] Available from: <http://www.springerlink.com/content/p5h2278x11m42682/> (Accessed 17 October 2011), 2011.

11. Appendices

11.1. SMPS Operation and Calibration

For YAWNS, the flow and electrical settings for the SMPS were set such that the measured diameter range for the particle size distributions was 20-800 nm. These settings are provided in Table 9.1 below.

Table 11.1. Operating parameters for the SMPS during YAWNS

Parameter	Value
<i>Lower Voltage Limit (V)</i>	20
<i>Upper Voltage Limit (V)</i>	9000
<i># of Bins per Scan</i>	50
<i>One-Way Scan Time (s)</i>	300
<i>Aerosol Flow (lpm)</i>	0.30
<i>Sheath Flow (lpm)</i>	3.0

Two types of data validation checks were applied to the SMPS to verify the instrument's performance during YAWNS. The first was a concentration verification of the CPC component of the system, performed approximately once per week. This occurred in two steps. First, a HEPA filter would be placed directly upstream to check for a zero reading. Background counts were consistently less than 0.1 cm^{-3} . Next the CPC connected to the SMPS was placed on the same sample line as the stand-alone CPC used during the study (see section 4.1.1). The two readings were expected to match to within $\sim 5\%$. This intercomparison was performed in place of a quantitative concentration calibration. Generating particle number concentration is exceptionally challenging, and standard procedure is for periodic (roughly annual)

factory calibrations to be validated qualitatively by intercomparisons. Both CPCs used in this study had had factory calibrations in the six months prior to YAWNS.

Size validations for the SMPS were done by generating dry particles of known size and then measuring the size distribution of this test aerosol to see if the measured peak diameter matched the known value. During YAWNS this test was performed frequently, since the SMPS was also used as a calibration instrument for the SP2 and HR-AMS. The size calibrations were performed using NIST-certified PSL nanospheres. The particles would be suspended in a dilute water mixture, and the mixture would be nebulized to form a mist. When the mist was dried, the resulting particles would be passed to the SMPS. Size calibrations typically involved sequentially generating 3-6 different monodisperse test PSL aerosols.

Final reported particle size distributions have been inverted from the directly measured distribution, in line with standard techniques. The basic process for this is shown in schematic form in Figure 9.1. As the SMPS scans through its voltage range, it records particle counts as a function of time $C(t)$. This time series of particle counts is converted directly to an instrument response $R(V)$, taking voltage as the independent variable, and accounting for the transmission time through the system and the scan direction. However, this instrument response still differs from the real size distribution. Many size-dependent factors affect how particles transmit through the SMPS. These factors include the voltage-size relationship, diffusional broadening within the DMA, multiple charging of particles, transmission efficiencies of the DMA and CPC, and so on. The total impacts of these effects are brought together into a mobility matrix, Γ . This matrix operates on the real size distribution

$N(D_p)$, to yield $R(V)$. Thus to determine $N(D_p)$ from $R(V)$, the equation must be numerically inverted. Our YAWNS measurements were inverted using a custom program developed using Igor Pro. This code has been tested extensively with our own data, and has been cross-validated against data and code developed at the National Center for Atmospheric Research.

SMPS Inversion Scheme

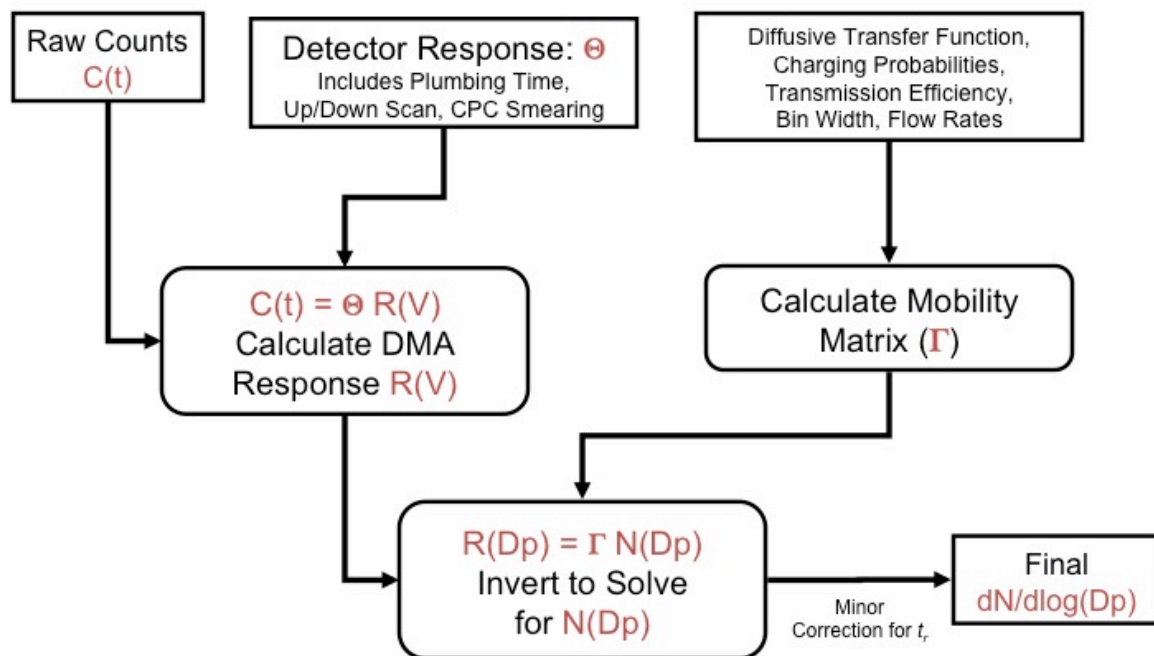


Figure 11.1. Schematic describing the data inversion approach to obtain particle size distributions from the SMPS.

11.2. HR-AMS Operation and Data Analysis

An Aerodyne high-resolution time-of-flight aerosol mass spectrometer (HR-AMS) allows for the direct separation and measurement of most ions at the same nominal m/z , quantification of organic and inorganic components, and the determination of the size distribution of all ions. The HR-AMS uses automated data analysis routines to classify the peaks in the mass spectrum into the following species classes: organics, ammonium, sulfate, nitrate, and chlorides. Concentrations for these species are given in near real-time. The instrument can operate under two ion optical modes, referred to as V-mode and W-mode. V-mode is a single-reflection configuration allowing for higher sensitivity at lower resolution, while W-mode is a two-reflection configuration offering a lower sensitivity but higher resolution. A schematic of HR-AMS found in Figure 11.2. Aerosol particles enter through a sampling inlet that restricted flow with a 110 μm critical orifice at a flow rate of approximately $1.5 \text{ cm}^3 \text{ s}^{-1}$ and into an aerodynamic lens. The aerodynamic lens focuses particles (ranging from 35 to 1500 nm) into a narrow beam using six apertures of sequentially decreasing size. At this stage most of the atmospheric gas surrounding the particles is removed.

After transmission through the aerodynamic lens, the focused aerosol beam is accelerated in a supersonic expansion caused by the difference in pressure between the sampling and sizing chambers. This acceleration results in different velocities for aerosols of different sizes. The instrument is typically alternated between two modes of operation that change how particle transmission through the sizing chamber occurs; these are mass spectrum (MS) mode and particle time-of-

flight (PToF) mode. These modes are controlled by the positioning of a mechanical chopper wheel, located directly after the particle beam exit from the aerodynamic lens. In MS mode, particles travel unimpeded until they impact onto a resistively-heated porous tungsten surface held at 600 °C. Here the volatile and semi-volatile portions of the aerosols are vaporized and then immediately ionized using 70-eV electron-impact ionization source. The mass spectrometer detects the positive ion fragments generated by the electron impact ionization and determines the mass-to-charge (m/z) distribution of the particle beam. When operating in PToF mode, particle size can be determined by measuring flight times across a fixed distance. The rotating chopper wheel consist of with two radial slits located 180° apart and when rotating intercepts the focused particle beam. As the particles travel on a straight path through the sizing chamber, they separate according to their size with the smaller particles traveling faster than the larger particles. Particles are thus classified by size in the sizing chamber and then also classified by their mass spectrum, allowing time-averaged composition-resolved size distributions to be obtained. The AMS detects non-refractory species which can evaporate rapidly at the AMS temperature and vacuum conditions (mostly volatile and semi-volatile components) sulfate, nitrate, ammonium, chloride, and total organic matter; while it does not measure non-volatile constituents like crustal oxides, sea salt, and black carbon. More detailed information on the HR-AMS can be found elsewhere (DeCarlo et al., 2006).

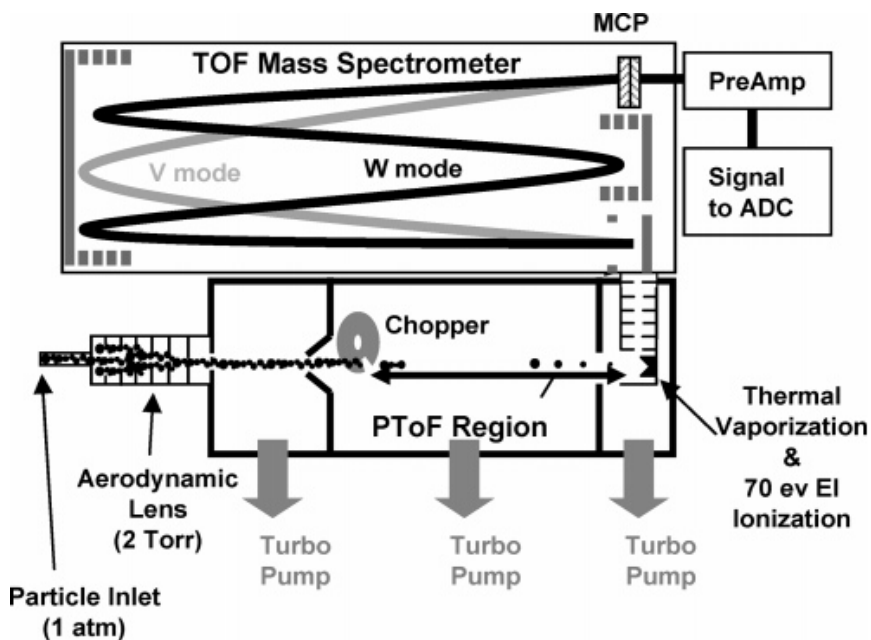


Figure 11.2. Schematic of the HR-AMS showing its two ion optical modes.

HR-AMS Operation

During YAWNS, the HR-AMS was operated at V-mode with a 2-minute averaging interval in both MS and PToF mode. The HR-AMS was alternated between modes every 15 seconds, producing time-averaged measurements for each. For YAWNS, the mass resolving power ($m/\Delta m$) was ~ 4000 at mass-to-charge (m/z) ratio 184 in “V” mode. All data were analyzed using standard AMS software (SQUIRREL v1.52G and PIKA v1.12G) within Igor Pro 6.21–6.31 (WaveMetrics, Lake Oswego, OR).

Instrument Calibrations

A series of calibrations were performed at the start of the campaign to ensure proper operation of the instrument. These included a lens alignment, flow calibration, m/z calibration, and particle size calibration. Each day the m/z calibration and tuning of the instrument was checked to maintain and ensure

quality measurements throughout the campaign. An Ionization Efficiency (IE) calibration was performed at the beginning, middle, and end of campaign. Table 11.2 details the major calibration activities for the HR-AMS during and YAWNS.

Table 11.2. Calibration activities for the HR-AMS during YAWNS.

Calibration	Date Performed
Lens Alignment	01/06/13
m/z Calibration	01/06/13
V-mode Tuning	01/06/13
Flow Calibration	01/07/13
Particle Size/Velocity Calibration	01/08/13
Ion Efficiency Calibration	01/09/13, 01/20/13, 01/26/13

The lens alignment is performed to ensure that the particle beam is properly focused through the chopper, across the sizing region, and onto the vaporizer. The particle beam path is controlled via the aerodynamic lens which needs to be adjusted each the instrument has been moved to ensure that the particle beam is aligned properly. This optimization of the beam alignment is performed with a strong concentration of ammonium nitrate generated particles and then small alignment changes of the lens are done until the measured bits per extraction (bpe) at m/z 46 (corresponding to NO₃⁻ ions) are maximized.

The HR-AMS sampling flow is controlled with a critical orifice located in the AMS inlet. The size of the critical orifice is chosen to ensure that the inlet pressure remains between 1.3-1.5 torr. This is the optimal pressure for the proper function of the aerodynamic lens in order to maximize particle transmission efficiency. A

flow calibration ensures that the proper critical orifice is used and thus that the particle transmission efficiency is optimized. Additionally, the flow calibration provides input parameters to the HR-AMS data acquisition system (DAQ) to allow the proper calculation of the inlet flow based on the measured inlet pressure. For this campaign a critical orifice size of 110 μm was determined to produce the proper inlet pressure. Using a Gilibrator to measure volumetric flow rates through the sample inlet and plotting against the measure inlet pressure for various critical orifice sizes provides the necessary slope and intercept for flow rate calculations throughout the campaign.

The purpose of the m/z calibration is to establish the relationship between recorded ion times-of-flight and ion m/z. The calibration in the DAQ software is based on a 3-point, linear least-squares fit. To calibrate, a mass spectrum is displayed in time-of-flight space. The user identifies the position of three peaks of known m/z, and the software calculates the linear fit. For this campaign the m/z calibration was based on m/z 14 (N⁺), m/z 28(N₂⁺), and m/z 184(W⁺); where the tungsten was being produced from the tungsten filament inside the AMS itself.

In PToF mode, the AMS outputs a vacuum aerodynamic particle size that is calculated based on the relationship between particle size and particle velocity. The "start time" is determined by the time the chopper opens and the "end time" is determined by the MS response. The timescale for the particle time-of-flight is milliseconds while the timescale for the ion time-of-flight in the MS is a microsecond; this difference in scale is why the detected MS spectrum can be linked to a specific particle size. The particle size /velocity calibration is performed using

monodisperse particles generated from an ammonium nitrate solution. The time-of-flight for various particle sizes are measured using the HR-AMS and then correlated into four parameters used in the DAQ to calculate the sample aerosol particle sizes based on the measured arrival times. Particle sizes of 100, 150, 200, 250, 300, 350, 400, 450, 500, 550, and 600 nm were used to generate the necessary parameters and m/z 46 (NO_3^-) was used to look at the ammonium nitrate particle arrival time in the MS. A sample particle velocity calibration plot is included below (Figure 11.3).

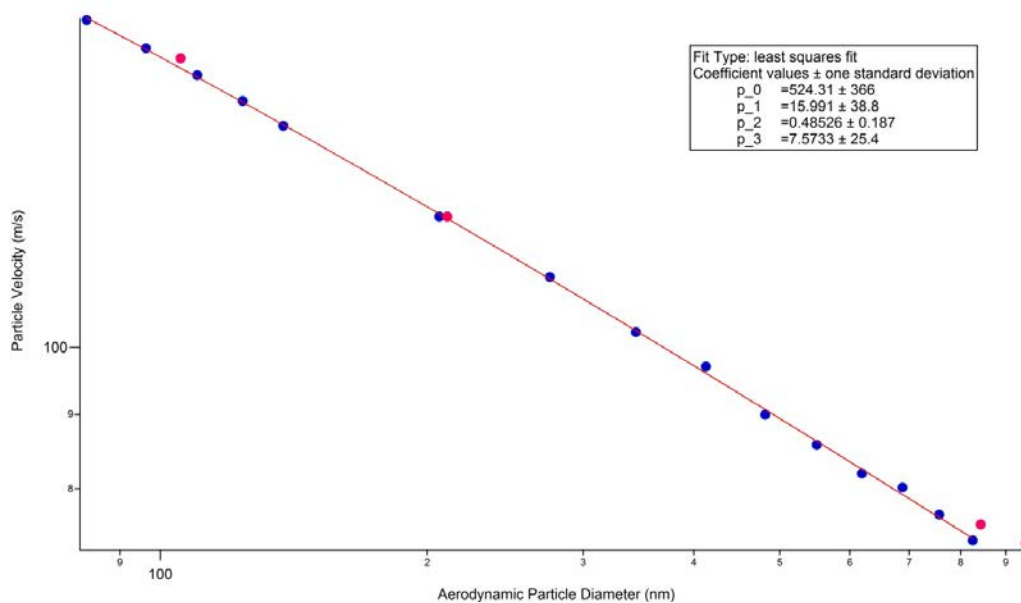


Figure 11.3. Particle velocity vs. size calibration plot.

The ionization efficiency (IE) calibration determines the ionization efficiency of ammonium nitrate. Quantification of all non-refractory HR-AMS components is based on the linearity of this IE. Nitrate ionization efficiency calibrations were performed three times during the campaign using 400nm mono-dispersed particles generated from ammonium nitrate solution as described by Jayne et al. (2000).

The IE is the number of ions measured by the MS from a known amount of mass entering the HR-AMS. Compounds are quantified by their relative response to nitrate. The relative ion efficiency (RIE) is the ratio of the IE of any given species to nitrate. Ammonium nitrate is used for this calibration. For this calibration to be accurate, all particles that enter the MS must be detected. Not all particles that enter the MS will produce the same number of ions. If only the particles that produce more ions are at a detectable signal, the IE calculated will be erroneously high and resulting ambient calculations will produce concentrations that are erroneously low. For the HR-AMS, the accepted particle size for performing this calibration is 400 nm in mobility diameter.

Filter Sampling

For five twenty-minute intervals during YAWNS, a Pall HEPA Filter was attached just prior to the AMS inlet on the sample line (Table 11.3). This intermittent sampling of the ambient aerosol through the HEPA filter allows for future calculation of species detection limits as well as study specific correction to the fragmentation table to account for deviations in the gas-phase from default settings.

Table 11.3. Table of HR-AMS filter samples and durations during YAWNS.

Filter Sample Date	Time (Duration)
01/09/13	12:43-13:03 (20 min)
01/11/13	12:43-13:04 (21 min)
01/15/13	16:52-17:19 (27 min)
01/20/13	14:27-14:50 (23 min)
01/26/13	09:33-10:10 (37 min)

Data Analysis

Figure 11.4 demonstrates some of the main operating parameters used during the YAWNS study. These values have all be post-study corrected following standard procedures (Jimenez Group Wiki, 2013).

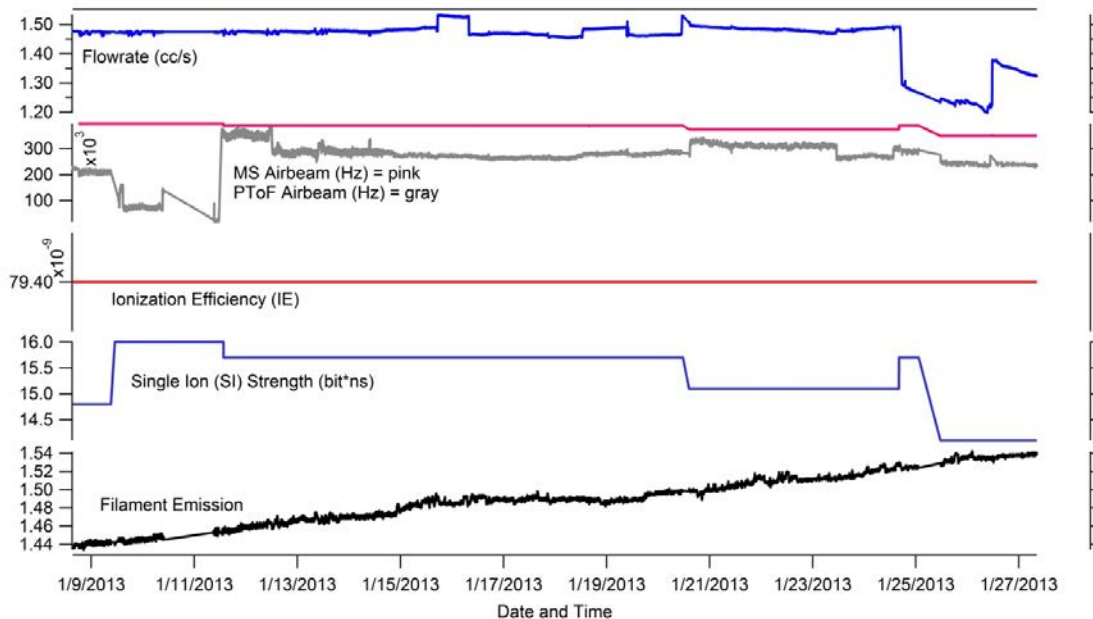


Figure 11.4. AMS operating diagnostics for YAWNS study. Including inlet flow rate (pressure corrected), MS and PToF Airbeam (AB), ionization efficiency (IE), Single Ion strength (SI), and filament emission.

Study Specific Corrections

Flow Corrections

Flow rate measurements are based on the pressure measured at the inlet and then scaled using the parameters from the flow calibration performed at the start of the study. For YAWNS the measured flow rate was corrected for the actual flow rate at ambient pressure. From the ideal gas law, one can relate the ratio of the line pressure (the pressure seen at the AMS inlet, P_{line}) and the ambient pressure

($P_{ambient}$) to the actual flow rate under ambient conditions ($\dot{V}_{ambient}$) and the measured flow rate at the AMS inlet (\dot{V}_{line}). By making this correction measured concentrations can be directly compared between all instrumentation.

Fragmentation Table Adjustments

The purpose of the fragmentation table is to apportion the AMS signal among the different chemical species present in the aerosol (ammonium, chloride, nitrate, sulfate, and organics). This table must be adjusted from study-to-study to account for small changes between instruments and measurement environments. Most of the necessary adjustments to the default fragmentation table have to do with air interferences. After making the appropriate fragmentation corrections for a given set of data the average mass spectra plots of all available filter samples are checked to ensure that the concentration of the five main components (Org, Chl, NH₄, NO₃, SO₄) are each approximately zero. A more detailed explanation of the fragmentation table is given by Allen et al. (2004).

CO₂ [44]

The default mixing ratio used for the apportionment of gas-phase of CO₂ in the atmosphere is 370ppm . The amount of signal at m/z 44 (mostly CO₂⁺) that is due to gas phase CO₂ and the amount of aerosol phase CO₂⁺ (and other small aerosol contributions at m/z 44) needs to be adjusted to reflect sampling conditions. Since external measurements of gas-phase CO₂ were being recorded during YAWNS, these time-dependent measurements were used to replace the default CO₂ mixing ratio.

Air [29]

Depending on the threshold setting and possible saturation effects, the amount of N¹⁵N at m/z 29 detected by the system may be slightly different than that predicted purely by an isotopic factor. In the case of this study a multiplier of 0.83 was used to adjust the predicted behavior.

Air [15]

Depending on the threshold setting and possible saturation effects, the amount of ¹⁵N at m/z 15 detected by the system may be slightly different than that predicted purely by an isotopic factor. In the case of this study a multiplier of 1.05 was used to adjust the predicted behavior.

O [16]

The O[16] fragment indicates the amount of gas phase signal due to O⁺ or a doubly charged O₂²⁺ ion. In turn this ratio impacts the ratio of NH₄[17] (NH₃⁺) vs NH₄[16] (NH₂⁺). This ratio should trend through the origin; since it did not a multiplier of 0.7 was used to correct the ratio so that the data would trend through the origin.

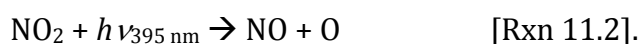
11.3. NO_x/NO_v Analyzer Operation and Calibration

The principal of measurement for this instrument is chemiluminescence, where NO reacts with ozone to produce a vibrationally excited NO₂ molecule:



This vibrationally excited NO₂ molecule then deactivates by colliding with another molecule or by releasing a photon with a wavelength of approximately 610 nm. This photon is then detected by a photomultiplier tube.

The instrument measures NO₂ by converting NO₂ to NO for detection by chemiluminescence. This is done with a photolytic NO₂ converter that uses light at a wavelength of 395 nm to convert NO₂ to NO by photolysis via the reaction:



NO_y is measured by reduction of oxidized nitrogen with a molybdenum oxide (MoO₂) catalyst heated to 310 C. This occurs via the reaction:



During the YAWNS campaign, this instrument was operated in NO_y/NO_x mode. That is to say that one channel was configured to measure NO_y and one was configured to measure NO_x. The NO_y channel was plumbed with sample air entering the inlet, running through the molybdenum catalyst and into the chemiluminescence analyzer. The NO_x channel was plumbed with sample air entering the inlet, passing through the NO₂ converter and finally into the chemiluminescence analyzer. The NO₂ converter was cycled on and off every 30 seconds so that NO and NO₂ could be measured on the same channel. Each channel was set to record data every second. For the NO_y channel, this means that there was an available data point every second. For the NO_x channel, the 30 second periods when the NO₂ converter was on or off were averaged, yielding 1 NO and 1 NO₂ point per minute. Background count rates

were measured every 30 minutes by diverting sample flow into a prereactor that removed NO from the sample by reaction with ozone:



This was done to characterize the background counts which can change quickly based on relative humidity and other factors. The instrument was calibrated about every other day based on an external NO standard of 500 ppmv diluted into the sample flow of 1 SLPM per channel, or a total of 2 SLPM. In addition, NO₂ conversion efficiency was measured on the same schedule. This was done by first measuring NO cal gas with the NO₂ converter off, second running the NO calibration mixture through an NO titration cell that converted about 50% of the NO into NO₂ and finally turning on the NO₂ converter to determine the amount of the NO that has been converted to NO₂ is converted back to NO by the NO₂ converter. Typical calibrations for the NO_y (channel 1) and NO_x channel (channel 2) are shown below (Figures 11.5-6).

Channel 1's sensitivity is calculated via the equation:

$$\text{Channel 1 Sensitivity} = \frac{\text{NO}_c - \text{NO}_{bck}}{\chi}$$

Where χ is the NO calibration mixture mixing ratio in ppbv.

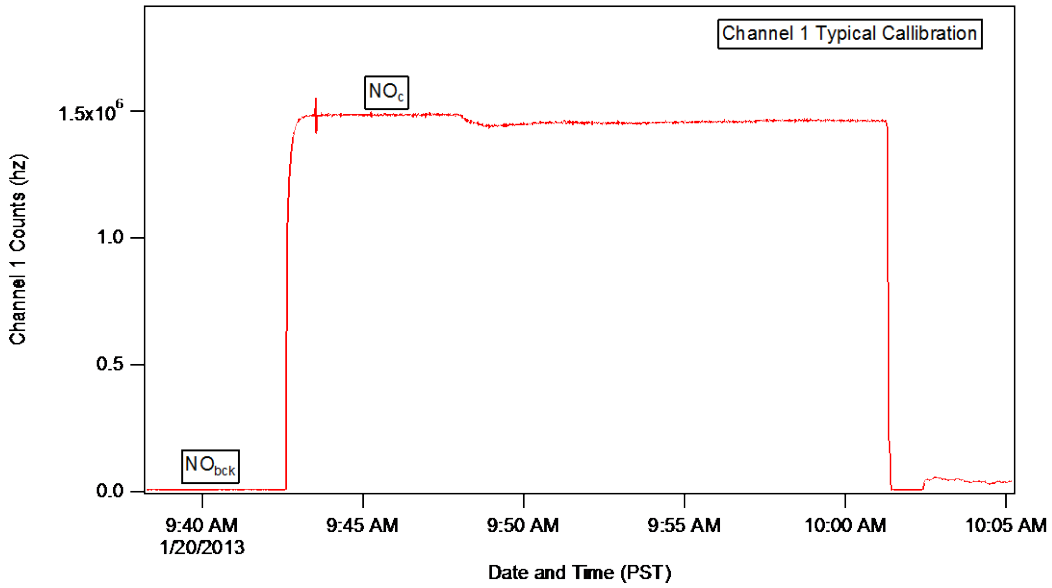


Figure 11.5. Typical calibration profile for the NO_y channel of the NO_x/NO_y analyzer.

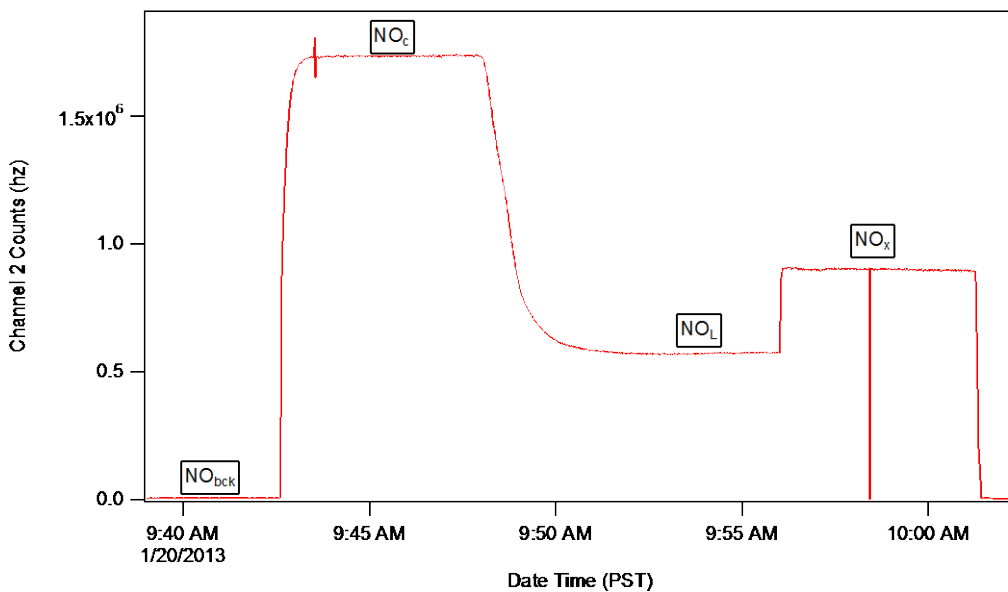


Figure 11.6. Typical calibration profile for the NO_x channel of the NO_x/NO_y analyzer.

Channel 2's sensitivity to NO in hz/ppbv is calculated via the equation:

$$\text{Channel 2 Sensitivity} = \frac{\text{NO}_c - \text{NO}_{bck}}{\chi}$$

Where χ is the NO calibration mixture mixing ratio in ppbv.

The NO₂ conversion efficiency is calculated via the formula:

$$\text{NO}_2 \text{ Conversion Efficiency} = \frac{\text{NO}_x - \text{NO}_L}{\text{NO}_C - \text{NO}_L}$$

The data work up procedure for this instrument involves first interpolating background counts, pulling out NO and NO₂ periods for the NO_x channel, and finally applying sensitivities to convert count rates into mixing ratios (ppbv). The backgrounds that were pulled out of the data for each channel and interpolated are shown below (Figures 11.7-8).

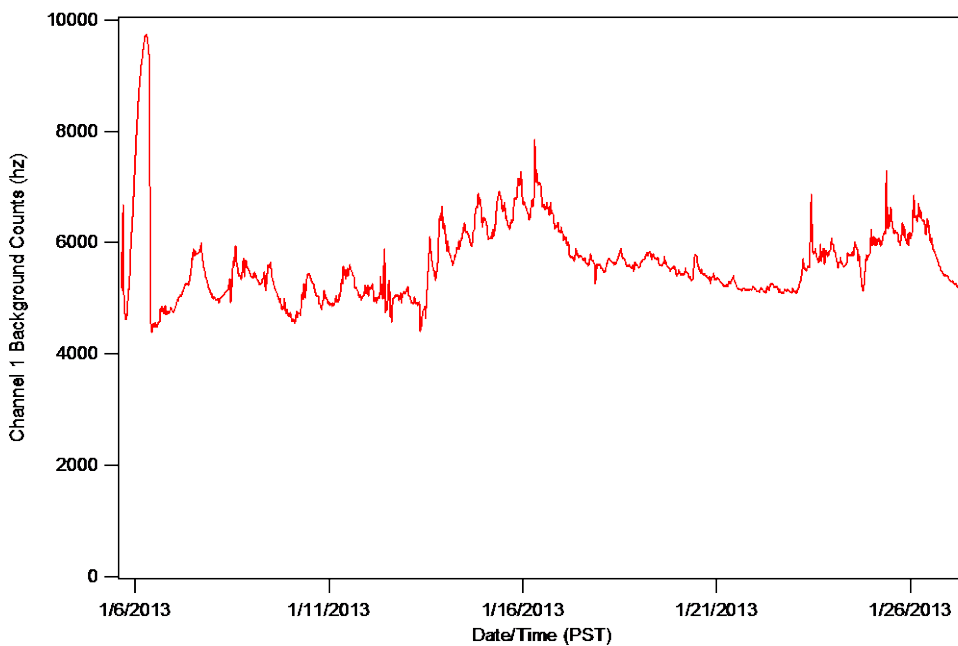


Figure 11.7. Background counts for channel 1 of the NO_x/NO_y analyzer during YAWNS.

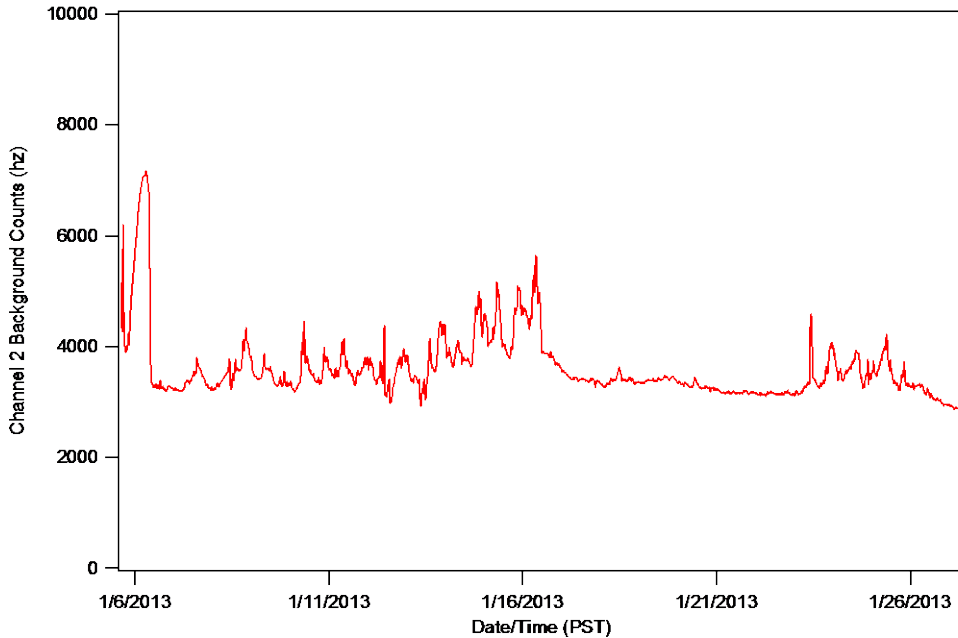


Figure 11.8. Background counts for channel 2 of the NO_x/NO_y analyzer during YAWNS.

For the NO_x channel, it is necessary to separate the periods in which the NO_2 converter is off and when the NO_2 converter is on. For each one-minute period, the converter is on for 30 seconds and off for 30 seconds. Each of these periods were pulled out, averaged and attributed to that minute. An example of how these periods look is shown below (Figure 11.9). The periods of high counts are when the NO_2 converter is on and the lower periods are when the NO_2 converter is off. The very low, flat periods at the beginning and end of this window are measurements of the channel's background count rate.

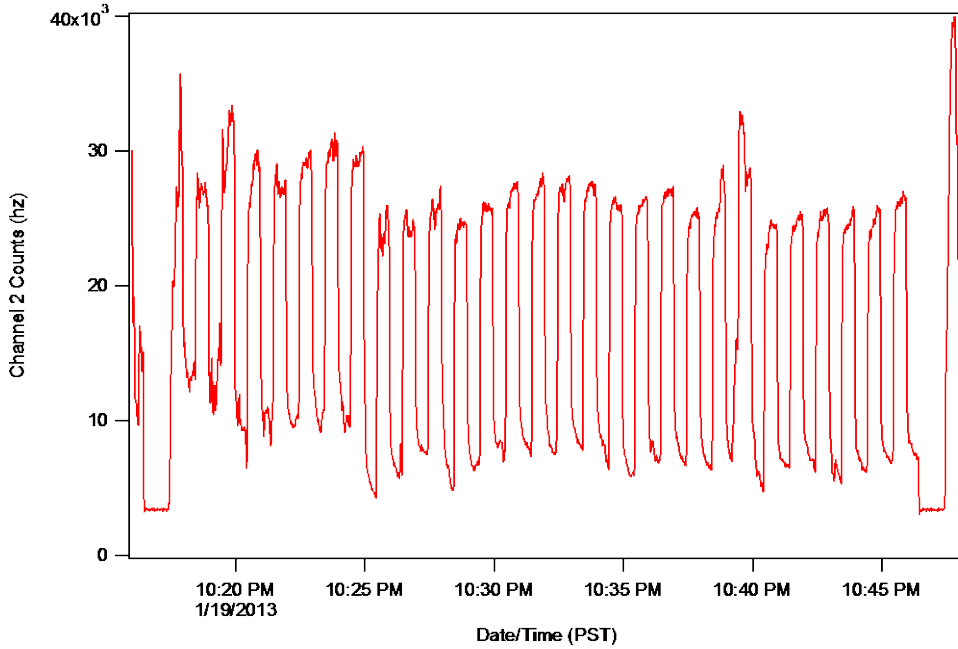


Figure 11.9. Representative time series of the raw count rate measured by channel 2 of the NO_x/NO_y analyzer. Explanation provided in the text.

To calculate NO_y mixing ratios, the interpolated background of channel 1 is simply subtracted from the overall channel 1 count rate and then divided by the sensitivity. This assumes that the conversion efficiency of the catalyst is 1.

$$\text{NO}_y \text{ (ppbv)} = \frac{\text{CH1 (hz)} - \text{CH1}_{bck} \text{ (hz)}}{\text{CH1}_{sens} \left(\frac{\text{hz}}{\text{ppbv}} \right)}$$

Where CH1 is the signal of channel 1, CH1_{bck} is the interpolated background, and CH1_{sens} is the sensitivity of channel 1. To calculate NO mixing ratios, the interpolated background of channel 2 is subtracted from the NO period averages and then divided by the channel 2 sensitivity.

$$\text{NO (ppbv)} = \frac{\text{CH2}_{NO} \text{ (hz)} - \text{CH2}_{bck} \text{ (hz)}}{\text{CH2}_{sens} \left(\frac{\text{hz}}{\text{ppbv}} \right)}$$

Where $CH2_{NO}$ is the average of the NO periods, $CH2_{bck}$ is the channel 2 background, and $CH2_{sens}$ is the channel 2 sensitivity.

NO_2 mixing ratios are calculated by removing the channel 2 background from both the NO and NO_2 periods. Then the background removed NO period signal is subtracted from the background removed NO_2 period signal and this is divided by the NO_2 conversion efficiency. This quotient is then divided by the NO_2 sensitivity.

$$NO_2 \text{ (ppbv)} = \frac{\frac{[CH2_{NO_2} \text{ (hz)} - CH2_{bck} \text{ (hz)}] - [CH2_{NO} \text{ (hz)} - CH2_{bck} \text{ (hz)}]}{NO_2 \text{ Conversion Efficiency}}}{CH2_{sens} \left(\frac{\text{hz}}{\text{ppbv}} \right)}$$

Where $CH2_{NO}$ is the averages of the NO periods, $CH2_{NO_2}$ is the averages of the NO_2 periods, $CH2_{bck}$ is the channel 2 background, and $CH2_{sens}$ is the channel 2 sensitivity.

11.4. Aerolaser VUV CO Instrument Operation and Calibration

In the field, the Aerolaser VUV CO instrument was configured to report data every second. Background count rates were measured every four hours by passing sample air through a SOFNOCAT 514 scrubber, which removes any CO from the sample. Calibrations were also done every 4 hours by mixing about 30 SCCM of an external CO standard of 101.6 ppmv in to the typical sample flow of approximately 800 SCCM. To account for ambient CO, ambient air is measured with no calibration (cal) gas addition before and after cal gas is measured. The average of these two periods is subtracted from the count rate observed when cal gas is introduced to determine the count rate that is attributable to only the cal gas. A typical background/calibration goes as follows: ambient air through SOFNOCAT 515 (instrument background), measure ambient air (calibration background 1), ambient sample with calibration gas added (calibration), and finally ambient air is measured again (calibration background 2). A typical calibration is shown below (Figure 11.10).

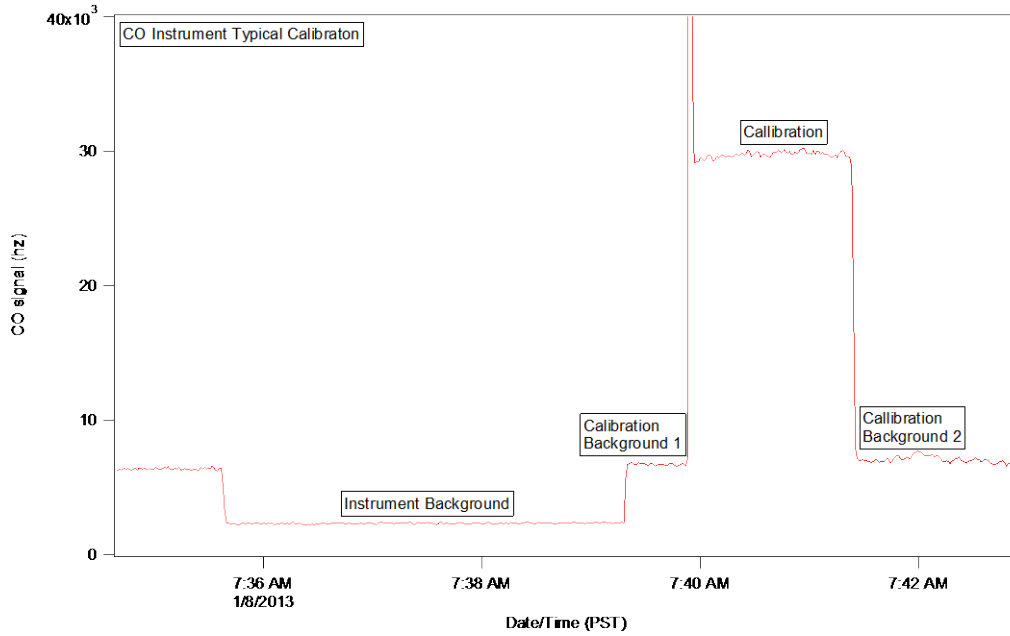


Figure 11.10. Typical calibration profile for the Aerolaser VUV CO instrument.

$$\text{CO sensitivity} \left(\frac{\text{hz}}{\text{ppbv}} \right) = \frac{\text{Calibration} - \frac{\text{Calibration Background 1} + \text{Calibration Background 2}}{2}}{\chi}$$

Where: χ is the calculated CO mixing ratio in the calibration, and the sample air mixture CO mixing ratios were determined by subtracting the interpolated backgrounds from the ambient signal and dividing by the sensitivity:

$$\text{CO (ppbv)} = \frac{\text{CO signal (hz)} - \text{CO background (hz)}}{\text{Sensitivity} \left(\frac{\text{hz}}{\text{ppbv}} \right)}$$

The interpolated backgrounds and sensitivities are shown below (Figures 11.11-12).

The sensitivities over the campaign were consistent and because of this, a constant value of 6 hz/ppbv was used to convert raw signal into mixing ratios.

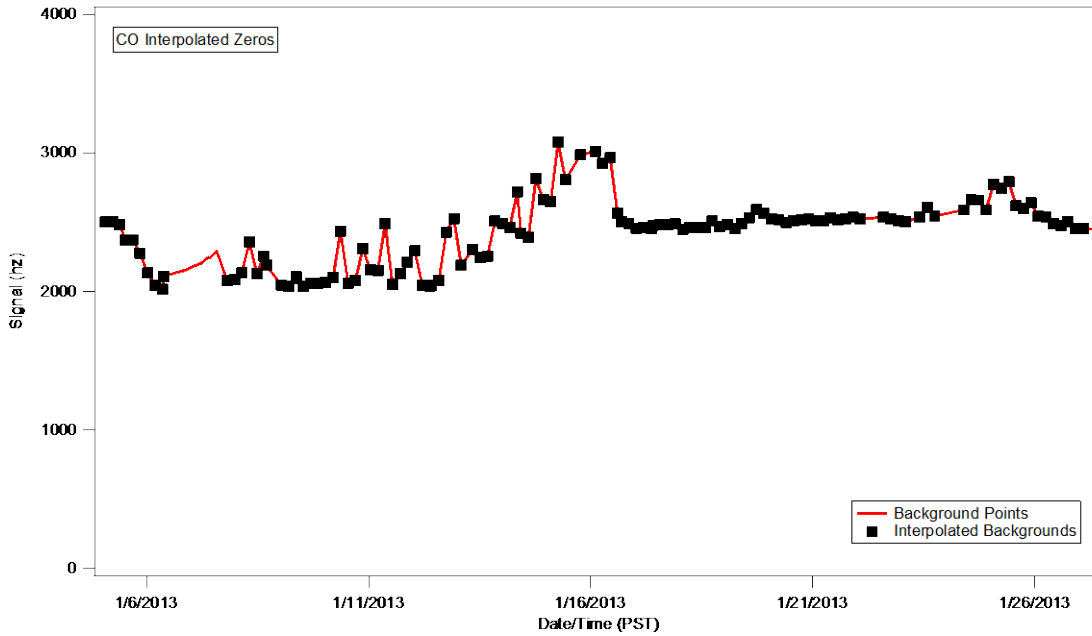


Figure 11.11. Interpolated background points for the VUV CO instrument during YAWNS.

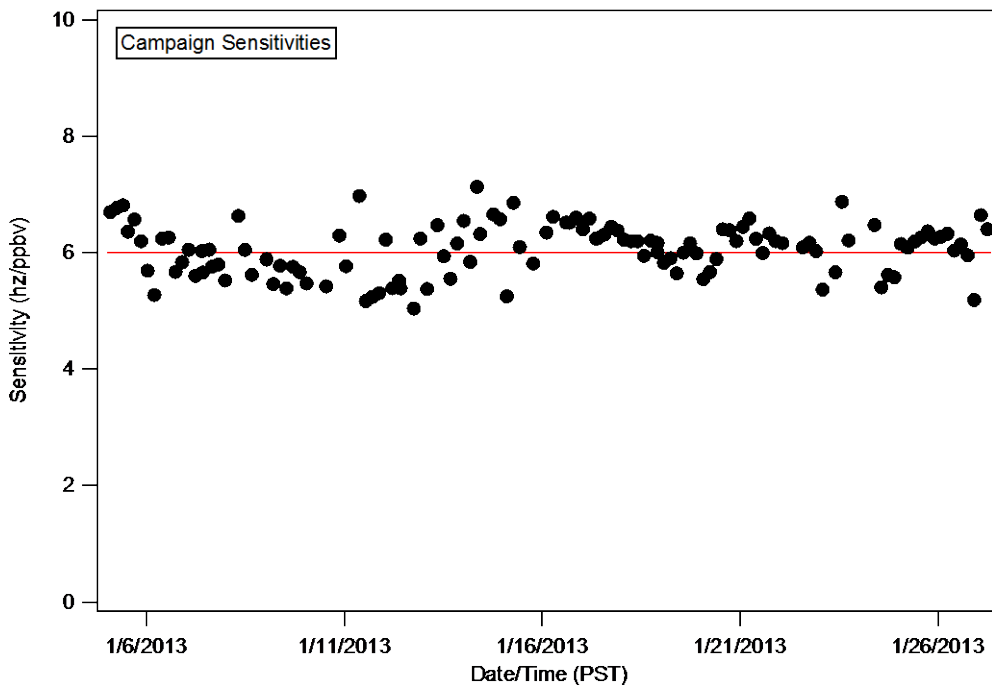


Figure 11.12. Calculated sensitivities for the VUV CO instrument during YAWNS.

11.5. PTR-MS Operation and Calibration

The PTR-MS can be operated at different drift pressures and electric field strengths. This is measured in units of Townsends (Td), which is a measure of the drift field strength (E) divided by the molecular number density in the drift tube (N). One Td is equal to $1 \times 10^{-17} \text{ V/cm}^2$. Operating at higher Td numbers limits water cluster formation ($\text{H}^+\text{H}_2\text{O}_2$) which allows for better understanding of instrument sensitivities, but this comes at the cost of forcing more ion dissociation in the drift tube.

Proton Transfer Reaction: $\text{R} + \text{H}_3\text{O}^+ \rightarrow \text{RH}^+ + \text{H}_2\text{O}$

Sample Dehumidification:

Sample dehumidification was employed during the YAWNS campaign to eliminate water vapor sensitivity dependence for polar molecules, and to greatly increase the sensitivity of the instrument to formaldehyde. In addition, dehumidifying the sample allows the PTR-MS to be operated at a lower Td number, by reducing the amount of water clustering that is normally present at lower Td numbers. Operation at lower Td numbers increases instrument sensitivity and decreases the amount of ion dissociation in the drift tube.

Sample dehumidification was done by passing sample air through a cold zone set to -30 C. The dehumidifier consisted of two stainless steel tubes mounted inside an aluminum block that was cooled by an immersion cooler probe. The immersion cooler probe cooled the tubes to about -50 C. The temperature of the tubes was controlled by resistive heating using a polyamide coated nichrome wire with a resistance of about 95 ohms that was coiled around the cold tubes. The

temperatures of the individual tubes were controlled by Watlow temperature controllers and the tube temperature was measured continuously using a thermocouple probe that was in contact with the inner wall of the tube.

In the field, the two tubes were operated in tandem so that measurements would remain continuous over the course of the campaign. Each tube operated in one of three states at any given time; sample, condition, or backflush. Sample mode was when ambient air was sampled by the PTR-MS through the cold tube. In backflush mode, the tube was heated up to 70 C and flush with dry N₂ to remove ice buildup that may have formed while sampling. Conditioning mode is when the tube is returned to the low temperature with ambient air flowing through before being used as a dehumidifier for the PTR-MS sample. At any given time, one tube was in sample mode, while the other was in the process of being backflushed and conditioned. This cycle was 20 minutes long, so each tube was used to dehumidify sample air for 20 minutes before being backflushed and reconditioned. This process was automated so that continuous measurements could be made without operators present.

IVOC Sampler:

Between January 12 and January 24, a thermal desorption system was used in conjunction with the PTR-MS to measure larger molecular weight VOC that were below the detection limit of the instrument. This system employed a Tenax trap to accumulate VOCs over a 20-minute sampling period while the PTR-MS was measuring ambient air. VOCs were desorbed and measured by the PTR-MS for 5-minute periods, during which the PTR-MS was not making ambient measurements.

Because of an issue of the sample line not being continuously conditioned, the IVOC data will not be presented in this report. However, being that the IVOC sampling cycle lasted about 30 minutes and the IVOC measure mode when the PTR-MS is not measuring ambient air lasted 5 minutes, it is important to note that 5 of every approximately 30 minutes of VOC sampling was lost.

In Field Operation:

During the measurement campaign, The PTR-MS was operated in one of three modes: 120 Td VOC mode, 80 Td VOC mode, and 80 Td VOC and IVOC mode. 120 Td VOC mode was when the PTR-MS sampled ambient air at 120 Td without dehumidifying the sample, 80 Td VOC mode was when the PTR-MS measured ambient air at 80 Td through the dehumidifier, and 80 Td VOC and IVOC mode was when the PTR-MS measured ambient air at 80 Td, but the thermal desorption sampler was also running and desorbing for PTR-MS measurements for 5 of every 30 minutes. Table 11.4 below shows operation modes during the different intervals of the study.

Table 11.4. PTR-MS operation modes during YAWNS.

Date	Td	Dehumidification	IVOC system
1/5 - 1/8	120	NO	NO
1/8 - 1/12	80	YES	NO
1/12 - 1/24	80	YES	YES
1/24 - 1/27	120	NO	NO

Calibration and Sensitivities:

The PTR-MS was calibrated 8 times over the course of the study. This was done by sampling about 10 SCCM of an external gas standard dilluted with approximately 1 SLPM of zero air. Backgrounds were also taken by measuring zero

air. Sensitivities were calculated in units of hz/Mhz H₃O⁺/ppbv. Raw counts were then converted to mixing ratios by first dividing by the reagent ion count rate, multiplying by 10⁶, subtracting off the normalized background countrate and dividing by the sensitivity. The averaged sensitivities for the campaign are shown in Table 11.5 below.

Table 11.5. YAWNS PTR-MS sensitivities, in ncps per ppbv.

<u>Compound</u>	<u>Mass</u>	<u>120 Td</u>	<u>80 Td Dehumidified</u>
Formaldehyde	m31	3.0	14.2
Methanol	m33	11.9	28.2
Acetonitrile	m42	20.8	59.6
Acetaldehyde	m45	15.7	44.8
Acetone	m59	18.0	54.3
Isoprene	m69	8.2	28.2
MVK	m71	6.5	21.6
MEK	m73	16.1	53.0
Benzene	m79	8.0	20.0
a-Pinene frag	m81	4.0	7.9
Toluene	m93	9.8	26.3
Styrene	m105	9.2	27.4
P-Xylene	m107	8.3	25.0
1,2,4-Trimethylbenzene	m121	6.6	20.3
Teramethylbenzene	m135	7.3	22.5
a-Pinene	m137	2.6	10.8

VOC mixing ratio calculation:

$$[VOC] = \frac{\frac{hz}{hz H3O^+ * 10^6} - \frac{hz bck}{hz H3O^+ bck * 10^6}}{Sensitivity}$$

11.6. Ammonia Denuder Preparation

PROCEDURE: Denuder coating for NH₃ analysis (1% H₃PO₄ in 10% MeOH)

Written by: J. Michal **Date:** March 30, 2009 **Revised:** Dec 4, 2013

Materials:

Denuders
10 mL pipette

Reagents:

Phosphoric acid (H₃PO₄)
Methanol (MeOH)
Deionized NH₃-free water

Preparation of Reagents:

To approximately 80 mL of deionized, NH₃-free water, add:

- 1 mL H₃PO₄
- 10 mL MeOH
- Mix
- Pour into a 100 mL graduated cylinder
- Bring total volume up to 100 mL with deionized, NH₃-free water.
- Mix and pour into bottle.
- Cap or cover with parafilm and store at room

Procedure:

1. Clean denuders
 - a. Cap one end
 - b. Add deionized NH₃-free water
 - c. Put cap on open end of denuder
 - d. Shake back and forth 30 times
 - e. Remove one end cap and shake water out of the denuder
 - f. Repeat for a total of 3 washes
 - g. Remove end caps and gently tap denuders on clean kimwipe to remove all liquid
 - h. Allow to air dry
2. Using a clean, dry denuder
 - a. Cap one end
 - b. Add 10 mL of coating solution

- c. Put cap with hole in end on the open end of the denuder
- d. Shake back and forth 30 times
- e. Remove end cap with the hole and tap denuder into plastic funnel placed on waste collection bottle. Tap gently until all liquid has been removed
- f. Tap denuder on clean kimwipe to remove any liquid
- g. Dry with nitrogen gas or zero air

11.7. Ammonia Denuder Analysis

PROCEDURE: NH₃-N analysis - denuders

Written by: J. Michal **Date:** March 30, 2009 **Revised:** Dec 4, 2013

Materials:

Denuders
10 mL pipette
1 mL pipetman w/tips
Test 'n tube kit, LR 0.02 to 2.50 mg/L, salicylate method 10023 (Hach)
1 – 100 mL volumetric flask
4 – 25 mL volumetric flasks
30 mL collection bottles for storage
spectrophotometer

Reagents:

Deionized NH₃-free water
NH₃-N standard (100 mg/L)

Preparation of Reagents:

Working stock NH₃-N solution preparation:

- To a 100 mL volumetric flask, add 4 mL of 100 mg/L NH₃-N standard.
- Add deionized water to the flask until the bottom of the meniscus is level with the 100 mL line on the volumetric flask.
- Cover top of flask with parafilm.
- Invert and shake vigorously.

NH₃-N standard curve

<i>Concentration (mg/L)</i>	<i>Working stock (mL)</i>
2.5	15.625
1.25	7.813
0.625	3.906
0.3125	1.953
0	0

Add the specified volume of working stock solution to a labeled 25 mL volumetric flask and bring the total volume up to 25 mL with deionized water. Cover with parafilm, invert and shake vigorously.

Procedure:

1. Elute NH₃-N from denuders
 - a. Remove cap from one end of the denuder.
 - b. Add 10 mL of deionized N_{H3}-free water
 - c. Put cap with hole in end on the open end of the denuder
 - d. Shake back and forth 30 times
 - e. Remove end cap with the hole and tap denuder into plastic funnel placed on a labeled sample collection bottle. Tap gently until all liquid has been removed
2. Turn the spectrophotometer on. Set wavelength to 655 nm.
3. Use 2 tubes from the kit per sample and standard. Label each tube.
4. Add 2.0 mL of standard , sample, or blank (deionized water) to each tube.
5. Add contents of one Ammonium Salicylate Reagent Powder envelope to each tube.
6. Add contents of one Ammonia Cyanurate Reagent Powder envelope to each tube.
7. Cap tubes tightly and shake thoroughly to dissolve the powder.
8. Allow to react for 20 min.
9. After 20 min, wipe the blank and insert it into the spectrophotometer.
10. Zero the spectrophotometer.
11. Wipe each tube and insert into spectrophotometer. Record absorbance.